TECHNISCHE UNIVERSITÄT MÜNCHEN

Klinik und Poliklinik für Innere Medizin II

Klinikum rechts der Isar

MODULATING CELLULAR PLASTICITY OF PANCREATIC CANCER-ASSOCIATED FIBROBLASTS DRIVEN BY PRRX1

Karin Feldmann

Vollständiger Abdruck der von der Fakultät für Medizin der Technischen Universität München zur Erlangung des akademischen Grades eines

Doktors der Naturwissenschaften (Dr. rer. nat.)

genehmigten Dissertation.

Vorsitzender:	Prof. Dr. Radu Roland Rad
Prüfer der Dissertation:	1. TUM Junior Fellow Dr. Maximilian Reichert
	2. apl. Prof. Dr. Dietmar Knopp

Die Dissertation wurde am 04.12.2019 bei der Technischen Universität München eingereicht und durch die Fakultät für Medizin am 07.04.2020 angenommen.

Acknowledgements

Writing a dissertation would not have been possible without the tremendous support of great people.

First of all, I would also like to thank the members of my doctoral committee, Prof. Dietmar Knopp and Dr. Günter Schneider, for their scientific input and fruitful discussions. In addition, I would like to thank Prof. Roland M. Schmid for giving me the opportunity to do my PhD research in his department, Klinik und Poliklinik für Innere Medizin II, and Prof. Dieter Saur for his support during the last years.

Above all, I would like to thank Dr. Maximilian Reichert for his support, guidance, and understanding during the last years. He motivated and supported me and contributed to the successful outcome of my dissertation.

I would also like to all members from the Reichert, Saur, Rad, Geisler, and Schneider group for their friendship, fruitful discussions, their constant help and support throughout the years. In particular, I would like to thank Dr. Alice Nomura, Katja Peschke, Dr. Kathleen Schuck, Dr. Sabine Klein, Dr. Angelika Krömer, Magdalena Zukowska and Dr. Zahra Dantes. In addition, I would like to thank Dr. Steffen Teller for his scientific input and for sharing his methodical knowledge about pancreatic stellate cells and 3D migration assays.

Finally, I would like to thank my family and friends. Especially I want to thank my husband for his support and advice, for his critical reading of my dissertation, his patience and help during the last years. Thank you for all your love and trust – thank you for always believing in me – thank you for everything.

Table of contents

Summary

Heterogeneity and plasticity are the key characteristics of one of the most malignant tumor diseases, namely pancreatic ductal adenocarcinoma (PDAC). The tumor stroma, known as desmoplastic reaction, is contributing to the complexity, as it facilitates tumor supportive and repressive functions. Specifically, cancer-associated fibroblasts (CAFs) play an important role, since they produce extracellular matrix (ECM) proteins in order to facilitate desmoplasia, a hallmark of PDAC.

Recently, the transcription factor *Prrx1* was identified as a plasticity driver during the process of embryonic development, pancreatitis and carcinogenesis. Remarkably, gene expression analysis revealed that *Prrx1* is highly upregulated in the stromal compartment, especially in CAFs. To address the question, which role *Prrx1* does play in the function of CAFs, a conditional knockout allele of *Prrx1* was developed to delete *Prrx1* genetically *in vitro* and *in vivo*. The *in vivo* findings demonstrate that *Prrx1* in CAFs restrains stromal expansion but promotes invasion of tumor cells. Hence, the tumor cells undergo epithelial to mesenchymal transition (EMT) and disseminate into the blood circulation and, therefore, metastasize. In contrast, *Prrx1*-deficient CAFs secrete a higher amount of extracellular matrix and limit the invasiveness of tumors.

Interestingly, *Prrx1* ablation in CAFs *in vitro* leads to increased fibroblast activation as shown by alpha smooth muscle actin (α-SMA) and collagen expression as well as stronger migration towards the tumor cells. In addition, these cells are also characterized by reduced plasticity and keep their tumor-restraining function. Both the *in vivo* and *in vitro* experiment results imply that targeting fibroblast plasticity directly changes the fibroblast-tumor cell interaction, the stroma contribution, and therefore the progression of the disease. These data highlight the possibilities of new treatment designs by converting tumor promoting CAFs into tumor-restraining CAF population.

Recently, Takano et al. showed that hepatocyte growth factor (HGF) is a transcriptional target of Prrx1b (Takano et al., 2016). To analyze the ability of *Prrx1* knockout fibroblasts to secrete HGF and thereby modulating the plasticity of tumor cells, *in vitro* co-culture experiments were used. Ablation of *Prrx1* in fibroblasts leads to reduced secretion of HGF which is companied by reduced expression of EMT markers in tumor cells.

Also, the orthotopic implantation model revealed decreased HGF expression in the pancreatic tumor and lower HGF levels in the serum of the mice, when *Prrx1* is ablated in the fibroblasts. The reduced PRRX1 levels correlate with better differentiated and less invasive tumors as well as fewer metastasis in the mouse model of pancreatic cancer. Hence, we hypothesize that

stromal PRRX1 correlates with pancreatic cancer subtypes. This might serve as a stratification for patients with pancreatic cancer to predict disease progression and metastatic spread – which, however, must be verified by future experiments.

In summary, the *Prrx1*-dependent modulation of the fibroblast plasticity and their secretome, specifically for HGF, influence the tumor cell plasticity and heterogeneity via EMT and their response to chemotherapy. This, once again, highlights the role of *Prrx1* as a master regulator of cellular plasticity.

Zusammenfassung

Das duktale Adenokarzinom des Pankreas (PDAC) ist eines der tödlichsten Tumorerkrankungen weltweit. Die Schwierigkeit, neue Therapiekonzepte abzuleiten, liegt in der Komplexität des Tumors. Die Tumorzellen sind umgeben vom Tumorstroma, auch extrazelluläre Matrix (ECM) genannt, bestehend aus zellulären und molekularen Bestandteilen, die das Tumorwachstum beeinflussen können.

Zu den molekularen Bestandteilen der ECM gehören u.a. Collagen, Fibronektin und Metalloproteasen, die zum größten Teil von Tumor-assoziierten Fibroblasten (CAFs) sezerniert werden. Neben den CAFs gehören auch Immunzellen und Endothelzellen zu dem zellulären Bestandteil der ECM. Die Hauptquelle der CAFs sind ruhende pankreatische Sternzellen (PSC), die sich durch Aktivierung in inflammatorische CAFs (iCAFs) oder myofibroblastische CAFs (myCAFs) differenzieren können – dieser Vorgang wird auch als zelluläre Plastizität bezeichnet. Die iCAFs und myCAFs sezernieren verschiedene Faktoren, die das Tumorwachstum begünstigen oder inhibieren können.

Die zelluläre Plastizität wird über Transkriptionsfaktoren, wie z.B. *Prrx1*, reguliert. PRRX1 reguliert die epitheliale Plastizität während der Embryonalentwicklung, ist aber auch während der Pankreatitis und Karzinogenese aktiv. Bisher ist jedoch wenig über dessen Funktion im Stroma bekannt. Erste Genexpressionsanalysen vom Tumorgewebe des PDAC zeigen, dass *PRRX1* im Tumorstroma hochgradig reguliert ist. Basierend auf diesen Erkenntnissen wird in dieser Dissertation die zelluläre Plastizität von CAFs in Abhängigkeit von Prrx1 untersucht.

Um die Rolle von *Prrx1* in CAFs *in vitro* und *in vivo* zu untersuchen, wurde ein konditionales Knockout-Allel von *Prrx1* entwickelt. Die *in vivo* Daten zeigen, dass *Prrx1* in CAFs die Sekretion der ECM Proteine beeinflusst, die Invasion von Tumorzellen durch epitheliale zu mesenchymale Transition (EMT) fördert und damit verbunden die Dissemination in den Blutkreislauf und deren Metastasierung.

Die Ablation von *Prrx1* in Fibroblasten führt zu einem stärker aktivierten Phänotyp *in vitro*. Die verstärkte Aktivierung zeichnet sich durch erhöhte Expression von α-SMA, vermehrter Kollagenproduktion sowie zu einer stärkeren Migration der Fibroblasten zu den Tumorzellen aus. *Prrx1* knockout Fibroblasten sind durch eine reduzierte Plastizität charakterisiert, d.h. diese Zellen können ihre Funktionalität nicht mehr ändern und verbleiben im „α-SMA high“ Status. Die *in vivo* und *in vitro* Ergebnisse legen nahe, dass die gezielte Veränderung der Plastizität der Fibroblasten direkt die Interaktion zwischen Fibroblasten und Tumorzellen, die Zusammensetzung der extrazellulären Matrix und damit die Tumorprogression beeinflusst.

In den letzten Jahren konnte gezeigt werden, dass der Hepatozyten-Wachstumsfaktor (HGF), transkriptionell von *Prrx1b* reguliert wird. HGF spielt eine wichtige Rolle in der Stroma-Tumor Interaktion. Aus diesem Grund wurde die Fähigkeit der *Prrx1* knockout Fibroblasten, HGF zu sezernieren und damit die Plastizität von Tumorzellen zu modulieren, in *in vitro* Co-Kulturen analysiert. Die Ablation von *Prrx1* in Fibroblasten führt zu einer geringeren Sekretion von HGF, die durch eine verminderte Expression von EMT-Markern in Tumorzellen und einem besseren Ansprechen auf Chemotherapeutika einhergeht.

Auch im murinen orthotopen Implantationsmodell konnte eine verminderte HGF-Expression im Pankreastumor und ein geringerer HGF-Spiegel im Serum gemessen werden. Die reduzierten HGF-Werte korrelieren mit besser differenzierten und weniger invasiven Tumoren sowie weniger Metastasen im Mausmodell.

Zusammenfassend zeigt sich, dass die Manipulation von *Prrx1* in Fibroblasten nicht nur die Plastizität der Fibroblasten verändert, sondern auch die Differenzierung von Tumorzellen. Darüber hinaus konnte eine Korrelation zwischen der PRRX1-HGF Achse und das Ansprechen auf Chemotherapeutika festgestellt werden. Anhand dieser Daten wird verdeutlicht, dass *Prrx1* die zelluläre Plastizität von Fibroblasten reguliert und somit sowohl Tumorwachstum begünstigen als auch inhibieren kann.

List of abbreviations

4-OHT	4-hydroxytamoxifen
AS	amino acid
a-SMA	alpha smooth muscle actin
BMDC	bone-marrow derived cell
BPE	bovine pituitary extract
BSA	bovine serum albumine
CAF	cancer associated fibroblast
CD31	platelet endothelial cell adhesion molecule
CK-19	cytokeratin-19
CRISPR-Cas	clustered regularly interspaced short palindromic repeats-CRISPR associated nuclease
CTC	circulating tumour cell
CTGF	connective tissue growth factor
CXCL12	stromal cell-derived factor 1
ddH_2O.	double-distilled water
DMEM	Dulbecco's modified Eagle's medium
DMSO	dimethyl sulfoxide
DNA	deoxyribonucleic acid
DPBS	Dulbecco’s phosphate-buffered saline
DRS	dual recombinase system
ECM	extracellular matrix
EDTA	ethylenediaminetetraacetic acid
EGF	epidermal growth factor

ELISA	enzyme-linked immunosorbent assay
EMT	epithelial to mesenchymal transition
EndMT	endothelial to mesenchymal transition
EpCAM	epithelial cell adhesion molecule
ER	estrogen receptor
ERT	truncated estrogen receptor
FACS	fluorescence-activated cell sorting
FAP	fibroblast activation protein
FBS	fetal bovine serum
FGF	fibroblast growth factor
Flp	flippase
FMI	forward migration index
FNA	fine-needle aspiration
FOLFIRI-NOX	fluorouracil, folonic acid; oxaliplatin and irinotecan
FRT	flippase recognition target
FSF	FRT-stop-FRT
GAP	GTPase activating protein
GBSS	Grey’s balanced salt solution
GEMM	genetically engineered mouse model
GFAP	glial fibrillary acidic protein
GFP	green fluorescent protein
GTP	guanosine-5'-triphosphate
H&E	haematoxylin and eosin staining

HGF	hepatocyte growth factor
HIF-1α	hypoxia-inducible factor 1α
HSP90	heat shock protein 90
iCAF	inflammatory cancer associated fibroblast
IF	immunofluorescence
IHC n	immunohistochemistry
IL-6	interleukin 6
IP	intraperitoneal
IPMN	intraductal papillary mucinous neoplasm
ITS	insulin/human transferring/selenous acid and linoleic acid
KC	*Pdx1-Cre*; *LSL-Kras*$^{G12D/+}$
KPC	*Pdx-1-Cre, LSL-Kras*$^{G12D/+}$*, LSL-Trp53*$^{R172H/+}$
KPF	*Pdx-Flp, FSF-Kras*^{G12D}*, p53*$^{frt/wt}$
LBD	ligand-binding domain
MCN	mucinous cystic neoplasm
MET	mesenchymal to epithelial transition
MMF	medetomidin, midazolam, fentanyl
MMP	matrix metalloproteinase
myCAF	myofibroblastic cancer associated fibroblast
OAR	otp, aristaless, rax
OTX	orthotopic implantation
PAF	pancreas associated fibroblast
PanIN	pancreatic intraepithelial neoplasia
PBS	phosphate-buffered saline

PDAC	pancreatic ductal adenocarcinoma
PDC	pancreatic ductal cell
PDGFRa	platelet-derived growth factor receptor A
Pdx1	pancreatic and duodenal homeobox gene 1
PFA	paraformaldehyde
Prrx1	paired-related homeobox 1 transcription factor
P/S	penicillin streptomycin
PSC	pancreatic stellate cell
Ptf1a	pancreatic transcription factor 1a
RT	room temperature
RT-PCR	reverse transcription polymerase chain reaction
SHH	sonic hedgehog
Slug	zinc finger protein SNAI2
SM22	smooth muscle protein 22
Snail	zinc finger protein SNAI1
SPARC	secreted protein acidic and rich in cysteine
STI	soybean trypsin inhibitor
TAE	TRIS-Acetate-EDTA
TAM	tamoxifen
TF	transcription factor
TGF-β	transforming growth factor β
TIMP	tissue inhibitor of metalloproteinases
TME	tumor microenvironment
Tn-C	tenascin-C

Twist	twist-related protein 1
VEGF	vascular endothelial growth factor
Zeb1/2	zinc finger E-box-binding homeobox 1/2
wt	wildtype

1 Introduction

1.1 Pancreatic ductal adenocarcinoma

Paul Ehrlich, the founder of chemotherapy, inspired generations of scientists with his “magic bullet” concept: a concept in which drugs go straight to their cell-structural targets without harming healthy tissue (Strebhardt and Ullrich, 2008).

To date, scientists have neither found a “magic bullet” to cure pancreatic cancer nor chemotherapeutics with tolerable side effects. At the moment, pancreatic cancer is the fourth leading cause of cancer death in developed countries (Jemal et al., 2011; Siegel et al., 2013); however, due to increasing incidence, it is expected to be the second leading cause of cancer death by 2030 (Rahib et al., 2014). The pancreatic ductal adenocarcinoma (PDAC) represents 90% of the pancreatic cancers and is one of the most aggressive solid malignancies (Adamska et al., 2017). Only 10-15% of patients being diagnosed with PDAC are eligible for surgery, which currently is the only potentially curative option (Ryan et al., 2014). The vast majority of PDAC patients are diagnosed with unresectable tumors and metastasis (Yachida and Iacobuzio-Donahue, 2009; Neesse et al., 2013; Heinemann et al., 2014) without any chance of cure.

Therefore, the five years survival rate remains around 5-7% (Vincent et al., 2011). The poor prognosis is caused by the lack of early symptoms, no reliable biomarkers for early diagnosis, and late unspecific symptoms, which lead to late diagnosis (Maitra and Hruban, 2008).

Additionally, tumor heterogeneity and plasticity contribute to the complexity of the disease as well as chemoresistance. Gemcitabine was established as a first line chemotherapeutic drug, but it extends the overall survival by only a few months (Heinemann et al., 2014). Improvement of the overall survival from 6.8 months to 11.1 months and treatment of metastatic disease were achieved by the harsh multiple drug regime FOLFIRINOX (fluorouracil, folonic acid; oxaliplatin and irinotecan) (Thibodeau and Voutsadakis, 2018). Another treatment option is the combination of nab-placitaxel and gemcitabine, which increase the overall survival from 6.8 months to 8.5 months (Conroy et al., 2011; Hoff et al., 2013). FOLFIRINOX and gemcitabine/nab-placitaxel are currently the standard care treatment options for advanced and metastatic PDAC; nevertheless, their efficacy still remains low with severe side effects. As a consequence, novel approaches to diagnose and treat PDAC are urgently needed.

1.1.1 Carcinogenesis of the pancreas

PDAC is a complex and heterogeneous disease compared to other human malignancies. It evolves through an increasing number of dysregulated cell-autonomous and non-tumor cell pathways, accompanied by morphological changes.

Pancreatic cancer can arise from distinct preneoplastic lesions. The most common route to pancreatic cancer is via intraepithelial neoplasia (PanIN). Less frequently, intraductal papillary mucinous neoplasm (IPMN) and mucinous cystic neoplasm (MCN) give rise to invasive PDAC (Vincent et al., 2011). The transdifferentiation from acinar to ductal cells, called acinar-to-ductal metaplasia (ADM), in acute or chronic pancreatitis, might be involved in the process of PanIN and PDAC development (Guerra et al., 2007; Reichert and Rustgi, 2011).

Based on their morphological appearance, they are classified as PanIN-1 (low-grade dysplasia), PanIN-2 (moderate dysplasia) or PanIN-3 (high-grade dysplasia) (Hruban et al., 2000). The normal ductal epithelium is characterized by a cuboidal layer of cells and the absence of mucin in the cytoplasma. In contrast, low grade PanIN lesions (PanIN-1) are further classified into PanIN-1a and PanIN-1b, and can be recognized by mucinous differentiation and elongation of the ductal cells, where their nuclei are orientated at the basal membrane. Low grade PanINs are very common in humans with increasing age (Hruban et al., 2004). The progression to PanIN-2 lesion is accompanied by cytological atypia as well as nuclear alterations like nuclear pleomorphism, hyperchromasia, and crowding. PanIN-3 lesions ("carcinoma *in situ*") are present in 30-50% of invasive PDACs and have the highest degree of dysplasia, although it is not invading into the basement membrane (Hruban et al., 2004). PanIN-3 lesions have papillary morphology and consist of dystrophic goblet cells.

PanINs are part of the multistep tumor progression model in pancreatic cancer and genetic alterations occur and accumulate during this process. Activating mutations in the KRAS oncogene represents a critical event and can be found as earliest genetic alteration in low-grade PanIN-1A lesions (Eser et al., 2014). KRAS is part of the RAS family and it requires GTPase activating proteins (GAPs) to convert guanosine triphosphate to guanosine diphosphate to modify downstream signals, thereby controlling proliferation, differentiation, and survival pathways (Schneider et al., 2017). The three major pathways regulated by KRAS signaling are RAF/MEK/ERK, PI3K/PDK1/AKT, and the Ral guanine nucleotide exchange factor pathway (Lim et al., 2005; Feldmann et al., 2010; Collisson et al., 2012). Additionally to KRAS activation, also telomere shorting is another early event, which leads to chromosomal instability (van Heek et al., 2002).

During the process of PanIN development additional mutations accumulate, mainly inactivation of the three tumor suppressor genes, *CDKN2A/INK4A*, *TP53,* and *DPC4/SMAD4/MADH4*. The

CDKN2A/INK4A gene encode the cell cycle checkpoint protein P16, which binds to CDK4 and CDK6 by causing a G1-S cell-cycle arrest (Sherr, 2000). Several mechanisms can lead to P16 inactivation such as homozygous deletion of *CDKN2A/INK4A,* intragenic mutation with loss of the second allele, and epigenetic silencing by promoter methylation (Schutte et al., 1997).

Another tumor suppressor is *TRP53* which is inactivated in 44% of pancreatic cancer (Schneider et al., 2017) mainly through a combination of intragenic mutation and loss of the second wild type allele (Redston et al., 1994). Losing the function of P53 allows the cell to bypass DNA damage checkpoints and apoptotic signals, which can contribute to genomic instability (Hingorani et al., 2005).

The inactivation of *DPC4/SMAD4/MADH4* leads to inference with the TGF-β signaling, resulting in decreased growth inhibition and uncontrolled proliferation (Feldmann et al., 2007). The frequency of *SMAD4* mutation occurs in 14% of human PDAC (Schneider et al., 2017).

Besides these by far most frequent genetic alterations, many other mutations in oncogenes, tumor suppressors, and other genes contributing to the complexity of the disease (Witkiewicz et al., 2015; Bailey et al., 2016). These genetic but also epigenetic alterations (DNA methylation, chromatin remodeling, and post-translational modification of histones) contribute to the lethal outcome of PDAC and therapeutic failure due to selection for resistance tumor cells under treatment (chemoresistance) and Darwinian evolution. The genetic heterogeneity is one of principal problems facing PDAC and its poor sensitivity towards treatment.

1.1.2 Model systems in pancreatic cancer

To begin unraveling the genetic alterations and epigenetic contributions underlying PDAC pathogenesis, a variety of model systems are needed.

More than 50 years ago, the first pancreatic cancer cell line was generated. Since that day several other PDAC cell lines were added, generated from primary tumors, liver metastasis, ascites, and lymph nodes (Dobrynin, 1963). Although these cell lines have many advantages (low costs, easy to cultivate, ability for genetic manipulation, and drug testing), there are also many limitations: for instance, passing these cells results in genetic drift (genetic instability) and cellular senescence (Lowy et al., 2008). One major limitation is the loss of the extracellular matrix and – with it – cellular and molecular interactions (Lowy et al., 2008).

To understand the complexity of the disease especially regarding cell-cell interaction, genetically engineered mouse models (GEMM) are needed, to establish practical approaches for early detection, and to test novel compounds of chemoprevention and chemotherapy.

In 2003, Hingorani et al. described the *Pdx1-Cre; LSL-Kras^{G12D}* mouse model, which recapitulates the molecular and histopathological evolution of human PDAC (Hingorani et al., 2003). The point mutation of the *Kras* oncogene on codon-12 leads to a permanent activation of the GTPase. This mouse model takes advantage of a *Lox-Stop-Lox* cassette inserted into the endogenous promoter upstream of exon 1 of *Kras^{G12D}*. Subsequent Cre activation in pancreatic progenitor cells allows the expression of oncogenic *Kras^{G12D}* and development of PDAC (Hingorani et al., 2003). To genetically target pancreatic cancer the Cre was introduced under the control of the Pancreatic and duodenal homeobox gene 1 (Pdx-1) and pancreatic transcription factor 1 α (Ptf1α) promoter (Hingorani et al., 2003). The mosaic expression of the *Pdx1-Cre* is detected in the pancreatic epithelium, antral stomach, and duodenum in neonates and in pancreatic beta islet cells in adults (Kim and MacDonald, 2002; Hingorani et al., 2003).

Since PDX1 expression can be detected at embryonic day 8.5 and Cre is active, the mice will develop a complete spectrum of PanINs (Hingorani et al., 2003). The PanIN lesions reflect the PanIN development in patients and the mice will ultimately develop PDAC with long latency (12-15 months) (Hingorani et al., 2003). Accelerating tumor formation (starting from 3-4 months timepoint) can be achieved by additional epigenetic and genetic somatic alterations, including inactivation or point mutation of *p53; Cdkn2a; Smad4, Tgfßrl* and *Tgfßrll* (Caldas et al., 1994; Redston et al., 1994; Hahn et al., 1996; Goggins et al., 1998; Aguirre et al., 2003; Bardeesy et al., 2006; Mueller et al., 2018). Similar to human PDAC, which metastasizes to the liver, lung, and lymph node, the GEMM recapitulates the same frequency of metastases (Aguirre et al., 2003; Bardeesy et al., 2006).

The tumor microenvironment (TME), known as desmoplastic reaction, increases tumor complexity and its function in the process of carcinogenesis is critical. The stroma comprises of an extracellular matrix, activated fibroblasts, inflammatory cells, blood and lymphatic vessels that interact with neoplastic cells during PDAC progression.

To manipulate the TME during PDAC formation, progression, and metastasis, the use of a single recombinase has limited ability. Therefore, an additional recombinase, the *Flippase (Flp)* recombinase, was introduced into the system. The *Flp* recombines genomic sequences flanked by *Flippase recognition target (FRT)* sites and allows cell-autonomous and non-cell autonomous activation and/or inactivation of genes in the same tumor at different stages during disease progression (Branda and Dymecki, 2004; Schönhuber et al., 2014).

The *Flp/FRT* recombination system is similar to the *Cre/loxP* system. For pancreas specific expression, the *Flp* recombinase is under the control of the *Pdx1* promoter and a *FRT*-flanked STOP cassette (FRT-stop-FRT, FSF) silenced the *Kras^{G12D}* expression (Schönhuber et al., 2014). The survival and the development of precursor lesions and PDAC are similar for the

Pdx1-Cre; *LSL-Kras*$^{G12D/+}$ (KC) mice and the *Pdx1-Flp; FSF-Kras*$^{G12D/+}$ (*KF*) mice (Schönhuber et al., 2014).

The dual recombinase system (DRS), the combination of the *FlpFRT* and the *Cre-LoxP/Cre*^{ERT2}*-LoxP* system, allows new experimental design with multistep carcinogenesis (Schönhuber et al., 2014). To allow a time-specific manipulation, the Cre*/loxP* system was altered by fusing the Cre recombinase to the ligand-binding domain (LBD) of the human estrogen receptor (ER) (Metzger et al., 1995), thereby the activity of the Cre depends on estradiol or tamoxifen (Metzger et al., 1995). To prevent activation of the Cre recombinase in mice by estradiol and specifically foster the Cre activation by tamoxifen administration, a point mutation (exchange of glycine to arginine at position 521 (G521R)) in the LBD was introduced (Feil et al., 1996). The fusion protein is called Cre^{ERT}. Without tamoxifen administration, the Cre^{ERT} is localized in the cytoplasma and binds to the heat shock protein 90 (HSP90). After tamoxifen administration, the Cre^{ERT} dissociates from the HSP90 and translocates to the nucleus. There, it recognizes the loxP sites and mediates the excision. To improve the ligand-activated site-specific recombination a triple mutant calling Cre^{ERT2} was introduced in the LBD of the estrogen receptor (G400V/M543A/L540A) to increase the sensitivity towards 4-hydroxytamoxifen (4-OHT) (Feil et al., 2009).

Using this next-generation dual recombinase system, Schönhuber and colleagues (Schönhuber et al., 2014) provided a tool, which allows for the manipulation of the tumor and the stroma at the same time, as illustrated in Figure 1.1 (Schönhuber et al., 2014) .

Nevertheless, generating such a mouse model is very expensive and time consuming. Furthermore, the gene mutations are being introduced in the germline of the mouse – in contrast to that, genetic alteration occurs somatically in humans.

To overcome the limitation of established cell lines and GEMM, Clevers' lab has developed a three-dimensional culture system of human pancreatic cells, called organoids (Boj et al., 2015). Organoids can be generated from small amounts of tissue from surgery samples or even from fine-needle aspiration (FNA) and biopsies. Especially the generation of organoids from FNA and biopsies allows scientist to maintain organoids from any disease stages to recapitulate all clinical conditions (Moreira et al., 2018). It has been shown that these isolated and cultivated cells maintain their identity of the original tissue for several passages. This advantage allows genomic, epigenomic, proteomic analyses as well as pharmacological screens of individual tumors, which will give insights into mutation-based drug sensitivities (Baker et al., 2016). A few years ago, in the field of colorectal cancer, a trial has already been started for the predictive value of personalized organoid screening (Clevers and Bender, 2015).

Due to their genetic stability, organoids also become attractive candidates for genetic manipulation e.g. via CRISPR/Cas 9 to study particular genes (Matano et al., 2015). Specially the ability to engineer sequential mutations might help to gain new insights into the identified subtypes of the PDAC (Bailey et al., 2016).

Although organoids are a powerful tool with high potential in diagnostics and personalized medicine, the molecular and cellular interactions (immune, stromal, and vascular compartments), which contribute to the success/failure of the chemotherapeutic drugs, are still missing.

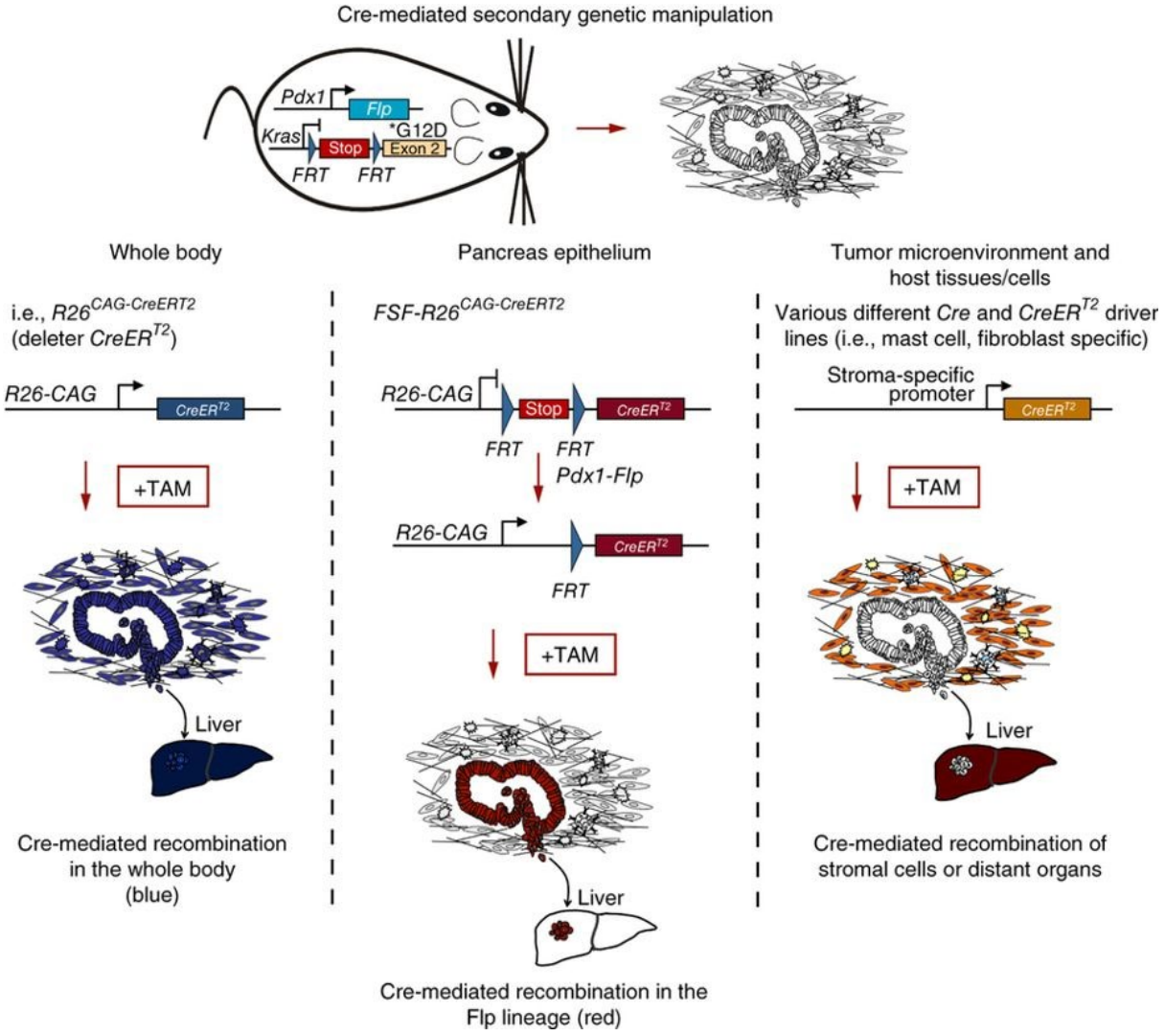

Figure 1.1 Schematic illustration of the usage of the dual recombinase system from Schönhuber et al. (Schönhuber et al., 2014). The usage of *Pdx1-Flp; FSF-Kras^{G12D}* leads to tumor formation in the pancreas (shown above). To gain additionally a whole body recombination, the *R26CAG-Cre^{ERT2}* can be crossed. The addition of Tamoxifen activates the Cre (time specific modulation) (left), to achieve an additional pancreas epithelium modification and a time-specific activation of the Cre, the *R26CAG-Cre^{ERT}* is flanked by FRT sides (middle). The usage of the of *Pdx1-Flp; FSF-Kras^{G12D}* in combination with another *Cre* or *CreERT2* driver lines, allows to target additionally various cell types (fibroblasts, immune cells etc.) or host tissue (for example the liver with the Alb-Cre) (right). Reprint with the permission of Springer Nature.

1.2 Tumor microenvironment of PDAC

PDAC is extremely rich of stroma and consists of up to 90% of a hard and scirrhous mass, which is called extracellular matrix (ECM) and which comprises activated fibroblasts, immune cells, blood vessels, neural cells, and a variety of proteins such as collagen type I and III, fibronectin, proteoglycans, hyaluronic acid, laminin as well as soluble proteins like matrix metalloproteinases (MMPs) and their inhibitors (TIMPs) (Chu et al., 2007; Hanahan and Weinberg, 2011; Feig et al., 2012; Apte et al., 2013; Moir et al., 2015; Kalluri, 2016).

The tumor microenvironment (TME) is not a static entity; rather, it is constantly changing in composition, especially in the progression from preneoplastic PanIN to invasive PDAC (Feig et al., 2012).

For a long time, it was believed that the TME is just a bystander reaction in cancer development and progression (Stoker et al., 1966). But research during the last years reveals that the TME plays an important role during tumor initiation, progression, and metastases (Kalluri, 2016).

On the one hand, the TME can act as a mechanical barrier to the tumor to prevent growth and spreading, but on the other hand, it can also increase the interstitial pressure and impair the vascularization, which limit the effective delivery of chemotherapeutics (Goel et al., 2011; Erkan et al., 2012b; Neesse et al., 2013). The increased hypoxia due to reduced blood perfusion and oxygen diffusion leads to a hypoxic environment and an upregulation of the hypoxia-inducible factor 1α (HIF-1α) protein, which activates various genes to promote cell survival, invasion and metastasis of the epithelial cells (Erkan et al., 2010). Hypoxia can also induce the production of collagen and vascular endothelial growth factor (VEGF) by pancreatic stellate cells, this promotes invasion and metastases (Erkan et al., 2010; Xu et al., 2014). Hypoxic cells are shown to maintain stemness, being more resistant towards radiotherapy and chemotherapy, which leads to a more aggressive disease, (Feig et al., 2012; Özdemir et al., 2014). This example highlights the controversy role of stroma and the challenges that have to be faced by targeting PDAC and by improving its treatment options.

One approach is to target MMPs, which are a large family of zinc-proteolytic enzymes and very important regarding ECM remodeling (Xu et al., 2014). The matrix-degrading enzymes provide favorable conditions regarding cancer cell migration and invasive cancer cell growth (Xu et al., 2014). The clinical phase III trial failed using the MMP inhibitor BAY 12-9566 because of the reduced survival compared to gemcitabine treatment (Moore et al., 2003), but also other approaches to target MMPs failed to be approved for clinical routine (Bramhall et al., 2001; Bramhall et al., 2002).

Moreover, extracellular matrix proteins came into focus for new treatment strategies. The depletion of hyaluronic acid, to release the high interstitial fluid pressure, using recombinant hyaluronidase which is PEGylated (PEGPH20), showed auspicious results in GEMMs (Provenzano et al., 2012; Jacobetz et al., 2013). The authors showed, that PEGPH20 results in re-expansion of blood vessels and improved drug delivery (Provenzano et al., 2012; Jacobetz et al., 2013). The beneficial role of PEGPH20, especially for patients with a high intratumorally content of hyaluronic acid, is currently in phase III of clinical trials (Doherty et al., 2018).

Other attempts for new therapies were waged e.g. inhibiting the sonic hedgehog (SHH) pathway, which is important for creating a fibroblast-rich desmoplastic stroma in pancreatic cancer (Rhim et al., 2014). Olive et al. found that inhibiting the SHH signaling pathway resulted in depletion of stromal components and increased intratumoral vascular density, leading to enhanced delivery of chemotherapeutics in GEMM (Olive et al., 2009). Surprisingly, the SHH inhibitor IPI-926 (saridegib) and GDC-0449 (vismodegib) both failed in phase II clinical trials (Neesse et al., 2013). To understand the reason for this failure, Rhim and colleagues chose the *ShhKPfl/+CY* model (Rhim et al., 2014). These mice show reduced stroma formation, but also earlier tumor formation, metastases and reduced survival compared to the KPC mice. The authors showed further that IPI-926 treatment also promotes cachexia in KPC mice (Rhim et al., 2014). This data revealed for the first time, that the TME can have also a protective role and targeting the stroma can lead to more aggressive tumors. These insights were supported by the publication of (Özdemir et al., 2014) showing that the depletion of α-SMA+ myofibroblasts resulted in undifferentiated and invasive tumors compared to the controlled group.

The failure of clinical trials targeting the stroma and the new insights regarding the protective role of TME highlights the need for investigating the TME and its role in tumor progression for better understanding.

1.2.1 The role of cancer-associated fibroblasts in PDAC

Pancreatic stellate cells (PSCs) and fibroblasts have emerged as the most important cell type in the desmoplastic reaction. Therein, PSCs are the main source of cancer associated fibroblasts (CAFs) (Erkan et al., 2012a; Moir et al., 2015). In healthy pancreas, quiescent PSCs are characterized by cytoplasmatic vitamin A storage lipid droplets (Nielsen et al., 2016). In 1998, PSCs were isolated and cultured for the first time (Apte et al., 1998; Bachem et al., 1998). These cells regulate the architecture in healthy tissue through synthesizing and degrading ECM components by secretion of MMPs and TIMPs (Moir et al., 2015; Bynigeri et al., 2017).

PSCs become activated in response to injury, inflammation, or paracrine signals secreted from tumor cells (Bachem et al., 2005; Vonlaufen et al., 2008; Pang et al., 2017). Once the PSCs

are activated, they lose their vitamin A storage, they change their morphology to a myofibroblast like structure and express α-SMA (Apte et al., 2012; Apte et al., 2013; Pang et al., 2017). The presence of lipid droplets together with expression of GFAP (glial fibrillary acidic protein), desmin, nestin (intermediate filament proteins), and vimentin is used to differentiate the PSCs from pancreatic fibroblasts (Omary et al., 2007).

However, once PSCs are activated, they start to proliferate, migrate, and produce excessive amounts of ECM proteins, resulting in a loss of the balance between ECM production and degradation, which can eventually lead to fibrosis (Wilson et al., 2014). Hence, PSCs can contribute to chronic pancreatitis, a risk factor for pancreatic cancer (Kalluri, 2016). In pancreatic cancer, activated PSCs contribute to the cell population of cancer-associated fibroblasts (CAFs). CAFs are a heterogenous population of mesenchymal cells including cells, which undergo EMT or EndMT, resident fibroblasts bone-marrow derived cells (BMDCs), and PSCs as the major source (Potenta et al., 2008; Shiga et al., 2015; Kalluri, 2016).

CAFs display an elongated, spindle shaped structure and are characterized by abundant expression of α-SMA. Functionally, CAFs are characterized by their production of various types of ECM proteins, cytokines, chemokines, metabolites, and enzymes (Kalluri, 2016). They influence cancer growth by supporting the proliferation of tumor cells associated with decreased apoptosis (Vonlaufen et al., 2008; Xu et al., 2010). They increase cancer cell stemness (Hamada et al., 2012), suppress the immune response (Ene-Obong et al., 2013; Mace et al., 2013), increase the migratory capability of tumor cells, and the angiogenesis (Xu et al., 2010) and resistance towards chemotherapy (Olive et al., 2009).

Pro-tumorigenic CAFs exhibit enhanced migratory capacity, autocrine growth factor induced signaling, and increased levels of secretory molecules that include growth factors and chemokines (Kalluri, 2016). CAFs can induce angiogenesis by secretion of CXCL12 (stromal cell-derived factor 1) (Zeisberg et al., 2000) or can impede tumor progression by enhancing proliferation, stemness, and survival of tumor cells, initiate metastasis and increase chemoresistance by secreting factors like TGF-β (Calon et al., 2014); FGF (Bai et al., 2015), HGF (Tyan et al., 2011; Straussman et al., 2012; Pothula et al., 2017), and periostin (Ratajczak-Wielgomas et al., 2016). Furthermore, the motility and invasiveness of tumor cells can be influenced by the secretion of MMPs from CAFs. The secreted MMPs can cleave E-Cadherin and thereby promote the epithelial to mesenchymal transition of the tumor cells (Lochter et al., 1997). Additionally, the secretion of metabolites as ketone bodies and lactate can support the proliferation of tumor cells and T-cells (Molon et al., 2016; LeBleu and Kalluri, 2018).

Recently, Öhlund et al. discovered distinct population of CAFs which either have a tumor promoting or tumor restraining effect (Öhlund et al., 2017). The myofibroblastic CAFs called myCAFs express abundant levels of α-SMA and contribute to the expression of ECM proteins as for instance collagen or periostin. These cells are resident in close proximity to the tumor cells. The inflammatory CAFs (iCAFs), which are located more distantly from the tumor cells, secrete IL-6 and other inflammatory mediators (Öhlund et al., 2017). Gene expressing profiling revealed that pathways as chemokine and cytokine signaling are enriched in iCAFs, underscoring a secretory phenotype of these cells, which modulate cancer and immune cells in a paracrine manner (Öhlund et al., 2017). The secretome of the iCAFs can contribute to tumor progression, chemoresistance, and systemic effects such as cachexia and immune suppression (Feig et al., 2013; Mace et al., 2013; Flint et al., 2016; Öhlund et al., 2017). Both cell states – the iCAFs as well as the myCAFs – are interconvertible; this contributes to the plasticity of the cell population.

While the pro-tumorigenic function of CAFs is mainly based on their secretome, latest insights in anti-stromal therapy showed that CAFs can also restrain tumor growth and invasiveness (Olive et al., 2009; Lee et al., 2014; Özdemir et al., 2014; Rhim et al., 2014). The heterogeneity of the cells might explain the diverse outcome of experimental studies regarding the function of CAFs (Öhlund et al., 2017; LeBleu and Kalluri, 2018) as depicted in Figure 1.2.

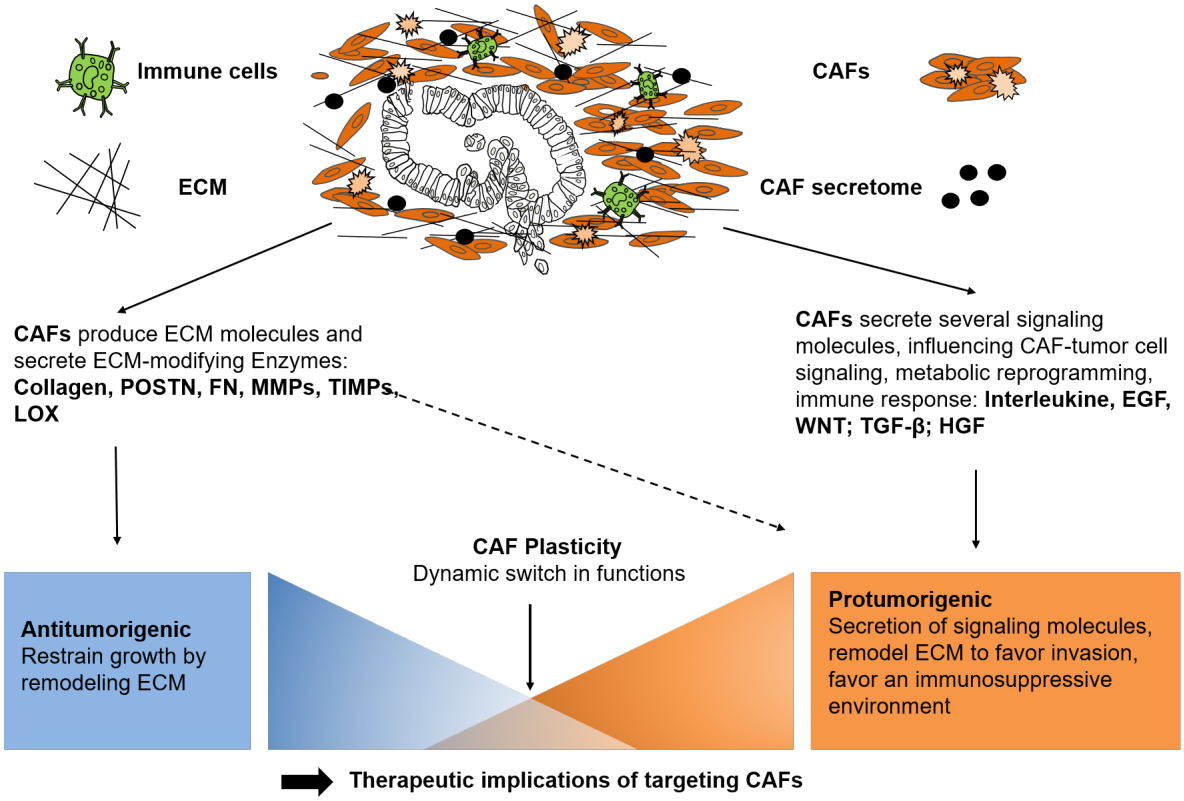

Figure 1.2 Schematic illustration of the composition of a PDAC and the special role of CAFs creating a antitumorigenic and a protumorigenic environment, modified from (LeBleu and Kalluri, 2018) and (Schönhuber et al., 2014)

1.3 Paired-related homeobox 1 transcription factor (Prrx1)

During embryonic development, a complex organism is formed from a single cell. Growth, differentiation, and migration are driven by transcriptional programs, directed by the expression and activity of transcription factors (TF) to form life. Involved in these carefully orchestrated processes are cell division, self-alignment, and specialization to form distinct organs and tissues. Key processes, to coordinate the migratory pattern and differentiation of these cells are the epithelial-to-mesenchymal transition (EMT) as well as the reverse phenomenon mesenchymal-to-epithelial transition (MET). Importantly, a subset of these transcriptional programs, which are activated during embryonic development, are also upregulated during carcinogenesis. Specifically, tumor cells acquire invasive and motility properties by undergoing EMT in order to metastasize to distant organs. MET is believed to be required for the metastatic outgrowth of the tumor cells (Hanahan and Weinberg, 2011).

The embryonic transcription factor PRRX1 is regarded as master regulator of cellular plasticity in various biological processes such as embryonic development, pancreatitis, and carcinogenesis (Reichert et al., 2013a). PRRX1 is a DNA-associated protein that localizes to the nucleus and harbors two main splice variants, *Prrx1a* and *Prrx1b* (Martin and Olson, 2000), highlighted in Figure 1.3. Although the first 199 amino acids (AA), including the homeobox domain, are identical, the C-terminus differs. Prrx1a harbors a so-called OAR (otp, aristaless, rax) domain named after three proteins that share this 15 amino-acid region. The OAR domain appears to be involved in modifying transactivation ability (Norris and Kern, 2001). The C-terminal end of *Prrx1b* lacks the OAR domain and therefore is designated as having an alternative C-terminus. The different functions of the dominant isoforms *Prrx1a* and *Prrx1b* are due to the C-terminus of the two proteins.

Recently, it was published for pancreatic cancer that *Prrx1a* fosters an epithelial phenotype regarding tumor differentiation and contribute in the process of metastases outgrowth by promoting mesenchymal-epithelial transition (MET) (Reichert et al., 2013a; Takano et al., 2016). In contrast, *Prrx1b* favors tumor cell invasion, tumor dedifferentiation, and epithelial-mesenchymal transition (EMT) (Reichert et al., 2013a; Takano et al., 2016).

Takano and colleagues describe that *Prrx1b* regulates the up-regulation of the hepatocyte growth factor (HGF) and therefore fosters the invasive phenotype of the tumor cells (Takano et al., 2016). Furthermore, the authors describe that targeting HGF with a neutralizing antibody in concert with gemcitabine reduces PDAC burden compared with gemcitabine treatment alone in preclinical studies (Takano et al., 2016). This highlights the importance of transcription factors and their regulated pathways as therapeutic targets.

Also, in other cancer types, for example in triple negative breast cancer, *Prrx1b* is significantly upregulated and associated with tumor size and vascular invasion (Lv et al., 2016). In a silencing approach of *Prrx1b* Lv et al could demonstrate an inhibition of the Wnt/β-catenin signaling pathway and an induction of MET (Lv et al., 2016). In gastric cancer, the expression of *Prrx1* is positively correlated with EMT induction and associated with invasive properties (Ocaña et al., 2012; Guo et al., 2015). This highlights the complex role of *Prrx1* as a plasticity driver.

Plasticity does not only play a role in tumor cells but also pancreatic stellate cells and fibroblasts. These cells can switch dynamically back and forth from quiescent to an activated phenotype, as well as from in an inflammatory (iCAFs) to a myofibroblastic phenotype (myCAFs). In search for an explanation for the fibroblast plasticity, Dr. Reicherts group (Klinikum rechts der Isar/ Technical University of Munich) found based on the data from Nicolle et. al that *Prrx1* is highly upregulated in the stromal compartment especially in fibroblasts in pancreatic cancer (Tomaru et al., 2014; Nicolle et al., 2017).

Although no further information is published regarding the role of *Prrx1* in pancreatic fibroblast, the recent study of Yeo et al. in colon, esophageal, and lung cancer showed, that Twist – another embryonic transcription factor – can induce the expression of *Prrx1* in a positive feed-forward loop in fibroblasts thereby activating the proliferation of these cells (Yeo et al., 2018).

The activation status of fibroblasts relates to their ability to secrete extracellular matrix proteins. Especially in liver fibrosis *Prrx1* is involved in modulating the expression of metalloproteinases MMP2 and MMP9, thereby modulating hepatic stellate cell (HSCs) migration (Gong et al., 2017).

In addition, C. Bousquet showed that the active form of FAK (FAK-pY397) is strongly expressed in CAFs and that this is linked to the migration of fibroblasts (Bousquet, 2017). The migration of fibroblasts and the formation of ECM may be related to the expression of PRRX1. McKean could already show that FAK induces the expression of PRRX1 and thus promotes a tenascin-C dependent migration of fibroblasts (McKean et al., 2003).

These publications just give a small insight in the complex regulated network by PRRX1 in fibroblasts and more research has to performed to unravel the mechanism beyond.

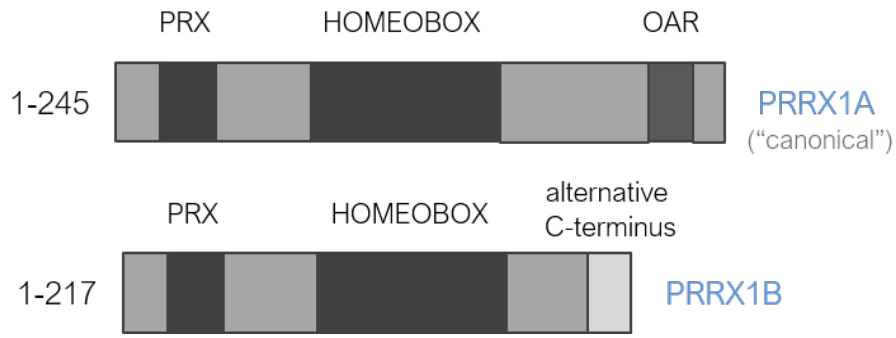

Figure 1.3 Schematic illustration of the splice variants *Prrx1a* and *Prrx1b*

1.4 Aim of this work

The extracellular matrix contributes up to 90% of the tumor mass in PDAC and thereby representing the largest part (Erkan et al., 2008; Neesse et al., 2013). In recent years, the stroma has increasingly moved into the focus of pancreatic cancer research and fueled the discussion whether the tumor stroma in PDAC is about "friend or foe" (Gore and Korc, 2014).

The transcription factor PRRX1 was recently described as a plasticity driver in the processes of embryonic development, pancreatitis, and carcinogenesis of the pancreas (Reichert et al., 2013a; Takano et al., 2016). In human cancer tissue, e.g. colon, esophageal, and lung cancer, it became apparent that PRRX1 is not exclusively expressed in the carcinoma but also in the stroma (Tomaru et al., 2014).

Based on the preliminary data, the question we asked is; which role does Prrx1 play in cellular plasticity of CAFs and how can this impact the shape of the tumor mass?

To answer the question a conditional knock-out allele of *Prrx1* was generated in Dr. Reichert's group (Klinikum rechts der Isar, Technical University of Munich). With the help of this mouse model we are able to analyze the role of PRRX1 in a tissue and cell specific context (in dependency of the Cre driver line) *in vivo* for the first time.

Therefore, the *Prrx1*$^{fl/fl}$ allele will be under control of an inducible fibroblast-specific *Cre* line (*Sm22-Cre*^{ERT}). Two different mouse models will be generated to analyze the role of *Prrx1* in CAFs during PDAC formation and progression. The first mouse model is the orthotopic implantation model, where tumor cells will be implanted orthotopically in the tail of pancreas in the *Sm22-Cre*^{ERT}*; Prrx1*$^{fl/fl}$ mouse model and tumors will be formed within two weeks. The second mouse model is the dual recombinase system (DRS). The DRS allows to drive pancreatic carcinogensis via the *Flp/Frt* system and manipulate *Prrx1* in CAFs in an inducible fashion via *Cre*^{ERT}*/LoxP* (*Pdx-Flp;FSF-Kras*^{G12D}*;p53*$^{frt/+}$*(KPF);Sm22-Cre*^{ERT}*; Prrx1*$^{fl/fl}$).

For both approaches histological analysis of the tumors as well as quantification for the ECM production will be performed. Furthermore, the frequency of metastases will be quantified and circulating tumor cells counted by FACS and survival curves generated to gain insights in the disease progression.

In addition, mouse derived primary fibroblasts and PSC will be generated for *in vitro* studies. The effect of *Prrx1* knockout on fibroblast functionality regarding ECM production, proliferation, migration, and plasticity will be assed.

Functional validation of the *in vivo* findings will be performed with the help of co-culture experiments *in vitro.* The same *in vitro* model will be used to decipher the role of *Prrx1* regarding chemotherapy resistance.

Through the combination of *in vivo* and *in vitro* experiments we will gain new insights in the *Prrx1* regulated network in fibroblasts in pancreatic cancer. With this dissertation we start our quest how does the plasticity of fibroblast influences the tumor burden and does the generated data have in respect of drug testing clinical relevance?

2 Materials

2.1 Technical equipment

Table 2.1 Technical equipment

Device	Supplier
AxioCam HRc	Carl Zeiss AG, Germany
AxioCam MRc	Carl Zeiss AG, Germany
Biometra Compact L/XL Agarose Gel Eletrophorsis	Analytik Jena AG, Germany
Centrifuge 5810R	Eppendorf AG, Germany
Centrifuge 5430R	Eppendorf AG, Germany
CO_2 incubator HERAcell 240	Thermo Fisher scientific, Inc. USA
Counting chamber; Neubauer improved, Brand®	Sigma-Aldrich Chemie GmbH, Germany
FACSAria™ III	BD Bioscience, USA
FACSAria™ Fusion	BD Bioscience, USA
Gel Doc™ XR + Gel Documentation System	Bio-Rad, California, USA
Glass ware, Schott Duran	Schott AG, Germany
Laminar flow HERAsafe	Thermo Fisher scientific, Inc., USA
Magnetic stirrer and hot plate; RCT basic Ikamag™	Sigma-Aldrich Chemie GmbH, Germany
Magnetic stirrer plate	Variomag®; USA
Microplate reader Multiskan® Ex	Thermo Fisher scientific, Inc., Waltham, MA, USA
Microscope Optech	Optech Microscope Services Limited; Oxfordshire, UK
Microscope Axio Imager. A1	Carl Zeiss AG, Germany
Microscope Axiovert 25	Carl Zeiss AG, Germany
Microscope Leica SP5	Leica Microsystems GmbH, Germany
Microwave	Siemens, München, Germany
Mini Centrifuge	Bio-Rad, California, USA
Mini Centrifuge PCR Stripes	Bio-Rad, California, USA
Multipipette Explorer	Eppendorf AG, Germany
Nanodrop	Thermo Fisher Scientific; Waltham, MA USA

Device	Supplier
pH Meter inoLab®	Xylem Analytics Germany Sales GmbH & Co. KG, Germany
Pipettes	Gilson Inc.; USA
Pipetboy Stripettor™	Corning Inc.; USA
Power Supplies; Power Pac Basic	Bio-Rad, USA
Multi-Flask Shaker + incubation chamber	Edmund Bühler GmbH; Germany
StepOnePlus System	Thermo Fisher Scientific, USA
Surgical instruments	Fine Science Tools GmbH, Germany
Thermocycler Mastercycler	Eppendorf AG, Germany
Thermocycler FlexCycler^2	Analytik Jena AG, Germany
Thermomixer compact	Eppendorf AG, Germany
Vortex-Genie 2	Scientific Industries, Inc. USA
Water bath	GFL Gesellschaft für Labortechnik GmbH; Germany

2.2 Chemicals, enzymes and kits

Table 2.2 Chemicals, enzymes and kits

Chemicals, enzymes and Kits	Supplier
1,4-Dithiothreitol (DTT)	Carl Roth GmbH& Co.KG, Germany
2-Log DNA Ladder (0.1-10.0 kb)	New England Biolabs GmbH, Germany
2-Mercaptoethanol, 98%	Sigma-Aldrich Chemie GmbH, Germany
2-Propanol	Carl Roth GmbH& Co.KG, Germany
3-(4,5-deimethylthiazol-2-yl)-2,5-diphenyl tetrazolium bromide (MTT)	Sigma-Aldrich Chemie GmbH
4-hydroxytamoxifen (4-OHT)	Sigma-Aldrich Chemie GmbH
Acetic acid	Carl Roth GmbH& Co.KG, Germany
Agarose	Biozym
ALLin™ Red Taq Mastermix	highQu GmbH, Kraichtal, Germany
Bovine serum albumin, lyophilized powder	Carl Roth GmbH& Co.KG, Germany
Calcium chloride	Carl Roth GmbH& Co.KG, Germany
Collagenase P	Roche GmbH, Germany
D (+) Saccharose	Carl Roth GmbH& Co.KG, Germany

Chemicals, enzymes and Kits	Supplier
Dexamethasone	Sigma-Aldrich Chemie GmbH, Germany
D-Glucose	Sigma-Aldrich Chemie GmbH, Germany
Dimethyl sulfoxide (DMSO, for MTT)	Carl Roth GmbH& Co.KG, Germany
Dnase	Roche GmbH, Germany
DNeasy Blood & Tissue Kits	QIAGEN GmbH, Germany
Ethanol	Carl Roth GmbH& Co.KG
Ethidium bromide	Carl Roth GmbH& Co.KG, Germany
Ethylenediaminetetraacetic acid (EDTA)	Sigma-Aldrich Chemie GmbH, Germany
Forene® isoflurane	Clinic pharmacy
Gelatin from cold-water fish skin	Sigma-Aldrich Chemie GmbH, Germany
Glucose	Sigma-Aldrich Chemie GmbH, Germany
Glycerol	Sigma-Aldrich Chemie GmbH, Germany
Glycine	Carl Roth GmbH& Co.KG, Germany
Hepes	Carl Roth GmbH& Co.KG, Germany
Histo-Clear™	Fisher Scientific GmbH
Histodenz (Nycodenz)	Sigma-Aldrich Chemie GmbH, Germany
Hydrochloride acid	Sigma-Aldrich Chemie GmbH, Germany
Magnesium chloride	Carl Roth GmbH& Co.KG, Germany
Magnesium sulfate	Sigma-Aldrich Chemie GmbH, Germany
Methanol	Sigma-Aldrich Chemie GmbH, Germany
Miglyol812	Caesar&Loretz GmbH, Germany
Murine HGF Quantikine ELISA Kit	R&D Systems®, Inc; USA
Murine TGF-β Quantikine ELISA Kit	R&D Systems®, Inc; USA
N,N-dimethyl formamide	Sigma-Aldrich Chemie GmbH, Germany
Nicotinamide	Sigma-Aldrich Chemie GmbH, Germany
Nonidet P40	Sigma-Aldrich Chemie GmbH, Germany
Potassium chloride	Carl Roth GmbH& Co.KG, Germany
Potassium phosphate monobasic	Carl Roth GmbH& Co.KG, Germany
Protease Typ14	Sigma-Aldrich Chemie GmbH, Germany
Proteinase K	Sigma-Aldrich Chemie GmbH, Germany
RNeasy Mini Kit	QIAGEN GmbH, Germany
SensiFast™ cDNA Synthesis Kit	Bioline, Meridian Life Science, Inc., USA
SensiFast™ SYBR® Hi-ROX Kit	Bioline, Meridian Life Science, Inc., USA
Sircol™ Soluble Collagen Assay	Biocolor Ltd., UK

Chemicals, enzymes and Kits	Supplier
Sodium bicarbonate	Sigma-Aldrich Chemie GmbH, Germany
Sodium chloride	Carl Roth GmbH& Co.KG, Germany
Sodium hydroxide solution	Carl Roth GmbH& Co.KG, Germany
sodium phosphate monobasic	Sigma-Aldrich Chemie GmbH, Germany
Tamoxifen	Sigma-Aldrich Chemie GmbH, Germany
Tissue-Tek® O.C.T. compound	VWR International GmbH, Germany
Tris hydrochloride	Sigma-Aldrich Chemie GmbH, Germany
Triton X-100	Sigma-Aldrich Chemie GmbH, Germany
Tween 20	Carl Roth GmbH& Co.KG, Germany

2.3 Antibodies

Table 2.3 Antibodies and used dilution in the experiments

Primary Antibodies	Supplier	Dilution
anti-CD31 antibody	Abcam plc, Germany	1:100
anti-Cytokeratin 19 antibody	Abcam plc, Germany	1:200
anti-Fibroblast activation protein, alpha antibody	Abcam plc, Germany	1:100
anti-Fibronectin antibody	Abcam plc, Germany	1:250
anti-GFAP antibody	Abcam plc, Germany	1:200
anti-GFP antibody	Abcam plc, Germany	1:500
anti-PRRX1 antibody	Merck KGaA, Germany	1:200
anti−smooth muscle actin antibody, mouse monoclonoal	Merck KGaA, Germany	1:500
CD140a (PDGFRA) Monoclonal antibody	eBioscience™; Thermo Fisher Scientific Inc; USA	1:100
CD326 (EpCAM) Monoclonal antibody, APC	eBioscience™; Thermo Fisher Scientific Inc; USA	1:200
Goat anti-type I collagen	Southern Biotech, USA	1:200
mouse HGF antibody	R&D Systems, Inc. USA	1:200
mouse SPARC antibody	R&D Systems, Inc. USA	1:50
Vimentin (D21H3) XP® Rabbit mAb	Cell Signaling Technology, Inc. USA	1:200
Secondary Antibodies	Supplier	Dilution
Alexa Fluor™ 594 Phalloidin	Thermo Fisher Scientific Inc; USA	1:40

Primary Antibodies	Supplier	Dilution
Alexa Fluor™ donkey anti-goat 647	Thermo Fisher Scientific Inc; USA	1:500
Alexa Fluor™ donkey anti-mouse 488	Thermo Fisher Scientific Inc; USA	1:500
Alexa Fluor™ donkey anti-mouse 594	Thermo Fisher Scientific Inc; USA	1:500
Alexa Fluor™ donkey anti-rabbit 488	Thermo Fisher Scientific Inc; USA	1:500
Alexa Fluor™ donkey anti-rabbit 594	Thermo Fisher Scientific Inc; USA	1:500
Alexa Fluor™ goat anti-chicken 488	Thermo Fisher Scientific Inc; USA	1:500
Alexa Fluor™ goat anti-mouse 647	Thermo Fisher Scientific Inc; USA	1:500
Alexa Fluor™ goat anti-rat 488	Thermo Fisher Scientific Inc; USA	1:500
Biotinylated anti-goat IgG (H+L)	Vector Laboratories, Inc., USA	1:500
Biotinylated anti-mouse IgG (H+L)	Vector Laboratories, Inc., USA	1:500
Biotinylated anti-rabbit IgG (H+L)	Vector Laboratories, Inc., USA	1:500
Biotinylated anti-rat IgG (H+L)	Vector Laboratories, Inc., USA	1:500
DAPI (4′,6-Diamidine-2′-phenylindole dihydrochloride)	Merck KGaA, Germany	1:1000

2.4 Disposables

Table 2.4 Disposables

Disposables	Source
4 well Nunc™ Lab-Tek™ Chamber Slide System	Thermo Fisher Scientific Inc., USA
Cell culture plastics	Greiner Bio-One GmbH, Germany; TPP, Techno Plastic, Products AG, Switzerland; Sarstedt AG & Co., Germany; Corning Inc., USA; Thermo Fisher Scientific Inc., USA
Cell scrapers	TPP Techno Plastic, Products AG, Switzerland
Combitips BioPur®	Eppendorf AG, Germany
Conical tubes, 15 mL and 50 mL	Sarstedt AG & Co., Germany
Cover slips	Gerhard Menzel, Glasverarbeitungswerk GmbH & Co. KG, Germany
Disposable scalpels	Feather Safety Razor Co., Ltd., Japan
Embedding cassettes	AMP Stensved, Denmark
Ethilon II	CLS Medizintechnik, Germany
Filtropur S 0.2 and S 0.45	Sarstedt AG & Co., Germany

Disposables	Source
Glass slides Superfrost® Plus	Gerhard Menzel, Glasverarbeitungswerk GmbH & Co. KG, Germany
Para film®	Bemis Company Inc., USA
Pasteur pipettes	Hirschmann Laborgeräte GmbH & Co. KG, Germany
PCR reaction tubes	Sarstedt AG & Co., Germany
Petri dishes	Sarstedt AG & Co., Germany
Pipette tips	Biozym Scientific GmbH, Germany
Reaction tubes, 0.5 mL, 1.5 mL and 2.0 mL	Eppendorf AG, Germany
Safe seal filter pipette tips	Biozym Scientific GmbH, Germany
Safe-lock reaction tubes BioPur®	Eppendorf AG, Germany
Serological pipettes	Sarstedt AG & Co., Germany
Single use needles Omnican ® 100	B. Braun Melsungen AG, Germany
Single use needles Sterican® 27 gauge	B. Braun Melsungen AG, Germany
Tissue-Tek® Cryomold®	VWR International GmbH, Germany,
Trans-well cell culture inserts (6 well and 96 well format, 0.45 µm pore size)	Corning Inc., USA
Wound clips	MEDICON AG, Germany

2.5 Buffer and solutions

Table 2.5 Composition list for buffer and solutions used in the methods part

Buffer/Solutions	Component
10x Gitschier's buffer	670 mM Tris, pH 8.8 166 mM (NH4)2SO4 67 mM MgCl2
50 x Tris acetate EDTA (TAE) buffer, pH 8.5	2 M Tris 50 mM EDTA 5.71 % Acetic acid
BSA Solution for PSC Isolation	0.3 % BSA in GBSS+NaCl
Enzyme Solution for PSC Isolation	1.3 mg/mL 1 mg/mL Protease

Buffer/Solutions	Component
	10 µg/mL Dnase in GBSS + NaCl
FACS Buffer	in DPBS 1 % BSA 1 mM EDTA
Grey's Balanced Salt Solution (GBSS)	g/500mL 0.105 g $MgCl_2$ $6H_2O$ 0.0171 g $MgSO_4$ anhydrous 0.185 g KCl 0.15 g KH_2PO_4 anhydrous 0.0598 g Na_2HPO_4 anhydrous 1.135 g $NaHCO_3$ 0.5 g Glucose 0.1126 g $CaCl_2$
Grey's Balanced Salt Solution (GBSS) + NaCl	g/500mL 0.105 g $MgCl_2$ $6H_2O$ 0.0171 g $MgSO_4$ anhydrous 0.185 g KCl 0.15 g KH_2PO_4 anhydrous 0.0598 g Na_2HPO_4 anhydrous 1.135 g $NaHCO_3$ 0.5 g Glucose 3.5 g NaCl 0.1126 g $CaCl_2$
Nycodenz Solution for PSC Isolation	28,7 % Nycodenz in GBSS
PCR lysis buffer (Soriano)	0.5 % Triton X-100 1 % 2-Mercaptoethanol 1 x Gitschier's buffer 400 µg/mL Proteinase K

2.6 Cell culture

Table 2.6 Reagents used in cell culture

Reagents	Supplier
10x Minimum essential medium, without glutamine (MEM, 10×)	Thermo Fisher Scientific; USA
(Z)-4-Hydroxytamoxifen	Sigma-Aldrich Chemie GmbH, Germany
Bovine collagen solution type I, Nutragen	Advanced BioMatrix, USA
Bovine pituitary extract (BPE)	Thermo Fisher Scientific, USA
Collagen rait tail type I	BD Bioscience, USA
Collagenase P	Roche GmbH, Germany
Collagenase type I	Worthington, USA
Collagenase type V	Sigma-Aldrich Chemie GmbH, Germany
Corning® Matrigel® Growth Factor Reduced (GFR) Basement Membrane Matrix, phenol red-free	Corning Inc., USA
Dimethyl sulfoxide (DMSO for cell culture)	Sigma-Aldrich Chemie GmbH, Germany
Dnase	Roche GmbH, Germany
Dulbecco's modified medium (D-MEM) with L-glutamin	Thermo Fisher Scientific, USA
Dulbecco's Modified Eagle Medium low glucose, low pyruvate	Thermo Fisher Scientific, USA
Dulbecco's Modified Eagle Medium/Nutrient Mixture F-12 (DMEM/F-12)	Thermo Fisher Scientific, USA
Dulbecco's phosphate-buffered saline (DPBS), no calcium, no magnesium	Thermo Fisher Scientific, USA
Epidermal growth factor	BD Bioscience, USA
Fetal Bovine Serum, qualified, E.U.-approved, South America origin	Thermo Fisher Scientific, USA
Fungizone® antimycotic	Thermo Fisher Scientific, USA
Gemcitabine	Clinic pharmacy
Hepes, 1M, pH7.6	Sigma-Aldrich Chemie GmbH, Germany

Reagents	Supplier
ITS$^+$ (insulin/human transferring/selenous acid and linoleic acid) premix	BD Bioscience, USA
L-Glutamine	Thermo Fisher Scientific, USA
Nu-Serum IV	BD Bioscience, USA
Penicillin-Streptomycin (10,000 U/mL)	Thermo Fisher Scientific, USA
Protease Typ14	Sigma-Aldrich Chemie GmbH, Germany
Recombinant mouse HGF Protein	R&D Systems, USA
Soybean trypsin inhibitor (STI)	Thermo Fisher Scientific, USA
Trypsin-EDTA (0.5%), no phenol red	Thermo Fisher Scientific, USA

Table 2.7 Composition of different cell culture media and cell culture matrix

Medium/ Matrix	Component
Collagen for culturing cells in 2D	2.31 mg/mL Collagen I 10% 10xDPBS 1,65% 1N NaOH Adjust volume with ddH_2O
4-Hydroxytamoxifen [stock: 10 mg/mL]	10 mg 4-Hydroxytamoxifen 1 mL Methanol
Collagen for culturing cells in 3D	200 mM L-Glutamine 7.5% $NaHCO_3$ 1:10.2 ratio MEM,10x 6 mg/mL Nutragen (bovine collagen I) 1:51 ratio 1M Hepes, pH 7.6 Adjust volume with ddH_2O
Freezing media	90% FBS 10% DMSO
PAF media	1:1 D-MEM low glucose, low pyruvate: DMEM F12 20% FBS 1% Penicillin-Streptomycin
PDC full media	In DMEM F12 5% Nu-Serum IV 1% P/S 25µg/mL BPE 2.5 mL ITS^+ premix 20 ng/mL EGF 100 ng/mL Cholera toxin 5 nM 3,3,5-Triiodo-L-thyronine 1 µM Dexamethasone 5 mg/mL Glucose 1.22 mg/mL Nicotinamide
Tumor cell media	D-MEM 10% FBS 1% Penicillin-Streptomycin

2.7 Histology

Table 2.8 Reagents and kits used for histological analysis

Reagents/Kits	Supplier
Acetic acid (glacial)	Merck KGaA, Germany
Alcian Blue 8 GX	Sigma-Aldrich Chemie GmbH, Germany
Antigen unmasking solution, citric acid based	Vector Laboratories, Inc., USA
Avidin/biotin blocking Kit	Vector Laboratories, Inc., USA
DAB peroxidase substrate kit	Vector Laboratories, Inc., USA
Direct Red 80	Sigma-Aldrich Chemie GmbH, Germany
Eosin	Waldeck GmbH & Co KG, Germany
Hematoxylin	Merck KGaA, Germany
Hydrogen peroxidase 30%	Merck KGaA, Germany
Pertex mounting medium	Medite GmbH, Germany
Picric acid	Sigma-Aldrich Chemie GmbH, Germany
StartingBlock™ (PBS) Blocking Buffer	Thermo Fisher Scientific Inc, USA
Roti Histofix 4%	Carl Roth GmbH & Co. KG, Germany
Roti Histol	Carl Roth GmbH & Co. KG, Germany
Toluidine Blue O	Sigma-Aldrich Chemie GmbH, Germany
Vectashield mounting medium	Vector Laboratories, Inc., USA
Vectastain elite ABC kit	Vector Laboratories, Inc., USA

2.8 Primers

All primers were generated by Eurofins MWG (Ebersberg) and dissolved in double-distilled water to a concentration of 10µM.

Table 2.9 Primer for gene expression analysis

qPCR Primer	Sequence
CDA	5’-AAGGCCATCTCCGAAGGGTA-3’
	5’-CAGTCGGTGCCAAACTCTCT-3’
ENT1	5’-ATGGCAAGGGCTCAATGG-3’
	5’-TGGAGTAAGCGGGCATCAGT-3’
Etv1	5’-GAAGGGTCCCAGGCAGTTCT-3’
	5’-AACTTCTCCGGGACCACACA-3’
Fibronectin (FN1)	5’-ATCACAGTAGTTGCGGCAGGAGAA-3’
	5’-TGTCATAGTCAATGCCAGGCTCCA-3’

qPCR Primer	Sequence
H-Actin	5’-GCA CCA CAC CTT CTA CAA TG-3’
	5’-TGC TTG CTG ATC CAC ATC TG-3’
HGF	5’-TTGGGATTCGCAGTACCCTCACAA-3’
	5’-TAGCCAACTCGGATGTTTGGGTCA-3’
hPrrx1a	5’-AATCCTACTCAGGAGACGTGACTG-3’
	5’-AATAAGTAGCCATGGCGCTGTACG-3’
hPrrx1b	5’-CATCGTACCTCGTCCTGCTC-3’
	5’-GCCCCTCGTGTAAACAACATC-3’
Nt5c1A	5’-GGGCCGGATAGAATCCGAGT-3’
	5’-TCGATGGCTTCTCGCACTTT-3’
Nt5c3	5’-GCTTGTCCGGTTACCTTCAGA-3’
	5’-ACAGGGATACCGTGCTGTTG-3’
Periostin	5′-GGGGTTGTCACTGTGAACTG-3′
	5′-CGGCTGCTCTAAATGATGAA-3′
Prrx1a	5’-ACAGCCTCTCCGTACAGCGC-3’
	5’-AGTCTCAGGTTGGCAATGCT-3’
Prrx1b	5’-CATCGTACCTCGTCCTGCTC-3’
	5’-GCCCCTCGTGTAAACAACAT-3’
Slug	5’-CCACACATTGCCTTGTGTCTGCAA-3’
	5’-TGTGCCCTCAGGTTTGATCTGTCT-3’
Tn-C	5′-TCAAGGAAGTCATTGTGGGGC-3′
	5′-CAGGAGTCCAATTGTTGTGAAG-3′
Twist	5’-GTCCGCAGTCTTACGAGGAG-3’
	5’-TGGAGGACCTGGTAGAGGAA-3’
Vimentin	5’-AAGCACCCTGCAGTCATTCAGA-3’
	5’-GCAAGGATTCCACTTTCCGTTC-3’
Zeb1	5’-TGAGCACACAGGTAAGAGGCC-3’
	5’-GGCTTTTCCCCAGAGTGCA-3’
β-Actin	5’-GTC GAG TCG CGT CCA CC-3’
	5’-GTC ATC CAT GGC GAA CTG GT-3’

Table 2.10 Genotyping primers

PCR name	Primer	Sequence (5‘-3‘)
Pdx-Flp	Pdx5ut-scUP	AGAGAGAAAATTGAAACAAGTGCAGGT
	Flpopt-scLP	CGTTGTAAGGGATGATGGTGAACT
	Gabra-UP	AACACACACTGGAGGACTGGCTAGG
	Gabra-LP	CAATGGTAGGCTCACTCTGGGAGATGATA
FSF-Kras^{G12D}	Kras-WT-UP1	CACCAGCTTCGGCTTCCTATT
	Kras-URP-LP1	AGCTAATGGCTCTCAAAGGAATGTA
	R26-Tva-SA-mut	GCGAAGAGTTTGTCCTCAACC
p53-frt	p53-ftr1	CAAGAGAACTGTGCCTAAGAG
	p53-frt2	CTTTCTAACAGCAAAGGCAAGC
Sm22-Cre^{ERT}	SER-WT-UP	CTCAGAGTGGAAGGCCTGCTT
	SER-WT-LP	CACACCATTCTTCAGCCACA
	SER-mut-LP	GGCGATCCCTGAACATGTCC
R26^{mTmG}	CAG-sc-LP	GTACTTGGCATATGATACACTTGATGTAC
	R26-Tva-GT-UP	AAAGTCGCTCTGAGTTGTTAT
	R26-Tva-GT-WT-LP	GGAGCGGGAGAAATGGATATG
Prrx1	ANIL4	ACGTCCTTAGCAAAGTACGACAGTC
	SC1	TGTTGCTCTGAATCAGTCACTGCC

Table 2.11 Recombination PCR primers

Recombination PCR	Primer name	Sequence
FSF-Kras recombined	FSF-Kras recombined F	5’-AGAATACCGCAAGGGTAGGTGTTG-3’
	FSF-Kras recombined R	5’-TGTAGCAGCTAATGGCTCTCAAA-3’
p53frt recombined	p53-frt forward	5’-CAAGAGAACTGTGCCTAAGAG-3’
	p53-frt recombined R	5’-CTTTCAACAGCAAAGGCAAGC-3’

3 Methods

3.1 Cell culture

3.1.1 Isolation, cultivation and cryopreservation of pancreatic ductal cells

Pancreatic ductal cells (PDC) were isolated by mechanical shredding of the pancreas with a sterile scalpel or scissor and washed with ice cold PBS. Afterwards, the tissue suspension was digested through collagenase V (1mg/mL) followed by subsequent trypsin digestion. The isolated cells were resuspended in PDC full media and plated on collagen plates.

Expanding of ductal cells followed the same protocol. The cells grown on the collagen layer were digested by a collagenase I (1.5mg/mL) to remove the collagen and, afterwards, were digested by trypsin to retain a single cell suspension. The digestion was stopped by adding soybean trypsin inhibitor. The cells were centrifuged and resuspended in an appropriate volume of PDC full media for expansion and plated on new collagen plates. Otherwise, the cells could be frozen down after the last centrifugation step by resuspending the cells in 5% DMSO in PDC full media and storing the cells short term by -80°C and long term in liquid nitrogen.

Detailed information for isolation and cultivation of ductal cells is provided in the publication of (Reichert et al., 2015).

3.1.2 Isolation, cultivation and cryopreservation of tumor cells

The isolation protocol for the tumor cells is similar to the ductal cell isolation protocol: mechanical shredding of the pancreas, collagenase and trypsin digestion. Afterwards, the cells were cultivated in DMEM with 10% FBS and 1% P/S.

The tumor cells could be easily expanded by removing the media, washing the cells with PBS and adding trypsin on cells. After the cells were detached from the plate, the cells were washed with PBS, transferred to a centrifugation tube and centrifuged. Afterwards the cells could be re-cultured on plastic plates or frozen down with 10% DMSO in FBS.

3.1.3 Isolation, cultivation and cryoconservation of quiescent pancreatic stellate cells and fibroblasts

Quiescent pancreatic stellate cells differ from activated fibroblasts through the presence lipid droplets together with expression of glial fibrillary acidic protein (GFAP), desmin, nestin (inter-

mediate filament proteins) and vimentin (Omary et al., 2007). Through the differences in density of quiescent pancreatic stellate cells and tumor cells or fibroblasts, quiescent PSC can be isolated through density gradient centrifugation as highlighted in Figure 3.1.

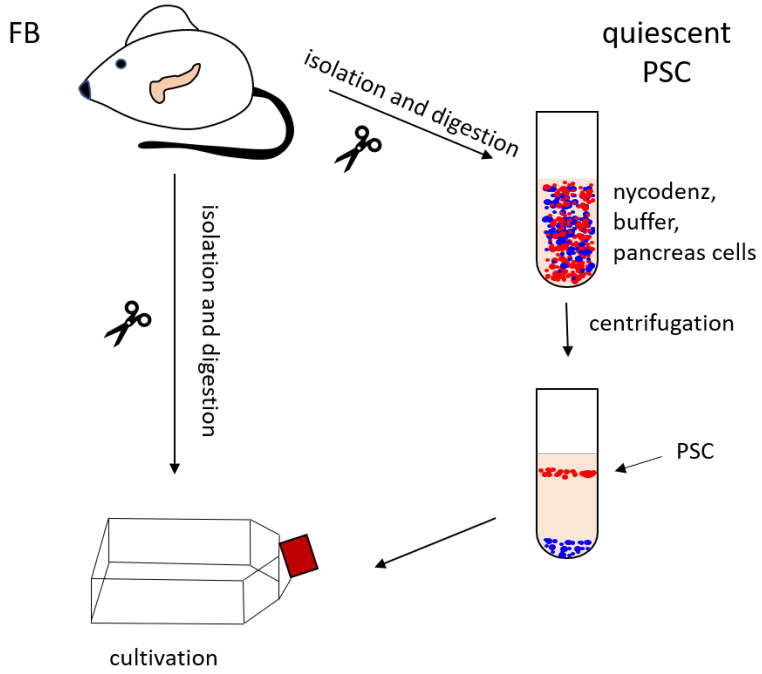

Figure 3.1 Schematic illustration of isolation of fibroblasts and quiescent pancreatic stellate cells

3.1.3.1 Quiescent pancreatic stellate cells

The freshly isolated pancreas was injected with GBSS/0.3% BSA/1mg/mL collagenase P solution and, subsequently, cut into small pieces. The tissue suspension was incubated at 37°C for a time period of approximately 15min – at the same time the suspension was stirred. Afterwards, the suspension was centrifuged (5min, 4°C, 300xg); the pellet was resuspended in GBSS/0.3% BSA/0.5% trypsin solution and incubated for 5min at 37°C. Subsequently, the suspension was filtered through a 100 µM nylon mesh and centrifuged. The pellet was resuspended in 4.75mL GBSS/0.3% BSA and 4mL of 28.7% Nycodenz solution in Gey's solution without NaCl was added. On top of the solution, another layer of 3mL GBSS/0.3% BSA was added. To build up a gradient, the solution was centrifuged for 20min, 1400xg, 4°C without break. The white layer above the interface was collected and resuspend in GBSS/0.3% BSA solution. After centrifugation, the cells were resuspended in PSC medium (20% FBS, 1% P/S in 50% DMEM-F12 and DMEM) and plated on plastic.

Detailed Information for isolation, cultivation and cryoconservation is provided in the publication by (Vonlaufen et al., 2010).

The PSC expansion and cryopreservation were performed identically to the ones of the tumor cells (section 3.1.2).

3.1.3.2 Fibroblasts

Fibroblasts were generated by complete digestion of the isolated pancreas via collagenase digestion by 37°C for approximately 20min under stirring. Subsequently, the suspension was centrifuged, and the pellet was resuspended in trypsin for an additional digestion step. Afterwards, the cells could be resuspended in PSC medium and cultured on plastic plates as illustrated in Figure 3.1.

The isolation protocol of the fibroblasts includes all mesenchymal cells, also tumor cells that undergo EMT. Therefore, fibroblast identity can be confirmed on the DNA level by Sanger sequencing to verify the wildtype status of Kras at codon 12 (forward primer 5'-CTGGTGGAGTATTTGATAGTG-3', reverse primer 5'-CTGTATCAAAGAATGGTCCTG-3') (Öhlund et al., 2017).

3.1.4 Isolation of EpCAM positive cells of the blood stream

The epithelial cell adhesion molecule (EpCAM) is exclusively expressed on epithelial and various cancer cells (Spizzo et al., 2011). The cells were isolated by draining blood from the heart of orthotopically transplanted mice (ca. 300-1000µL per mice) with a G27 needle (#2050864, B. Braun). The blood was collected within an EDTA tube. After washing the blood with DPBS and centrifugation (300xg, 5min, 4°C) the cells were frozen down in FBS with 10% DMSO or used directly for FACS (see section 3.1.8).

3.1.5 In *in vitro* recombination

Isolated *Sm22-Cre^{ERT}, R26^{mTmG}* or *Sm22-Cre^{ERT}, Prrx1$^{fl/fl}$, R26^{mTmG}* fibroblasts can be recombined *in vitro* if the cells are not recombined *in vivo*. For in *in vitro* recombination, fibroblasts were treated with 4-hydroxytamoxifen (final concentration of 500nM) three times every second day. Afterwards, the cells were cultured for another two days without tamoxifen before the cells were used for further experiments like drug screens, co-culture experiments or migration assays. The recombination efficiency was determined via FACS analysis (GFP positive cells), Gel electrophoresis (forward primer 5'-TGTTGCTCTGAATCAGTCACTGCC-3' and reverse primer 5'-ATTTCACTGCAGGTAGACGTTGGG -3', one band after successful recombination) or reverse transcriptase polymerase chain reaction (RT-PCR).

3.1.6 3D culture and 3D co-culture of ductal cells and fibroblasts

3.1.6.1 3D culture of PSC

Primary PSC were detached from the plate by trypsin digestion, counted (5,000 cells/50µL Matrigel) and resuspended in 50µL Matrigel and seeded into 4 well chamber slides. After solidification of the Matrigel, 500µL media was added on top of the cells. The cells were cultured 3-7 days. Further Information is provided in (Öhlund et al., 2017).

3.1.6.2 3D co-culture

3D pancreatic cell culture is performed as described previously (Reichert et al., 2013b; Reichert et al., 2013a). Using this method for co-culturing the cells, the primary fibroblasts were seeded on the bottom of the 4 well chamber slide before the collagen layer with the tumor cells was poured above. Tumor cells and fibroblasts are seeded in equal amounts.

3.1.6.3 Immunofluorescence staining

After culturing the cells, the cells were fixed with a 4% PFA solution for 30 min at RT and washed three times with PBS+. To facilitate the penetration of the antibody through the membrane and the cells, a permeabilization step at RT while rocking with the following solution was necessary: 0.35g fish skin gelatin and 250µl Triton X-100 diluted in 50mL of PBS with Ca2+ and Mg2+ for 30min. The primary antibodies were diluted in permeabilization solution and incubated overnight at 4°C. After washing with PBS+ three times for 5min, the secondary antibody was diluted in permeabilization solution and incubated either overnight at 4°C or for 3h at RT in the dark. Subsequent washing steps with permeabilization solution and PBS were followed before the cells are mounted with a coverslip and imaged on a confocal microscope. Detailed information is provided in (Reichert et al., 2013b).

3.1.7 Immunofluorescent staining of 2D culture

The protocol is similar to the one used for the 3D culture (see section 3.1.6). To facilitate the staining, the cells were grown on cover slips either coated with 3% poly-L-Lysin or with collagen I (diluted 1:10 in 30% ethanol) in a 6 well plate. Between 25,000 and 100,000 cells were seeded in a well and were cultured for 2-3 days. After the desired confluency was achieved, the media was removed, the cells washed 3 times with DPBS and fixed with 4% PFA for 10min. Subsequently, the cells were washed again and permeabilized for 10min at RT, before adding the primary antibody diluted in permeabilization solution for overnight incubation by 4°C. Afterwards, the cells were washed three times and the secondary antibody diluted in permeabilization solution was added to the cells. After overnight incubation at 4°C or for 3h at RT in the

dark, the cells were washed again and mounted with mounting media before they were analyzed by fluorescence microscopy.

3.1.8 FACS

Either freshly isolated cells from the pancreas or blood or thawed cells were used for FACS experiments. After preparation of a single cell suspension by filtering the cells through a 30µm cell strainer, the cells were washed three times with PBS and can be stained with EpCAM specific antibody (#17-5791-82); DAPI (#268298-10MG) (live dead staining) in FACS buffer (1x DPBS, 1% BSA, 1mM EDTA) for 30min at 4°C. Afterwards the cells were washed 3 times with FACS buffer and filtered through 30µM syringe filcons (#340626) and stored on ice until they were analyzed with the ARIA III fusion. Analysis was performed with the help of the FlowJo software (Becton, Dickinson and Company, 2018).

3.1.9 3D migration assay

The 3D migration assay was performed in a cooperation with Dr. Steffen Teller (Department of Surgery, MRI/TUM). To determine the forward migration index and the Euclidian distance of the fibroblasts, for each cell line (fibroblasts and tumor cells) 25,000 cells were resuspended in 25 µL Matrigel. The tumor cells resuspended in Matrigel were placed in the middle of the small petri dish (35mm x 15mm). The two fibroblast populations were placed in 6mm distance to tumor cells on the right-hand and on the left-hand side. As a control, an empty Matrigel drop (without cells) is placed above the tumor cells. The Matrigel is dried at 37°C for 10min in an incubator. Afterwards, the Matrigel drops were connected with a Matrigel bridge to each other. A Matrigel bridge is built by carefully pipetting of 3µL Matrigel in between the drops. After solidification of the Matrigel (10min, 37°C incubation), 2mL of the PSC medium were added. A picture was taken from the same area by the microscope every 30min for 48h. Detailed information according to the protocol is provided in (Ceyhan et al., 2008).

The euclidian distance and the forward migration index (FMI) were determined using the ImageJ software, as described in (National Institutes of Health, 2018; Ceyhan et al., 2008) For this purpose, the plugins (Cordelieres, 2004) and (Trapp and Horn, 2006) for FlowJo were used. Table 3.1 indicates the parameters used throughout the analysis with ImageJ. We identified that at least 30 cells must be tracked to obtain processable results. A detailed protocol to reproduce our results is provided in the appendix of this dissertation in section 9.2.

Table 3.1 ImageJ parameters used throughout 3D migration assay

Parameter	Value
Sequence format	TIF, scale image 70%
Time interval	30min
Duration	48h
X/y calibration	0.645 µm
Z calibration	0.3 µm
Search square size for centering	1.025 px
Dot size	6
Line width	3
Font size	12

3.1.10 Co-culture in a transwell approach

For co-cultures in a 6 well plate, tumor cells were seeded in a ratio of between 10 000 to 20 000 cells in the bottom layer, the PAFs/CAFs were seeded in an equal cell number on top of the trans-well membrane (0.45 µm pore size). The cells were cultured for 3 days in 50% DMEM F12 and 50% DMEM low glucose; 2% FBS and 1% P/S. Afterwards, the supernatant was filtered through a 0.45 µM filter and stored at -80°C for further analysis, e.g. ELISA. Additionally, the RNA was harvested from cells and used for gene expression analysis.

Additionally, the co-culture experiments were also used to examine the influence of Gemcitabine (600nM) or to perform rescue experiments with recombinant HGF (10ng/mL).

3.1.11 Drug testing and viability assay

Drug testing, viability assay and cell growth were performed in a 96 well format using either a 96 well plate or a 96 trans well plate for co-cultures. 1000 cells were seeded per well, for co-culture experiments 1000 cells were seeded in the bottom as well as in the top layer (trans-well membrane, 0.45µm pore size). The cells were cultured in 50% DMEM F12 and 50% DMEM low glucose; 10% FBS and 1% P/S for approximately 12 to 16h, before Gemcitabine was added to the cells (in a range of 100 to 1,000 nM). The MTT reagent was added after either 0h, 24h, 48h, 72h or 96h to each plate and the absorbance was measured 4h after adding the MTT reagent (Sigma # M5655). The MTT assay was performed according to the manufacturer's protocol.

3.2 Mouse experiments

The animal procedures have been approved by the Regierung von Oberbayern and are listed as follows: 55.2-1-54-2532-1-2017 “Tumor-Stroma Interaktion via Prrx1 im duktalen Adenokarzinoms des Pankreas“ and 55.2-1-54-2532.0-54-2016 “Übungsprojekt für MD/PhD Studenten und naturwissenschaftlichen Doktoranden (Ausbildung in gastrointestinalen Tumormodellen der Maus)“.

3.2.1 Mouse strains and breeding

The inducible dual-recombination *Flp/frt*; *Cre^{ERT}/loxP* system is used for analysis fibroblasts during PDAC formation and progression (Feil et al., 1996; Schönhuber et al., 2014). The *Pdx1-Flp* directs the oncogenic *Kras$^{G12D/+}$* expression as well as the loss of the *p53* allele directly to the pancreas. Using the tamoxifen inducible *Sm22-Cre^{ERT}* allows to disrupt the *Prrx1* gene flanked by two *loxP* sites time specifically in fibroblasts.

All animals were on a mixed *C57BL/6* genetic background. In the following, all mouse lines used for the experiments in the context of this dissertation are explained in detail.

Pdx1-Flp (Schönhuber et al., 2014). This transgenic mouse line was generated by Prof. Dr. Saur (Klinikum rechts der Isar, Technical University of Munich). The *Flp* recombinase is expressed under the control of the *Pdx1* promoter, which results in expression in pancreatic progenitor cells and in adult pancreatic islets.

FSF-Kras^{G12D} (Schönhuber et al., 2014). This knock-in mouse line was generated by Prof. Dr. Saur (Klinikum rechts der Isar, Technical University of Munich). The expression of the oncogenic *Kras^{G12D}* is blocked by a FSF cassette. The STOP cassette can be removed by *Flp* recombination and the oncogenic *Kras* can be expressed.

p53^{frt} (Lee et al., 2012). The exons 2 to 6 of the *p53* gene are flanked by *frt*-sites. These exons encode the DNA binding domain of the *p53* protein, which is necessary for *p53*-dependent tumor suppression. Through *Flp* activation, *p53* can be inactivated by excision of these exons.

R26^{mTmG} (Muzumdar et al., 2007). This knock-in mouse line was generated by introducing a loxP flanked tandem dimer Tomato and enhanced green fluorescent protein into the first intron of the Rosa26 locus. The *Cre*-mediated excision of the loxP flanked tdTomato cassette allows the expression of eGFP.

Sm22-Cre^{ERT} (Kühbandner et al., 2000): The *SM22-Cre^{ERT}* mouse is a transgenic mouse line expressing a tamoxifen-activatable *Cre* recombinase. The knock-in of the *Cre^{ERT}* construct was introduced in the second exon of the SM22 Locus. The *Cre^{ERT}* construct is under the control

of the Sm22 promoter, which is specific for vascular and visceral smooth muscle cells as well as fibroblasts.

***Prrx1fl/fl*:** This transgene mouse line *Prrx1tm1MR* (*Prrx1 F*; conditional floxed Prrx1 knock-out mouse line): was generated in Dr. Reichert's laboratories (Klinikum rechts der Isar, Technical University of Munich). A conditional knock-out allele was introduced by introducing two loxP sites into exon 2 of the *Prrx1* gene. Through *Cre*-mediated activation, *Prrx1* can be inactivated by excision of this exon.

3.2.2 Ear marks

The mice were weaned and marked at an age of 3 to 4 weeks after birth. For distinguishing the mice from each other, each mouse received an explicit ear marking, which represents the respective mouse number. The tissue coming from the ear marks is used for DNA isolation and PCR genotyping.

3.2.3 Tamoxifen treatment

To activate the inducible *Sm22-Cre^{ERT}*, the mice were treated with Tamoxifen (concentration 5mg/30g mice) solved in neutral Oil Miglyol812 at the age of 8 to 10 weeks. The tamoxifen was injected intraperitoneally (i.p.) into the mice three times every second day.

3.2.4 Orthotopic implantation of ductal adenocarcinoma cells into the pancreas

Sm22-Cre^{ERT2}/Sm22-Cre^{ERT2}; Prrx1$^{fl/fl}$ mice (± Tamoxifen) within an age of 12 to 16 weeks were used for orthotopic implantation. Anesthesia of the mice was performed with MMF (Medetomidin, Midazolam, Fentanyl with a mixing ratio 1:5:0.05 mg/mL). Adequate anesthesia was determined by loss of limb reaction. The hair of the animals was removed before opening the peritoneal cavity. Afterwards, the spleen was located and exteriorized onto a sterile field surrounding the incision site. 500,000 primary pancreatic tumor cells (resuspended in PBS with 10% Matrigel) were injected into the tail of the pancreas via a 1mL insulin syringe. A successful implantation could be visualized by the appearance of a liquid bubble in the pancreas. Thereafter, the pancreas and spleen were carefully replaced back into the cavity and the incision was closed. The anesthesia was antagonized by Atipamezol; Flumazenil and Naloxon (mixing ratio 5:0.1:0.4). Buprenorphine and Metacam were provided for analgesia. If a leakage was suspected during implantation, the respective mouse was excluded from the studies.

3.2.5 Tissue dissection

The mice were euthanized with isoflurane or MMF as well as through cervical dislocation. Afterwards, they were fixed, disinfected with 70% ethanol and the abdomen was opened. 2mm pieces of the pancreatic tissue were snap frozen and stored at -80°C for later analysis (RNA or protein). Additionally, blood was taken from the heart (300-1000µL) for serum extraction or isolation of circulating tumor cells. Afterwards, measurements of the pancreas/pancreatic tumor were taken (size of the tumor). All necessary organs (pancreas and spleen, intestine, liver, heart and lung) were fixed overnight in 4% PFA for histological analysis. Samples of cryosections were only fixed for 1.5 to 2h depending on tissue size for further histological analysis.

3.2.6 Serum collection

After collecting the blood from the mice in a 1.5mL reaction tube, the blood was left at RT for 30min for clotting. After centrifugation (4°C, 2,000xg; 10min), the supernatant (serum) could be aliquoted and stored at -80°C until usage. The serum is mainly used for ELISA.

3.3 Molecular biology

3.3.1 Reverse transcriptase polymerase chain reaction (RT-PCR)

RNA was isolated using RNeasy Mini Kit (QIAGEN #74106). 1µg of RNA was transcribed into cDNA (SensiFast™ cDNA Synthesis Kit) and assayed utilizing quantitative real-time PCR with SensiFast™ SYBR Hi-Rox Kit on the StepOnePlus System (Applied Biosystems).

3.3.2 Collagen assay

The Sircol collagen assay was performed according to the manufacturer's protocol (Biocolor #S1000).

3.3.3 Enzyme-linked immunosorbent assay

The serum or the supernatant of the co-culture experiments was analyzed according to the manufacturers protocol for mouse/rat ELISA Kit for HGF or TGFβ (R&D System, #MHG00, #MB100B).

3.3.4 DNA analysis

3.3.4.1 Genomic DNA Isolation

Genomic DNA isolation from ear marks or from the pancreas (to analyze the successful recombination in the tissue) was conducted after the Soriano protocol. The tissue was incubated in PCR lysis buffer (with freshly added proteinase K) for 90min at 55°C. To inactivate proteinase K, samples were incubated at 95°C for 15min. Afterwards, samples were mixed thoroughly and centrifuged (10min, 16,000xg). The supernatant that contains the DNA was transferred into a new tube and PCR analysis could be performed.

DNA isolation from cells and blood was performed by using the DNeasy Blood & Tissue Kits from Qiagen (# 69504).

3.3.4.2 PCR

To determine the exact genotype of each mouse, a PCR analysis was performed. The PCR was conducted after the manufacturer's protocol (ALLin™ Red Taq Mastermix, HighQu). The general composition of the reaction mix as well as the PCR conditions are highlighted in Table 3.2. For each reaction, 1µL of isolated DNA was used and amplification was done for 40 cycles. PCR products were visualized directly by performing agarose gel electrophoresis or stored at 4°C until usage.

Table 3.2 Reaction mix and PCR conditions

Reaction mix	PCR conditions
12.5 µL 2x Mastermix ((ALLin™ Red Taq Mastermix)	95°C - 3 min (initial denaturation)
0.25-2 µL forward primer (10µM)	95°C - 30 s (denaturation)
0.25-2 µL reverse primer (10µM)	55-65°C – 45 s (annealing)
1 µL isolated DNA	72°C - 90 s (elongation)
Add 25 µL ddH_2O	12°C (pause)

3.3.4.2.1 Genotyping PCRs

The isolated genomic DNA from the ear marks was used to analyze the different genotypes of mice. Specific primers were designed for each allele. PCR conditions are listed in Table 3.3.

Table 3.3 Genotyping PCR settings and expected band size of the PCR product

Genotyping PCR	Annealing temperature	PCR products
Pdx-Flp	55°C	300 bp (wt) 620 bp (mut)
FSF-Kras^{G12D}	56°C	270 bp (wt) 351 bp (mut)
p53^{frt}	57°C	292 bp (mut) 258 bp (wt)
Sm22Cre^{ERT}	60°C	220 bp (mut) 280 bp (wtt)
Prrx1	60°C	438 bp (wt) 595bp (mut)
R26^{mT-mG}	62°C	450 bp (wt) 650 bp (mut)

3.3.4.2.2 Recombination PCRs

The isolated genomic DNA from the pancreas was used to analyze the activity of *Flp* recombinase via recombination PCRs. The PCRs and their products are shown in Table 3.4.

Table 3.4 Recombination PCR settings and expected band size of the PCR product

Recombination PCR	Annealing temperature	PCR product
FSF-Kras del	60°C	196 bp
p53-frt recombined	55°C	352 bp

3.3.4.3 Agarose gel electrophorese

The PCR products were visualized by agarose gel electrophoresis using 1.5-2% agarose gels (in 1xTAE) containing ethidium bromide. The gels were loaded with 12.5µL of each PCR sample and run for 1.5h at 120V. Separated bands were detected and documented with the Gel Doc™ XR+ Gel Documentation System.

3.4 Histological techniques

3.4.1 Tissue fixation and tissue section

For paraffin sections, tissue was fixed overnight in 4% PFA at 4°C and afterwards stored in PBS at 4°C until dehydration. The dehydration of the tissue as well as the embedding in paraffin of the organs was performed by the institute of pathology (Dr. K. Steiger, Klinikum rechts der Isar, Technical University of Munich). The paraffin blocks could be stored at RT until further use. For histological analysis, series of 2.5µm sections were prepared of the tissue.

Tissue samples for cryosections were fixed for 2h in 4% PFA on ice and transferred to 15% sucrose for dehydration and incubated for 4h at 4°C. For further dehydration, the tissue was transferred to 30% sucrose overnight at 4°C. Afterwards, the tissue was embedded in Tissue-Tek® O.C.T. and stored for long term at -80°C. Series of 5µm sections were prepared by the institute of pathology (Dr. K. Steiger, Klinikum rechts der Isar, Technical University of Munich). Sections were stored at -80°C until further use.

3.4.2 Hematoxilyn and eosin staining

The hematoxilyn and eosin staining (H&E) was mainly performed by the institute of pathology (Dr. K. Steiger, MRI/TUM), otherwise the following protocol was used: Paraffin-embedded tissue sections were dewaxed in xylene for 2 x 5min and rehydrated in a decreasing ethanol series (twice 99.8%, twice 96% and twice 80% – each for 1min). Sections were stained with hematoxylin for 10s and washed with water for 10min. Afterwards, the sections were stained with eosin for 15s followed by 3 washing steps with ddH_2O. Afterwards, the slides were dehydrated using an increasing ethanol series (twice 80%, twice 96% and twice 99.8% – each 1min) and incubated for 2 x 5min in xylene. Subsequently, the slides were mounted with Pertex mounting medium (#LEIC811).

3.4.3 Picrosirius Red Staining

The sections were dewaxed and hydrated as described for the H&E. Afterwards, the nuclei were stained with hematoxylin for 8min and washed with water. The sections were stained for 1h in picro-sirus red (0.5g Direct Red 80 and 500mL saturated aqueous solution of picric acid. Afterwards, the sections were washed twice in acidified water (0.5% acetic actic) and dehydrated in 100% ethanol (3 x 2min). The sections were cleared in xylene and mounted.

3.4.4 Elastica von Gieson staining

The sections were dewaxed and hydrated as described for the H&E. Afterwards, the sections were stained for 20min in Resorcinfuchsin solution and washed 2 x 1.5min in 96% ethanol. Subsequently, they were incubated for 8min in the HTX-Weigerts solution and washed for 5min in water, before they were incubated for 2min in the picrofusin solution. Subsequently, the slides were dehydrated using an increasing ethanol series (96% and twice 100%, each 30s) and incubated 2 x 1.5min in xylene and mounted.

3.4.5 Immunohistochemistry

The sections were deparaffinized by warming up to 60°C for 15min, subsequent Xylene incubation for 2 x 5min, rehydrated in a decreasing ethanol series (twice 99.8%, twice 96% and twice 80% – each for 1min) and hydrating the slide by incubation in water. The sections were immersed in antigen unmasking solution (followed manufacturer's protocol, vector laboratories (#H-3300)) while microwaving. After cooling down for approximately 20min, the sections were washed with water. The endogenous peroxidase was quenched with 3% hydrogen peroxidase for 10min, followed by a washing step with ddH_2O and PBS. The sections were blocked with avidin D block reagent, washed with PBS, blocked with biotin blocking reagent and washed in PBS (followed manufacturer's protocol, vector laboratories). Afterwards, the sections were blocked with protein blocking agent (StartingBlock™ Blocking Buffer (# 37578)) for 10min. The primary antibody was diluted in PBT and incubated overnight. The sections were washed twice with PBS and the secondary antibody conjugated to biotin was incubated for 30min at 37°C. Additional washing steps with PBS were performed, before the HRP-conjugated ABC reagent (vector laboratories) was added for 30min at 37°C. 2 to 3 washes with PBS were performed prior to developing the signal with DAB substrate kit (vector laboratories (#SK-4100)). The reaction was stopped with ddH_2O. For counter staining the hematoxylin staining was used, see chapter 3.4.2.

3.4.6 Immunofluorescence staining

Paraffin embedded sections were deparaffinized and hydrated (see chapter 3.4.5). Frozen sections were dried on air, fixed for 10min with 4% PFA and rinsed in water.

The sections were immersed in antigen unmasking solution (followed manufacturer's protocol, vector laboratories) while microwaving. After cooling down approximately 20min, the sections weree washed with water. Afterwards, the sections were blocked with StartingBlock™ (PBS) blocking buffer for 10min. The primary antibody was diluted in PBT and incubated overnight. The sections were washed twice with PBS and the secondary antibody as well as the counter

stain was incubated for 30min at 37°C in the dark. The slides were washed twice with PBS and mounted with mounting media (#H-1000) before taking images on the fluorescence microscope.

3.4.7 Quantification of single-color immunofluorescence signals

Semiquantitative grading was performed using semi-automated ImageJ software analysis with the same threshold for each stain. The results were expressed as percentage staining per visual field (Sparc, α-SMA, Collagen I).

The quantification protocol was provided by Koushik Das, MD (Washington University School of Medicine, St. Louis, USA) within the publication (Heeg et al., 2016). The protocol can be found in the appendix of this dissertation (see section 9.1).

3.5 Statistical analysis

The GraphPad Prism7 (Motulsky) software was used to perform graphical depiction, data correlation and statistical analysis. A p-value of less than 0.05 is considered to be statistically significant. The significance used for each experiment is described in the respective figure legends. In addition, the symbols as denoted in Table 3.5 are used to indicate p-value ranges. Survival curves were created by using the Kaplan-Meier survival analysis.

Table 3.5 Symbols used to denote the p-values ranges in the figure legends according to standard of GraphPad Prism7 (Motulsky) software

Symbol	Meaning
*	p≤0.05
**	p≤0.01
***	p≤0.001
****	p≤0.0001

4 Results

4.1 PRRX1 expression is higher in CAFs than in pancreatic cancer cells

The transcription factor PRRX1 was recently described as a plasticity driver in the processes of embryonic development, pancreatitis, and carcinogenesis in the pancreas (Reichert et al., 2013a; Takano et al., 2016). In human cancer tissue e.g. colon, esophageal, and lung cancer it became apparent, that PRRX1 is not exclusively expressed in the carcinoma but also in the stroma (Tomaru et al., 2014). Performing histological analysis of the PRRX1A and PRRX1B expression in our own cohort of murine (*Pdx1-Cre; Kras*$^{G12D/+}$*; Ink4/ARF*$^{fl/+}$ mouse model) as well as in human PDAC tissue confirmed that *PRRX1* expression is not restricted to the tumor compartment (Figure 4.1 A-B). The PRRX1 expression is also found in cells adjacent to the tumor cells, most likely cancer associated fibroblasts.

Of note, Nicolle et al. found an elegant way to reveal the complex interplay between tumor cells und stroma in PDAC (Nicolle et al., 2017). In this publication, the authors analyzed 29 xenografts from PDAC patients and performed RNA profiling of bulk tumors to identify gene expression in the tumor (human origin) and in the stroma (murine origin) (Nicolle et al., 2017). We analyzed the data regarding *Prrx1* expression in both compartments (tumor and stroma). Interestingly, *Prrx1* was highly up-regulated in the stromal compartment (Figure 4.1 C).

To confirm that the *PRRX1* expression is not limited to PDAC cells, CAFs and PSCs were isolated from human pancreatic cancer tissue specimen. The tissues were minced and digested with collagenase to gain either tumor cells or fibroblasts via outgrowth or a nycodenz gradient centrifugation step was performed to obtain pancreatic stellate cells (Vonlaufen et al., 2010). Gene expression analysis of the primary cultured cells revealed that the *PRRX1* levels are significantly higher in CAFs compared to PDAC cells in a human context (Figure 4.1 D).

To further evaluate the findings in the murine model system pancreatic ductal cells (PDCs), fibroblasts (FB), and pancreatic stellate cells (PSCs) were isolated from the *C57BL/6* mice as well as Pancreatic Intraepithelial Neoplasia (PanIN) cells and PanIN associated fibroblasts from the *Pdx1-Cre; Kras*$^{G12D/+}$ mice. Gene expression analysis for *Prrx1a* and *Prrx1b* could further confirm that both splice variants of *Prrx1* are significantly upregulated in different fibroblast entities compared to cancer cells (Figure 4.1E-F).

Mostly the different fibroblast entities arise from pancreatic stellate cells, which are the major source for activated fibroblasts, called myofibroblasts. Once activated, the fibroblast contributes massively to the secretion of extracellular matrix proteins. Fibroblasts become activated in response to injury, inflammation, or to paracrine signals secreted from tumor cells (Bachem

et al., 2005; Vonlaufen et al., 2008; Pang et al., 2017). *In vitro* fibroblasts become activated by culturing them on plastic or treating them with cytokines e.g. TGF-β (Öhlund et al., 2017). This data indicates that *Prrx1* is highly expressed in the stromal compartment, especially in myofibroblasts.

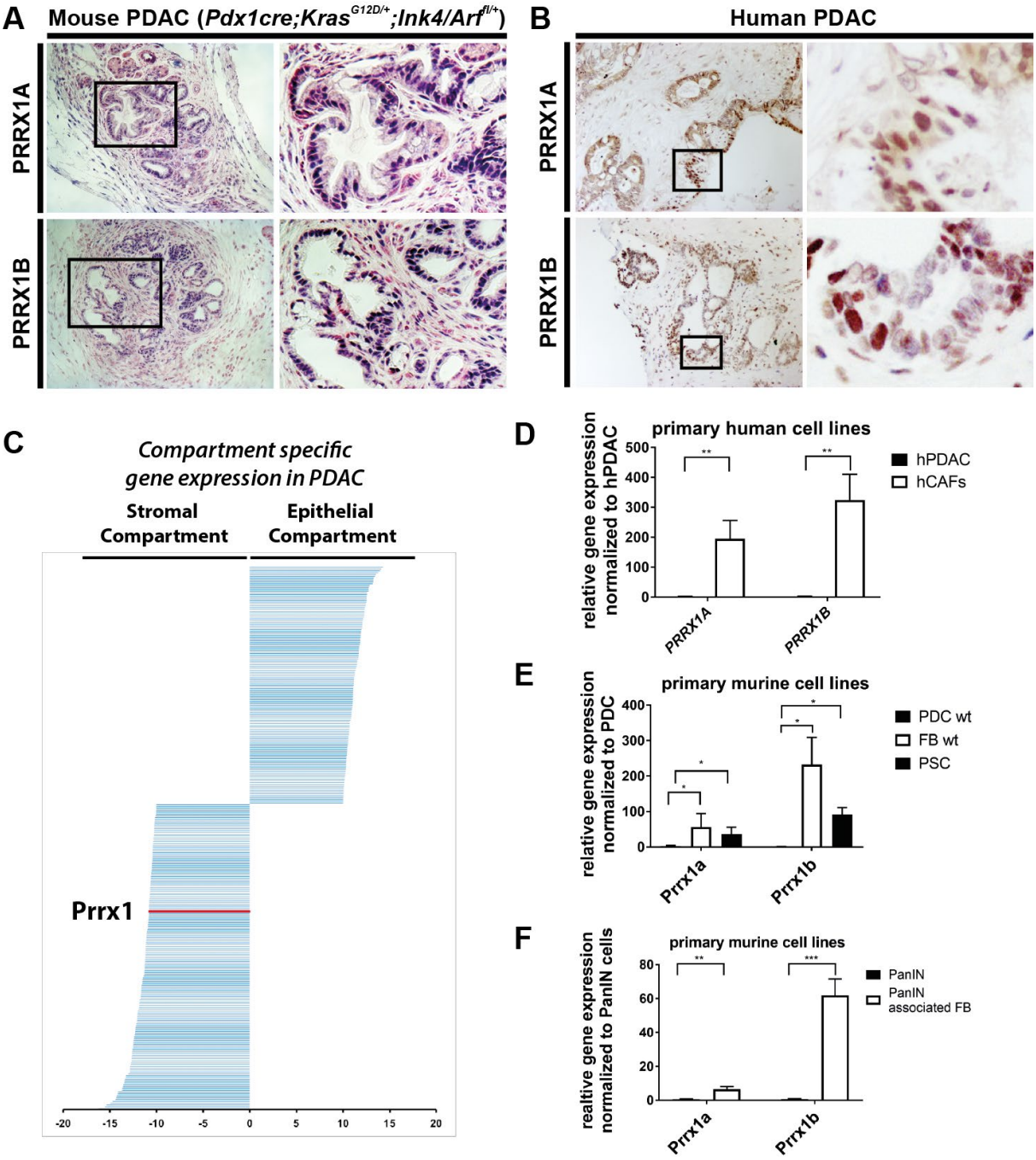

Figure 4.1 Prrx1 expression in murine as well as human tissues and cell lines. A) PRRX1A and PRRX1B immunohistochemistry in mouse sections with the indicated genotype. Expression of PRRX1 in the ductal compartment as well as in the stromal compartment. **B)** PRRX1A and PRRX1B immunohistochemistry in human sections; Expression of Prrx1 in the ductal compartment as well as in the stromal compartment. **C)** Compartment specific gene expression in PDAC based on the data from (Nicolle et al., 2017). High Prrx1 expression in the stromal compartment. **D)** Quantitative PCR analysis of PRRX1A und PRRX1B expression in primary human cell lines isolated

from surgery specimens, 2way ANOVA; **p-value 0.0012**. E)** Quantitative PCR analysis of Prrx1a und Prrx1b expression in primary murine cell lines isolated from a wt mice, 2way ANOVA; *p-value≤0.05**. F)** Quantitative PCR analysis of Prrx1a and Prrx1b expression in primary murine cell lines isolated from Pdx1-Cre; LSL-Kras^{G12D} mice. 2way ANOVA; **p-value: 0.005; ***p-value: 0.0005

4.2 Genetic manipulation of Prrx1 in fibroblasts *in vitro*

Given these initial findings, the following question was put into focus: Which role does *Prrx1* play in the fibroblasts? A global knockout of *Prrx1* is lethal as described in Martin et al. and there is no published data available about the lethality of a compartment specific ablation of *Prrx1* (Martin et al., 1995). Therefore, an inducible mouse model was used. The *Sm22-Cre^{ERT}* mouse model, a knock-in into the *Sm22* (smooth muscle protein 22 alpha) promotor, was used to target specifically fibroblasts and smooth muscle cells (Kühbandner et al., 2000). The administration of tamoxifen and its binding to the mutated estrogen receptor domain leads to the dissociation of HSP90 and the recombinase can translocate to the nucleus. There, it mediates the excision of the DNA fragments flanked by loxP sites. In case of the *Sm22-Cre^{ERT}, Prrx1$^{fl/fl}$, R26^{mTmG}* GEMM, the activation of the *Sm22-Cre^{ERT}* leads to a partial excision of *Prrx1* and excision Tomato and therefore to a switch to membrane-bound GFP (Figure 4.2 A).

To validate the functionality of the *Sm22-Cre^{ERT}, Prrx1$^{fl/fl}$* mouse model *in vitro*, pancreatic fibroblasts were isolated and cultured on plastic. To guarantee a successful recombination, the cells were treated three times with tamoxifen at an interval of two days. To avoid unspecific side effects, the cells were washed and left at least 3 days without tamoxifen before using the cells in an experiment.

The successful *in vitro* recombination of fibroblasts can be visualized by fluorescence microscopy, when these cells harbor the fluorescence reporter in their Rosa26 locus by switching the expression from Tomato to GFP (Figure 4.2 B, first row). Additional characterization of the cells confirmed that fibroblast grown on plastic express mainly all activation markers like α-SMA, Vimentin, PDGFRα, GFAP, and FAP and therefore show a myofibroblast phenotype (Figure 4.2 B). Although all markers were expressed regardless of the *Prrx1* status, it seems that the fibroblasts treated with tamoxifen express higher levels of these markers.

Gene expression analysis revealed that 5 days of tamoxifen treatment led to a significant reduction of the *Prrx1a* and *Prrx1b* levels (Figure 4.2 C). Furthermore, FACS analysis revealed that a recombination efficiency up to 90% could be achieved *in vitro* (Figure 4.2 D). Also, the PRRX1 staining demonstrated a significant drop of PRRX1 expression on protein level (Figure 4.2 E).

This data proves a successful *in vitro* recombination of isolated fibroblasts, termed myofibroblasts, from the *Sm22-Cre^{ERT}, Prrx1$^{fl/fl}$* mouse model.

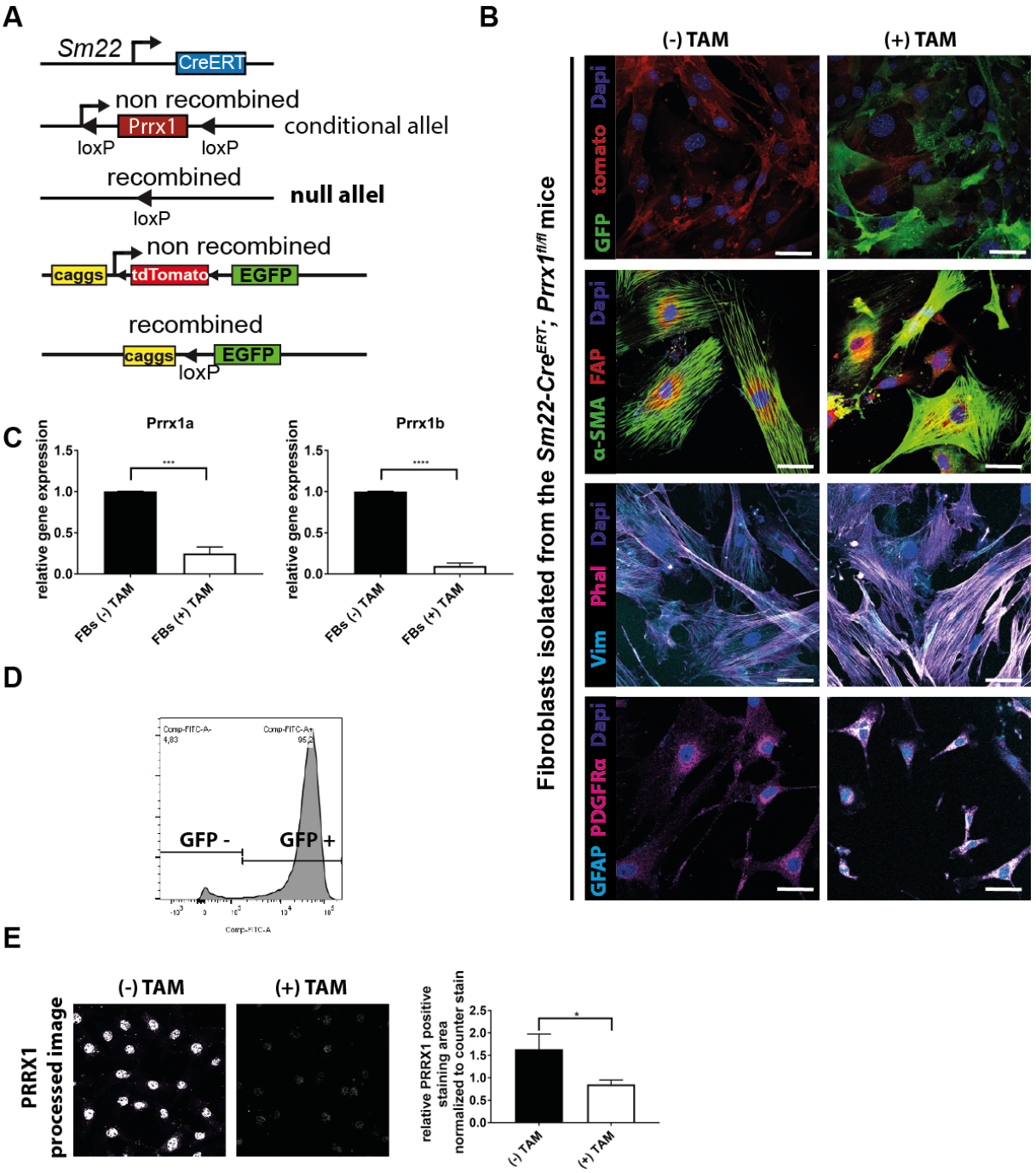

Figure 4.2 Analyzing the recombination efficiency of fibroblasts *in vitro*. A) Schematic illustration of the used mouse model. **B)** Representative IF image of fibroblasts of endogenous tdTomato and eGFP signal; nuclear staining with Dapi; GFAP, α-SMA; Vimentin, Phalloidin, FAP 50 µM scale bar. **C)** Quantitative PCR analysis of *Prrx1a* and *Prrx1b* expression in primary murine cell lines, unpaired-t test; ***p-value: 0.0007; ****p-value: <0.0001. **D)** FACS Analysis of isolated fibroblast cell lines TAM treatment, Sort of GFP+ (FITC) cells. **E**) Semi-quantitative processed image of the PRRX1 staining. Quantification of the PRRX1 positive staining area normalized to the nuclear counter stain; *p-value: 0.0359

4.2.1 *Prrx1* knockout fibroblasts are activated and highly migratory

During the process of characterization of *Prrx1* wildtype and *Prrx1* knockout fibroblasts regarding different fibroblast markers, it became obvious that the *Prrx1* knockout fibroblast expresses higher α-SMA levels compared to the wildtype fibroblast (Figure 4.3 A-B). Quantification of the

α-SMA positive staining showed a significant enrichment for α-SMA (Figure 4.3 B). In addition to this phenotype, a higher collagen production was measured in these cells (Figure 4.3 C). To exclude that the higher amount of collagen production is due to stronger proliferation of the cells, a proliferation assay was performed. Nevertheless, there was no significant difference between both groups, indicating a correlation between the activation status of cells and the secretion of ECM proteins (Figure 4.3 D).

To answer the question, how the altered activation status of the fibroblasts influences their functionality, a 3D migration assay was performed to determine the ability of fibroblasts to migrate toward the tumor cells. Within the experimental set-up, as illustrated in Figure 4.3 E, each cell type (fibroblasts and PDAC cells) was placed separately in a Matrigel drop in a small dish. After the Matrigel was solidified, a bridge was placed between the tumor cells and fibroblasts, which enabled the cells to migrate to each other. Based on the proliferation data, which showed no differences between both groups, we can already exclude, that the observed cell migration is due to cell proliferation. Surprisingly, after 16h, it became obvious that the recombined *Prrx1*$^{fl/fl}$ FBs start to migrate directly to the tumor cells (Figure 4.3 F). In contrast to that, the *Prrx1* wildtype FBs have not yet started to migrate at this time point. Analysis after 48h of incubation revealed that the recombined *Prrx1*$^{fl/fl}$ FBs are able to migrate faster (Euclidean distance) as well as specifically towards the tumor cells (forward migration index) (Figure 4.3 I-J), indicating that *Prrx1* influence the migration behavior of the fibroblasts.

In order to summarize the insights, we gained from the experiments, we can say that *Prrx1* influences the activation status, the cell migration and the ECM secretion of fibroblast.

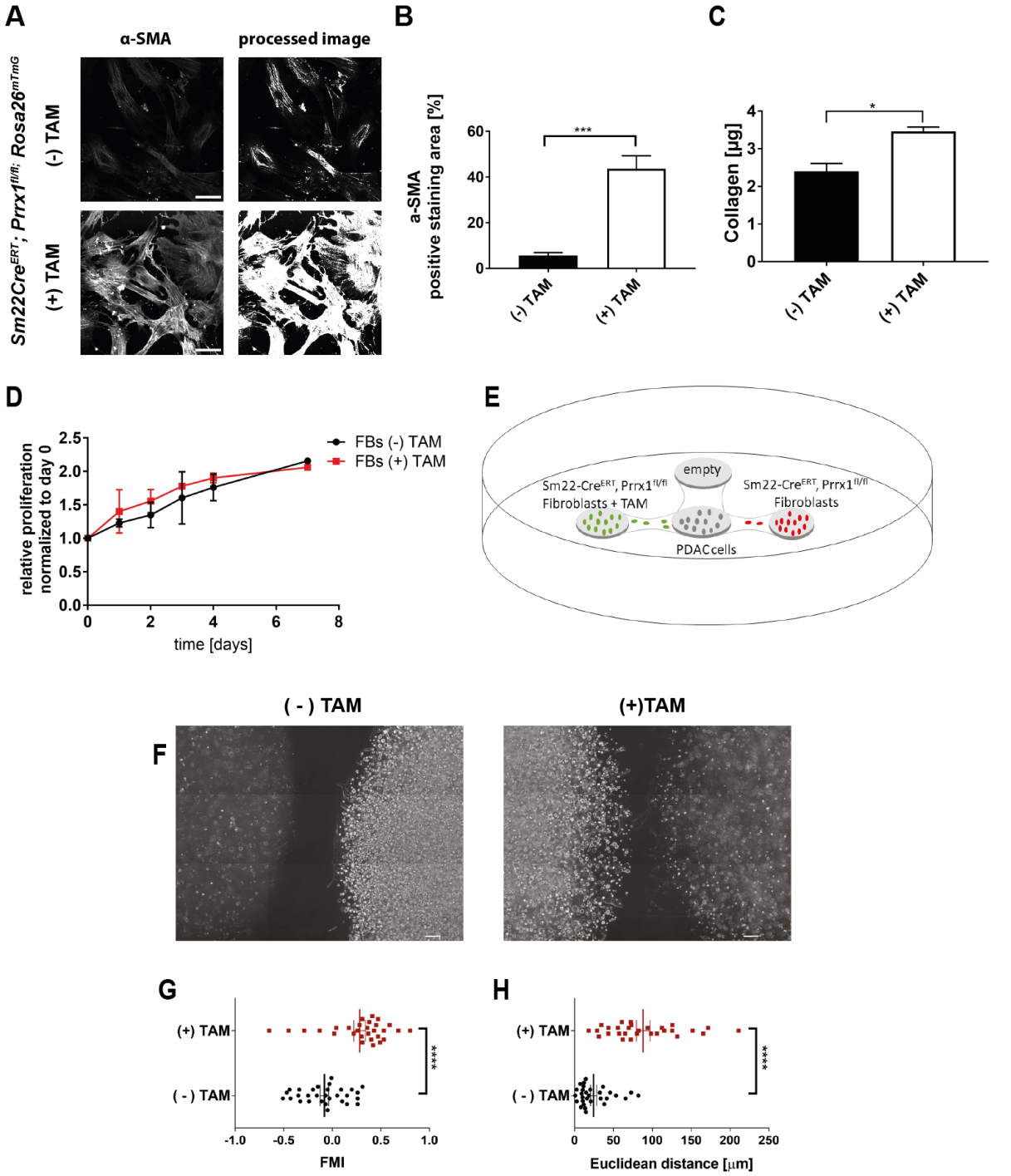

Figure 4.3 Prrx1 ablation in PAFs *in vitro* alters the functionality of these cells. A) Representative IF staining of α-SMA; 50µM scale bar+ semi-quantitative processed image of the α-SMA staining. **B)** Quantification of the α-SMA positive staining area of fibroblasts, unpaired t-test, ***p-value: 0.008. **C)** Determination of the collagen content in the cell lysat of the fibroblasts, unpaired t-test, *p-value: 0.0115. **D)** Determination of the cell proliferation via MTT. **E)** Schematic illustration of the 3D migration assay. **F)** Light microscope pictures 16h after experiment start, 100µM scale bar; left picture: tumor cells were seeded on the left hand side and fibroblasts on the right hand side; right picture: fibroblasts were seeded on the left hand side fibroblasts and tumor cells on the right hand side. **G)** Diagram shows the forward migration index of n=30 per group, unpaired t-test; ****p-value: <0.0001. **H)** Euclidian distance indicates how fast the fibroblasts migrates forward n=30 per group unpaired t-test; ****p-value: <0.0001

4.3 Stromal compartment specific manipulation of *Prrx1 in vivo*

The generated *in vitro* data showed that *Prrx1* plays an important role in fibroblasts concerning ECM protein secretion and migration towards tumour cells. To gain insights into the functionality of *Prrx1 in vivo*, an orthotopic implantation model was used. Within the experimental set up, tumour cells were transplanted orthotopically into the tail of the pancreas. A compartment specific ablation of *Prrx1* in an orthotopic transplantation model has not been performed yet in the context of pancreatic cancer. Therefore, a pilot experiment was conducted to answer the following questions: What is the best timepoint to activate the promotor by tamoxifen injections? Does tamoxifen alter the architecture of the pancreas?

To answer these questions, the *Sm22-Cre^{ERT}, R26^{mTmG}* mouse model is used (Figure 4.4 A) instead of the *Sm22-Cre^{ERT}, Prrx1$^{fl/fl}$, R26^{mTmG}* to avoid *Prrx1* dependent effects.

As indicated in Figure 4.4 B, the tamoxifen treatment does not influence the architecture of the organs neither macroscopically nor microscopically. The recombination in the normal pancreas is very low, because mostly quiescent, non-proliferative fibroblast are resident in the pancreas (Figure 4.4 B).

Therefore, the pancreas was challenged by orthotopic implantation of the tumor cells (PPT 8025, isolated from a *p48-Cre; LSL-Kras^{G12D}* tumor mouse with a C57BL/6 background) into the pancreas of the *Sm22-Cre^{ERT}, R26^{mTmG}* mice. Two different approaches (three mice with TAM and one without TAM per group) were used to analyze the best timepoint for tamoxifen treatment to gain the highest recombination efficiency of the *Sm22-Cre^{ERT}* positive fibroblasts: Within the first approach, the mice were treated 2 weeks prior to the implantation. Within the second approach, the mice were treated with tamoxifen 1 week after implantation. The experimental procedure is highlighted in Figure 4.4 C. Due to toxicity of the tamoxifen treatment, the recovering time from the treatment had to be extended towards 4 weeks prior to the tumor cells being implanted into the pancreas.

Nevertheless, histological analysis of the 2 weeks' timepoints revealed a macroscopic tumor formation (Figure 4.4 D) as well as moderately differentiated tumors. IF analysis of the pancreas tumor revealed that the *Sm22-Cre^{ERT}* positive cells (eGFP+ cells) are recruited from the healthy pancreas (tdTomato+ cells) to the tumor cells. Spontaneous recombination without tamoxifen treatment can be excluded.

To confirm a CAF phenotype of the *Sm22-Cre^{ERT}* positive cells, α-SMA staining was performed. The coverage of α-SMA+ and GFP+ double positive cells referred to the α-SMA positive cells is around 70%, indicating a CAF/myofibroblast phenotype of the *Sm22-Cre^{ERT}* positive cells Figure 4.6 F.

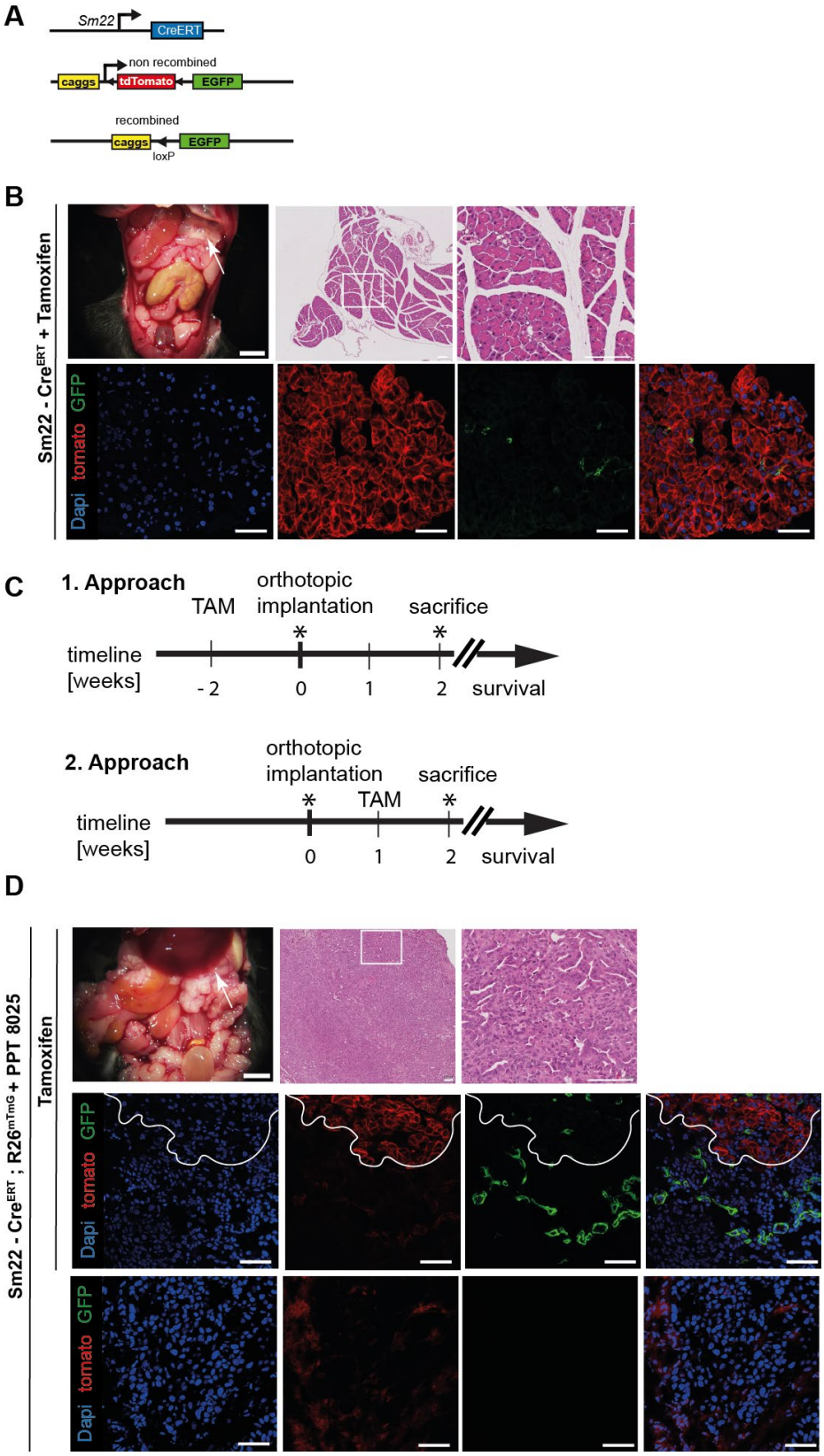

Figure 4.4 Validation of the Sm22-Cre^{ERT}, Rosa26^{mTmG} mouse model to target fibroblasts. A) Schematic illustration of the used mouse model. **B)** Upper row: macroscopic picture of the organs, H&E staining of the pancreas, 100µM scale bar. Lower row: representative IF picture of the pancreas, nuclear staining with Dapi, 50µM scale bar. **C)** Experimental procedure of the implantation experiment. **D)** Orthotopic implantation of the PPT 8025 cell lines into the tail of the pancreas, upper row: microscope picture of the organs, white arrow showing PDAC, H&E staining of PDAC, scale bar 100µM. Lower rows: IF picture of the PDAC, nuclear staining with Dapi, 50µM scale bar

4.3.1 *Prrx1* loss in fibroblasts leads to better differentiated tumors

Prrx1 is crucial during embryonic development (McKean et al., 2003; Reichert et al., 2013a) and therefore the functional consequence of *Prrx1* ablation in fibroblasts via tamoxifen administration at an age of 6-8 weeks after birth was evaluated in the *Sm22-Cre^{ERT}; Prrx1$^{fl/fl}$*; Reporter mouse model (Figure 4.5 A). As indicated by the representative H&E stainings of pancreas, liver, lung, and intestine for a 3-month-old mouse, the ablation of *Prrx1* within an age of 6 weeks has no influence on the development and the architecture of the organs (Figure 4.5 B). FACS and IF analysis revealed that only few fibroblasts are resident in the healthy pancreas and spontaneous recombination of the *Sm22-Cre^{ERT}* without tamoxifen administration was excluded (Figure 4.5 C-D).

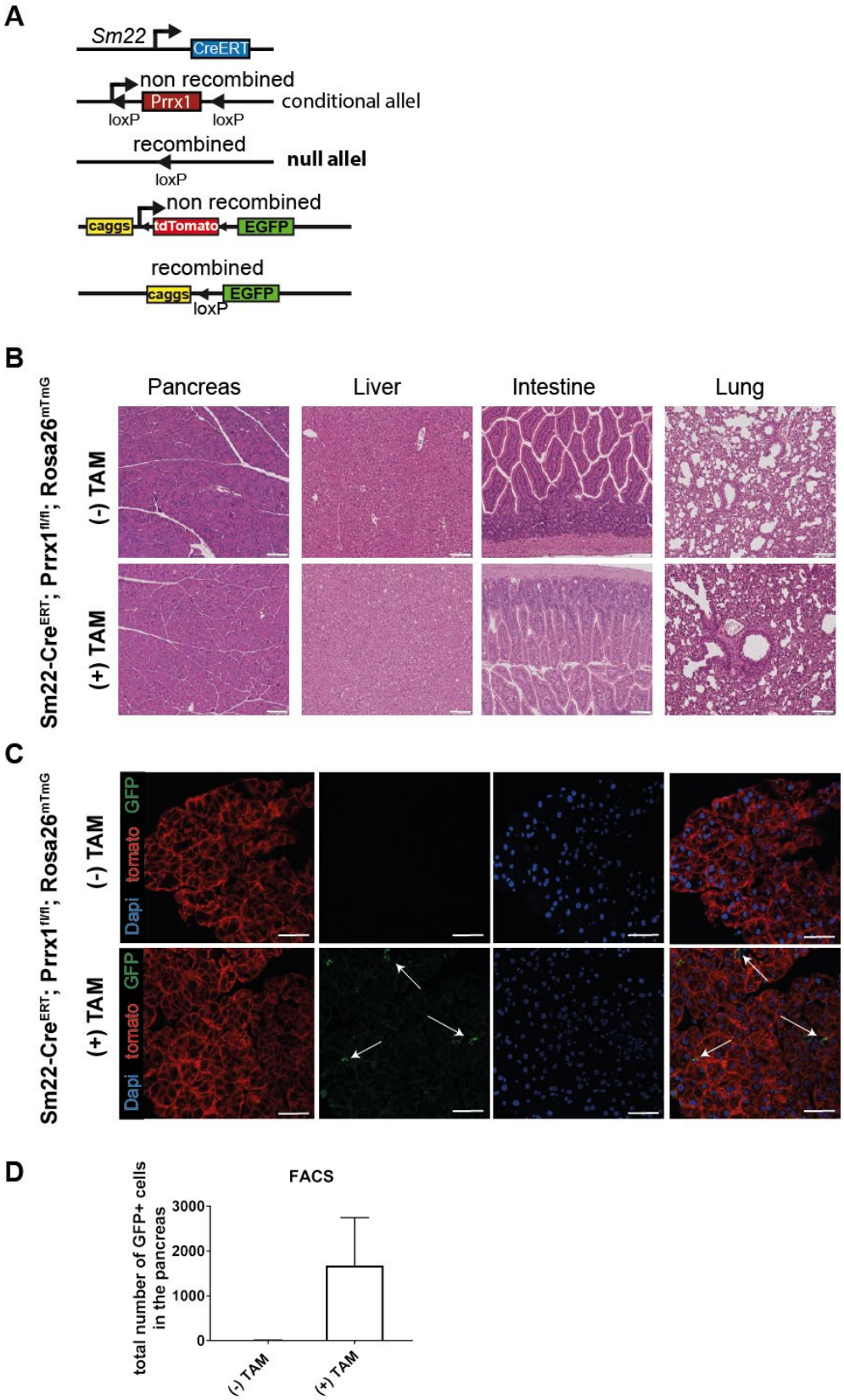

Figure 4.5 Altering Prrx1 Levels of Sm22-Cre^{ERT} positive fibroblasts in healthy tissue. A) Schematic illustration of the used mouse model. **B)** Representative H&E staining of pancreas, liver, lung and intestine of 3-month-old mice, n=3 per group; 100µm scale bar. **C)** Representative IF image of cryosection with endogenous tdTomato and eGFP signal; counterstain with DAPI; 50µM scale bar, white arrows indicate recombined cells. **D)** FACS sort of GFP+ cells of the entire pancreas, n=3 per group

For this reason, an orthotopic implantation model was chosen to study the role of *Prrx1* ablation in CAFs. The experimental design of this study is illustrated in Figure 4.6 A. For orthotopic implantation the same cell line 8025 PPT (isolated from a *p48-Cre; LSL-Kras^{G12D}* mouse in a C57BL background) as previously used for the validation experiment was injected into the tail of the pancreas. The mice were either scarified after 14 days for time specific analysis or kept for the survival study.

14 days after implantation the pancreas was completely penetrated by the tumor which could be confirmed via palpation as well as macro- and microscopically analysis. Histological analysis of 21 pancreatic tumors revealed that *Prrx1* ablation in CAFs leads to more differentiated tumors (more tumors with G2 grading and less tumors with G3 grading) compared to the control group (*Prrx1* proficient CAFs, (-) TAM) (Figure 4.6 B). Furthermore, to validate the ablation of *Prrx1* in CAFs, PRRX1 staining was performed in tumor section and a significant reduction of the PRRX1 signal was detected in the tamoxifen treated group, especially in the CAFs (GFP+ positive cells) PRRX1 staining was observed less (Figure 4.6 B and C). Nevertheless, the ablation of *Prrx1* does not significantly alter the survival of the mice nor the tumor volume (Figure 4.6 D and E). Additionally, there was no clear difference detectable in the CAFs distribution and recombination efficiency (GFP and α-SMA double positive cells) between both groups as shown in Figure 4.6 F and G.

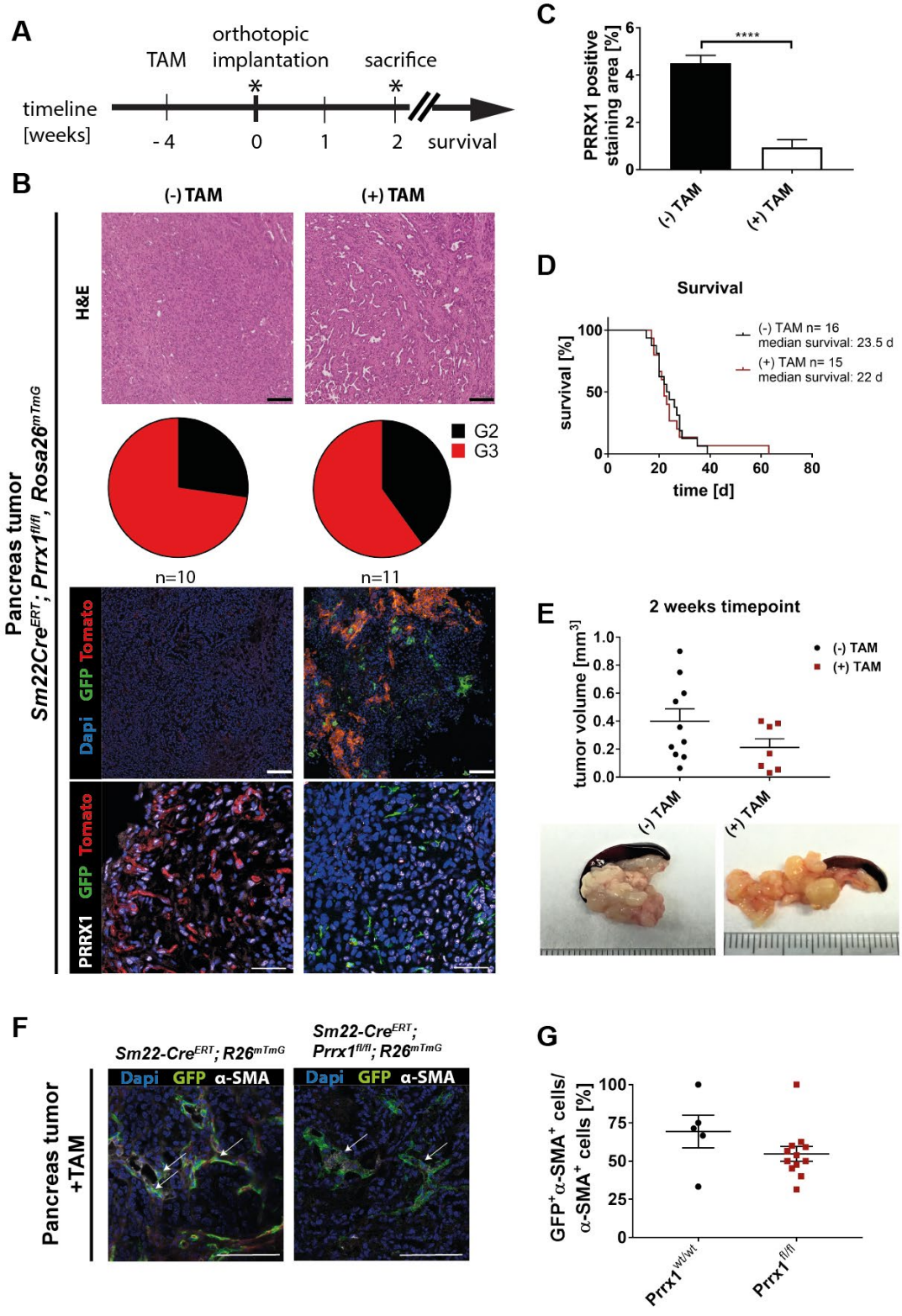

Figure 4.6 Orthotopic implantation of tumor cells in the *Sm22-Cre^{ERT}, Prrx1$^{fl/fl}$* mouse model. A) Experimental design of orthotopic implantation experiment with *p48-Cre; LSL-Kras^{G12D}* cell line. **B)** Upper row: Hematoxylin/Eosin staining of PDAC in control ((-) TAM) and *Prrx1$^{fl/fl}$* ((+) TAM) treated mice, 100µM scale bar, tumor grading of the two weeks' timepoint; IF stainings of cryosection with endogenous Tomato and GFP signal; DAPI and PRRX1 staining; 100µM scale bar. **C**) Semi-quantitative image processing was used to quantify the PRRX1 staining, unpaired t-test; **** p-value: < 0.0001. **D)** Survival curve of the implantation model. **E)** Tumor volume of the two weeks timepoint, (-) TAM n=10; (+) TAM n=7; picture of the tumor. **F)** Compartment specific recombination of *Prrx1*; IF staining of the pancreatic tumor for α-SMA (white), recombined cells (green, GFP) nuclear counterstain (blue, Dapi), arrows indicate double positive cells for α-SMA and *Prrx1$^{fl/fl}$*. **G)** Manually counted GFP and α-SMA positive cells per field of view

4.3.2 *Prrx1* ablation in CAFs leads to reduced metastatic burden in the orthotopic implantation model

Pancreatic cancer is known for its metastatic spread to other parts of the body, mostly to the liver. During this process the tumor cells adapt to different steps via EMT and MET (to disseminate from the tumor, to go into circulation of the blood stream, and to co-localize to different organs). Each of these steps is highly inefficient and only a small fraction of the circulating tumour cells develops into metastases (Gupta et al., 2005). Rhim et al. showed that an inflammatory stroma is necessary for EMT and dissemination (Rhim et al., 2012). Reichert et al. recently published the role of *Prrx1* as an EMT-Inducer (Reichert et al., 2013a). This led to the question, does Prrx1 ablation in the stromal compartment alter the metastatic burden? Therefore, histological lung and liver sections of the orthotopic implantation model were examined. The analysis revealed, that more liver and lung metastases were detected in the control group (-) TAM compared to the experimental group ((+) TAM, $Prrx1^{-/-}$ in CAFs) (Figure 4.7 A and B). Additional FACS analysis of blood samples regarding circulating tumor cells, characterized by EpCAM expression, underscore the histological findings. Significantly less CTC were counted in the blood samples in *Sm22-Cre*^{ERT}*, Prrx1*$^{fl/fl}$ (+) TAM compared to the control group (Figure 4.7 C).

This finding leads to the hypothesis, that *Prrx1* ablation in CAFs changes the CAF-tumor cell crosstalk by modulating tumor cell plasticity resulting in changes of the tumor architecture as well as invasiveness of the tumor cells.

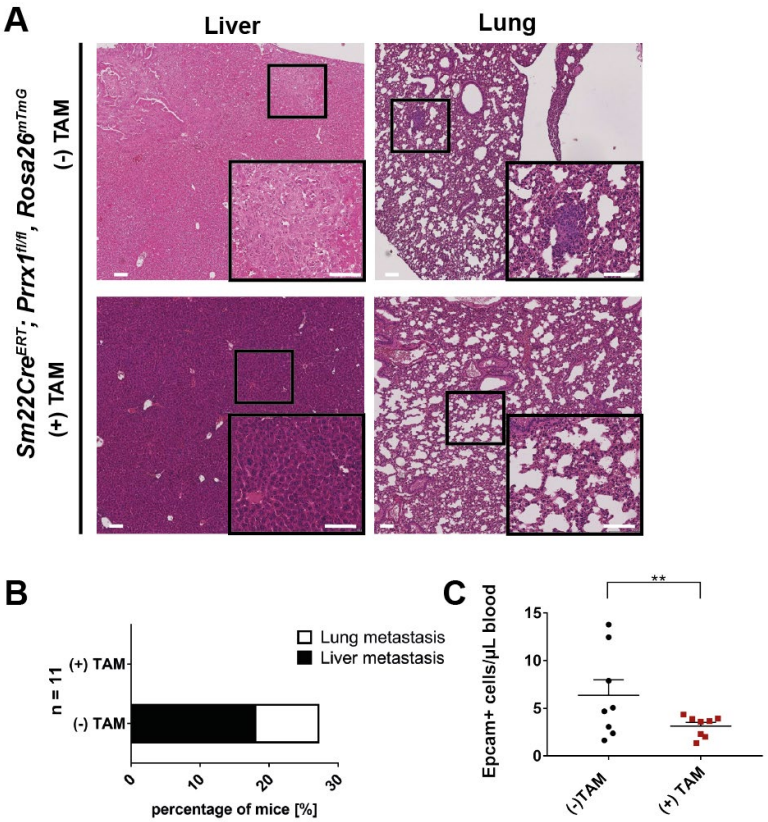

Figure 4.7 *Prrx1* ablation CAFs leads to reduced tumor formation. A) Hematoxylin/Eosin staining of liver and lung tissue of the two weeks timepoint, upper row control mouse with lung and liver metastasis; lower row (+) TAM: normal lung and liver tissue, no metastasis. **B)** Quantification of liver and lung metastasis of n=11 per group. **C)** FACS analysis of EpCAM+ cells isolated from the whole-body blood of the mice; n=8 per group, unpaired t-test **p-value: <0.05

4.3.3 Increased extracellular matrix secretion through *Prrx1* ablation in CAFs

The ECM plays an important role in cell signaling through binding directly to cell surface receptors or as ECM-derived peptides (Monboisse et al., 2014). Besides the biochemical signaling, the ECM also provides mechanical properties (tissue tension) to cells, which in turn influence the intracellular signaling cascades (Laklai et al., 2016). Paszek et al. describe that a stiff stroma reduces tissue polarity and destroys adherent junctions (Paszek et al., 2005). Influencing the biochemical signaling as well as the mechanical cues highlights the importance of the ECM in tumor development, progression and metastasis. Beside the differences in tumor grading, also changes in the contribution of the extracellular matrix (ECM) was observed during histological examination of the implanted pancreas tumor.

For evaluation of the composition of ECM in our implantation model, three mice per group of the two weeks' timepoint were analyzed.

To gain an overview of the contribution of the extracellular matrix, the Elastica van Gieson staining was performed. Thereby the elastic fibers were stained violet-black, cytoplasm and

muscles yellow and collagen red. Figure 4.8 A reveals that the conditional knockout of *Prrx1* in fibroblasts leads to an increase of collagen and elastic fibers.

Collagen is one of the most abundant and well characterized components of the ECM. Although 28 types of collagen are described (Ricard-Blum, 2011), Collagen I contributes mostly to the desmoplastic reaction in PDAC. The secretion of collagen leads to various effects, e.g. disrupting the basement membrane and foster invasion. But collagen can also act as a signaling molecule, e.g. binding of Collagen I to integrins promotes proliferation and migration but also leads to the activation of the focal adhesion kinase (FAK) pathway, resulting in self-renewal and EMT of the tumor cells in PDAC (Armstrong et al., 2004; Begum et al., 2017).

Histological stainings of collagen were performed, because of it is the major composition of the ECM. To gain an overview of the total collagen content, a Picrosirus Red staining was performed. The conditional knockout of *Prrx1* in fibroblasts leads to an increase of collagen production (Figure 4.8 B and C). To evaluate, whether the collagen I content is also altered, an additional IF staining was performed. Also, here an increase of collagen I content in *Prrx1* knockout fibroblasts was observed (Figure 4.8 E).

The Elastica van Gieson staining also revealed an increase in elastic fibres, including glycoproteins, which also have an important impact on tumour cells. The glycoprotein fibronectin similar to collagen is able to bind to integrin receptor (α5β1) and activates the FAK pathway (Giancotti and Ruoslahti, 1999), but fibronectin can also support the function of collagen by acting as a linker protein between collagen and integrins. Because of its impact on PDAC biology, a fibronectin staining was performed additionally. IHC analysis in Figure 4.8 D shows an increase of fibronectin in the conditional knockout model of *Prrx1*.

Interestingly, fibronectin plays an important role in amplifying ECM synthesis by pancreatic stellate cells. Fibronectin binds to the latent TGF-β binding protein, which allows the release of active TGF-β, which in turn activates PSCs (Dallas et al., 2005).

Activated stellate cells are characterized by abundant α-SMA expression. Therefore, α-SMA staining was performed. Associated with higher extracellular matrix content, also higher levels of α-SMA expression in the fibroblasts were quantified via immunofluorescence analysis. This indicates that *Prrx1* ablation in CAFs leads to a higher activation of fibroblasts (Figure 4.8).

The generated data shows that the desmoplastic stroma is a dynamic compartment which might also influence the vascularity of the tumour mass. Dependent on their activation status, PSC secrete pro-angiogenic factors such as VEGF or contribute an anti-angiogenic stroma

through the excessive ECM protein secretion. To gain insights into the endothelial vessel density, CD31 staining was performed. Surprisingly, there is no significant difference between both groups (Figure 4.8 G).

The observed differences in the ECM protein secretion in the analyzed PDAC tissue underscore the hypothesis that *Prrx1* ablation in CAFs leads to significant changes in the contribution of the ECM and thereby restrains the invasiveness of the tumor.

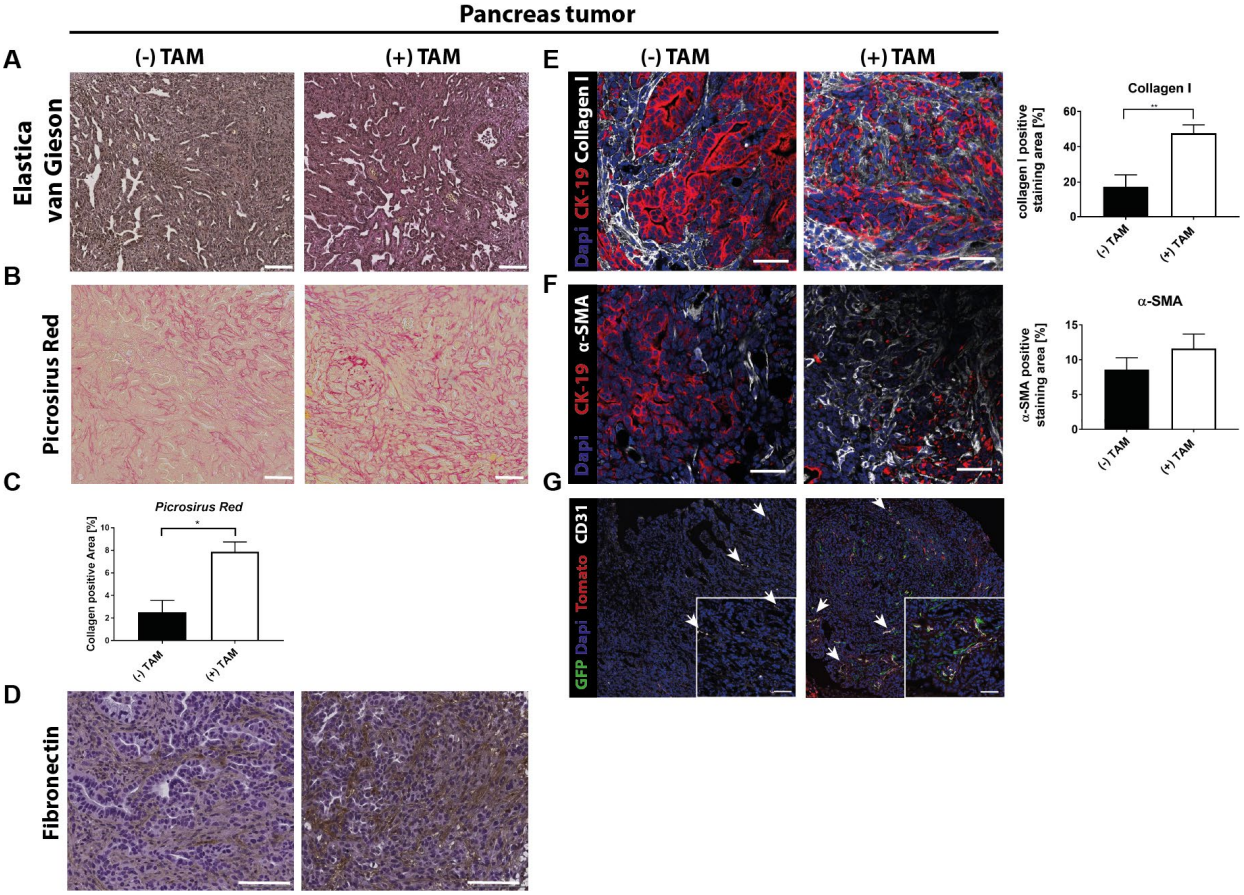

Figure 4.8 Loss of *Prrx1* in fibroblasts leads to dramatic changes of the TME in the OTX model of *Sm22-Cre^{ERT}, Prrx1$^{fl/fl}$* mouse model. A) Representative picture of Elastica von Gieson staining, 100µM scale bar. **B)** Representative picture of Picrosirius Red staining, 100µM scale bar. **C)** Quantification of the Picrosirius Red via ImageJ, 4 pictures were taken of each slide and 3 slides per group were analyzed, unpaired t-test **p-value: 0.0169. **D)** Representative picture of Fibronectin staining, 100µM scale bar. E) Representative IF staining for CK-19, Collagen I und Dapi; n=3 per group; 50µM scale bar, semi-quantitative image processing was used to quantify the collagen staining; unpaired t-test, p-value: 0.0047. **F)** Representative IF staining for CK-19, α-SMA and Dapi; n=3 per group; 50µM scale bar; semi-quantitative image processing was used to quantify the α-SMA staining. **G)** Representative IF staining for CD31 and Dapi, endogenous fluorescence signal of GFP and Tomato in the implantation model, 50µM scale bar

In order to examine the role of *Prrx1* ablation in CAFs during tumorigenesis and progression, we crossed the *Sm22-Cre^{ERT}, Prrx1$^{fl/fl}$* mice with the KPF (*Pdx-Flp; FSF-Kras^{G12D}; p53$^{frt/wt}$*) mice to receive the final genotype: *Pdx-Flp; FSF-Kras$^{G12D/+}$; p53$^{frt/wt}$; Sm22-Cre^{ERT}, Prrx1$^{fl/fl}$* as illustrated in Figure 4.9 A. The usage of the dual recombinase system allows the induction of

stroma rich tumors by *Pdx1-Flp* mediated activation of an FRT-stop-FRT (FSF) silenced oncogenic *Kras*^{G12D} allele as well as heterozygous inactivation of *p53* (Schönhuber et al., 2014). Analysis of the KPF model showed, that the mice developed a broad spectrum of PDAC reaching from well differentiated to poorly differentiated tumors with a median survival of 183 days (Schönhuber et al., 2014).

Additional usage of the *Sm22-Cre*^{ERT} line allows the genetic manipulation of *Prrx1* in CAFs during tumor formation and progression.

A preliminary evaluation of the survival data revealed, that heterogeneous ablation of *Prrx1* in CAFs in the KPF model does not alter the survival of the mice (*Prrx1*$^{fl/+-}$ 178 days to *Prrx1*$^{+/+}$ 187.5 days) (Figure 4.9 B). Interestingly the homozygous deletion of *Prrx1* in CAFs in the KPF model seems to shorten the survival to 136.5 days, but because of small animal cohort a conclusion is not possible (Figure 4.9 B).

Histological analysis of the pancreatic tumors of both groups (*Prrx*$^{fl/fl}$ and *Prrx1*$^{+/+}$ (+TAM)) confirmed the heterogeneity of these tumors, showing moderately to poorly differentiated areas within the same tumor Figure 4.9 C.

Nevertheless, staining for ECM protein within the tumors showed an increase of α-SMA positive cells in the tumors of *Prrx1* knockout fibroblasts as well as a significant increase of collagen secretion in the ECM of the tumors (Figure 4.9 D). This preliminary data supports our findings that *Prrx1* in CAFs can influence the secretion and modulation of the extracellular matrix *in vivo*.

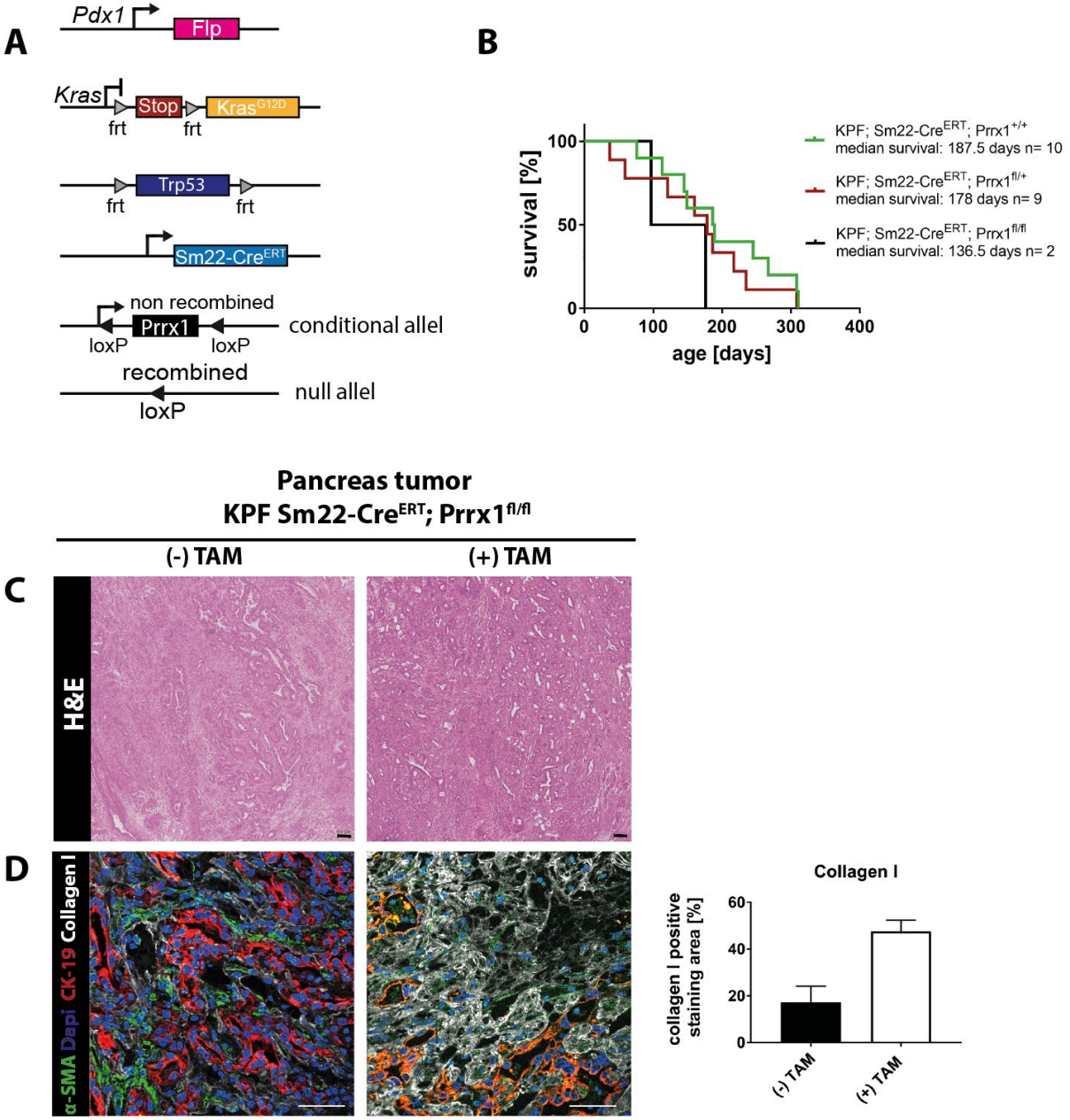

Figure 4.9 *Prrx1* ablation in CAFs leads to changes in the ECM in the endogenous *Pdx-Flp; FSF-Kras^{G12D}; p53$^{frt/+}$* (KPF); *Sm22-Cre^{ERT}; Prrx1$^{fl/fl}$* mouse model. A) Schematic illustration of the endogenous KPF mouse model. **B)** Kaplan-Meier survival curve for the indicated genotypes. **C)** Representative H&E staining of the pancreas tumor, scale bar 100µm. **D)** Representative IF staining for CK-19, Dapi; Collagen; α-SMA, 50µm scale bar; semi-quantitative image processing was used to quantify Collagen I staining, unpaired t-test; 50µM scale bar

4.4 *Prrx1* alters the plasticity of fibroblasts

The generated *in vitro* and *in vivo* data indicates that *Prrx1 knockout fibroblasts* express more α-SMA, secrete more ECM proteins, and migrate faster towards the tumor cells compared to the *Prrx1* proficient fibroblasts. The observed differences and the finding that *Prrx1* plays an important role as a plasticity driver in epithelial ductal cells in the pancreas leads to the hypothesis that *Prrx1* might impair the activation status of the fibroblasts (Reichert et al., 2013a;

Takano et al., 2016). Quiescent pancreatic stellate cells are characterized by a low ECM protein synthesis, no α-SMA expression, and storage of lipid droplets (Erkan et al., 2012a; Moir et al., 2015). Once they are activated, they start to express α-SMA and secrete ECM proteins. The relationship between the quiescent and activated phenotype is dynamic and might be regulated by transcriptions factors such as *Prrx1*. To examine the plasticity of fibroblasts, isolated PSCs were cultured in Matrigel, as illustrated in Figure 4.10 A, because PSCs cultured in Matrigel can revert to their quiescence state (Jesnowski et al., 2005; Öhlund et al., 2017).

The exposure of PSCs to TGF-β, which is an activator of PSCs, induces the expression of TGF-β target genes, such as connective tissue growth factor (*Ctgf)* or *Acta2* (encoding α-SMA) and therefore promoting a myofibroblastic phenotype (Öhlund et al., 2017).

To evaluate their plasticity, the PSCs were cultured for 4 days in Matrigel before 20ng/mL TGF-β was added. Afterwards the cells were cultured for another 4 days and then fixed and stained for immunofluorescent analysis.

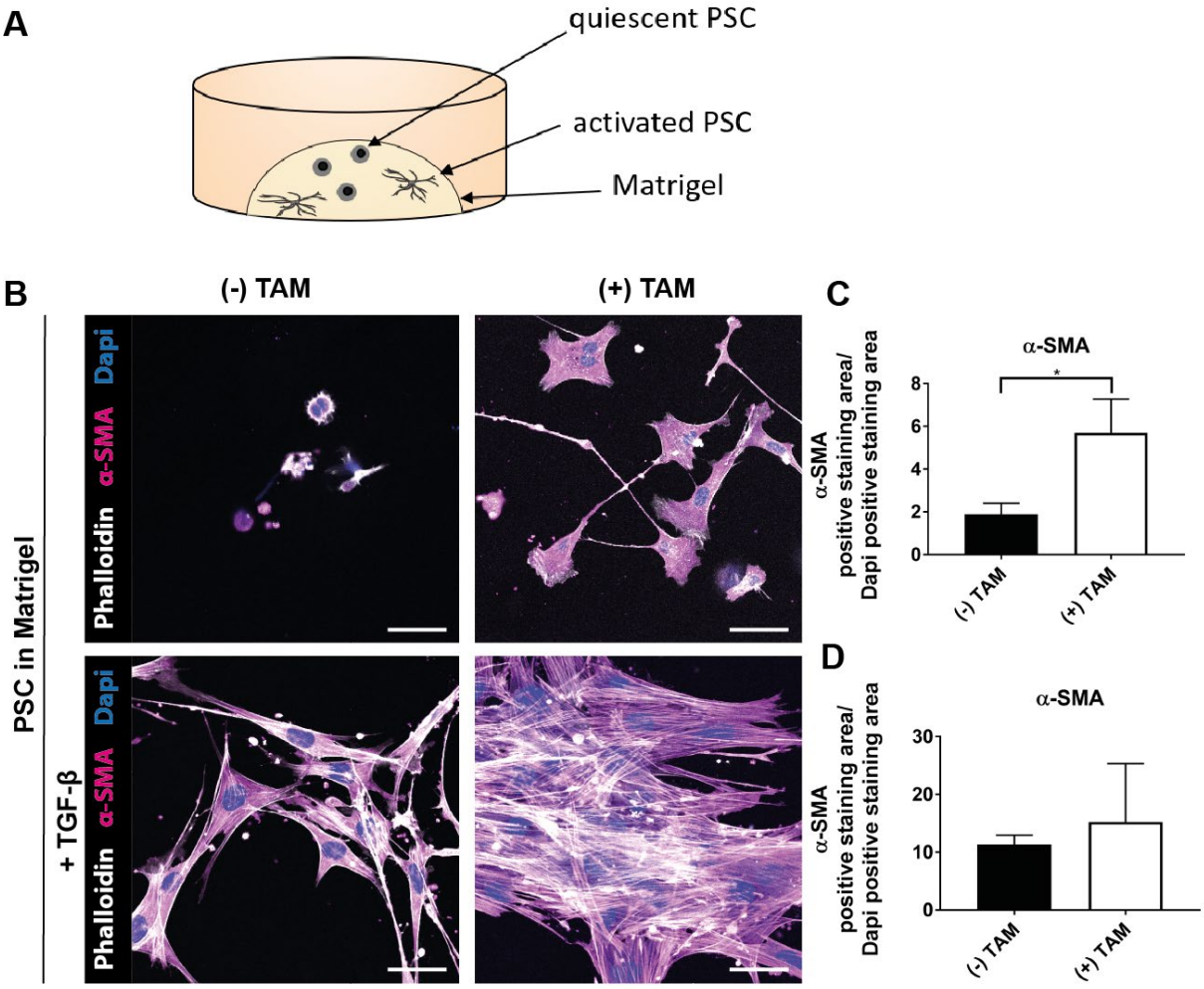

Figure 4.10 Reduced plasticity in *Prrx1*$^{fl/fl}$ PSCs. A) Schematic illustration of experimental set up. **B)** PSCs cultured in Matrigel, representative IF staining for Phalloidin, α-SMA and Dapi, 50µM scale bar low row: + TGF-β. **C+D)** Semi-quantitative image processing was used to quantify the α-SMA staining normalized to the Dapi staining, unpaired t-test, *p-value: 0.0468

Astonishingly, the *Prrx1* ablation in PSCs kept these cells in a myofibroblast-like phenotype with significant higher α-SMA expression and a spindle shaped structure. These cells show a reduced plasticity, indicating that the *Prrx1*$^{fl/fl}$ PSCs are kept in their activated state. In contrast to that, *Prrx1* wildtype PSCs are able to revert to their quiescence state, indicated by lower α-SMA expression and the round structure of the cells (Figure 4.10 B and C).

The addition of TGF-β to cell culture medium leads to the activation of the TGF-β signaling pathway, shown by increased α-SMA expression and the cell morphology in both groups (Figure 4.10 B and D).

This data underscores the importance of *Prrx1* as a plasticity driver in fibroblasts.

4.5 *Prrx1* in CAFs alters tumor differentiation by paracrine HGF signaling

The orthotopic implantation model showed that *Prrx1* can alter the tumor progression *in vivo* and plays an important role as a plasticity driver in fibroblasts. For this reason, the tumor-CAF crosstalk came more into focus. It is known that tumor cells turn activate fibroblasts into cancer-associated fibroblasts (CAFs) through the secretion of paracrine growth factors (Kalluri and Zeisberg, 2006). The CAFs can promote on the one hand cell survival, growth, and progression of cancer cells (Erkan et al., 2010; Bussard et al., 2016; Bynigeri et al., 2017; LeBleu and Kalluri, 2018) and on the other hand they can restrain tumor growth (Özdemir et al., 2014; Rhim et al., 2014). The CAFs secrete several soluble factors like TGF-β; HGF, CXCL12 to induce EMT and chemoresistance in tumor cells (Wendt et al., 2010; Kalluri, 2016).

To analyze the influence of paracrine factors regarding tumor progression, both cell types (tumor cells and fibroblasts) must be kept separately via a permeable membrane as illustrated in Figure 4.11 A. Only the crosstalk via soluble factors (secretome) is possible.

Gene expression analysis of the co-culture experiment confirmed that the fibroblasts can influence tumor cells to undergo EMT (Figure 4.11 B) (Kalluri, 2016).

Interestingly, co-culturing tumor cells with *Prrx1*$^{-/-}$ FBs overrides the effect and leads to significantly reduced expression levels of EMT markers like *Hgf; Twist, Zeb1, Slug, Etv1*, *Postn*, and *Tnc* (Figure 4.11 B).

To evaluate, whether TGF-β is the source for the induction of the EMT (Yu et al., 2014), a TGF-β ELISA was performed. The TGF-β ELISA of the supernatant of the co-culture experiment shows no significant differences between *Prrx1* wildtype and *Prrx1* knockout fibroblasts, indicating that there is no *Prrx1* dependent regulation of this growth factor (Figure 4.11 C).

As recently published, *Prrx1b* regulates the HGF-dependent MET activation and plays an important role in stimulating epithelial-mesenchymal transition (EMT) in tumor cells, resulting in increased invasion and metastasis (Takano et al., 2016). To examine differences in the concentration of secreted HGF in the supernatant of the co-culture experiment, an HGF ELISA was performed. Indeed, the ELISA data revealed that significantly less amount of HGF is secreted into the supernatant while co-culturing PDAC cells with *Prrx1* knockout FBs (Figure 4.11 D). This indicates that changes in the secretome of the CAFs can influence the invasiveness of the tumor cells.

IHC analysis of the pancreas tumor of the orthotopic implantation model revealed less HGF expression in the tamoxifen (*Prrx1*$^{-/-}$) treated group *in vivo (*Figure 4.11E). Furthermore, the

analysis of the blood serum of the mice confirmed the hypothesis, that *Prrx1* ablation in fibroblasts leads to reduced HGF levels (Figure 4.11 F).

To evaluate if the increased gene expression of EMT markers while co-culturing the tumor cells with the fibroblasts also alters the epithelial integrity of the tumor cells, a three-dimensional collagen assay was performed. Therefore, the FBs were grown on plastic and the tumor cells were layered on top of the fibroblast, embedded in a collagen matrix, as illustrated in Figure 4.11 G. Visualizing the sphere formation capacity of the tumor cells via IF staining demonstrates, that the tumor cells co-cultured with wildtype FBs have reduced epithelial integrity. This is demonstrated by a reduced sphere formation capacity and expression of high levels of α-SMA, supporting the gene expression data and an EMT phenotype. In contrast to that, tumor cells co-cultured with *Prrx1* knockout FBs keep their epithelial integrity and form organized spheroidal structures with no α-SMA expression (Figure 4.11 H).

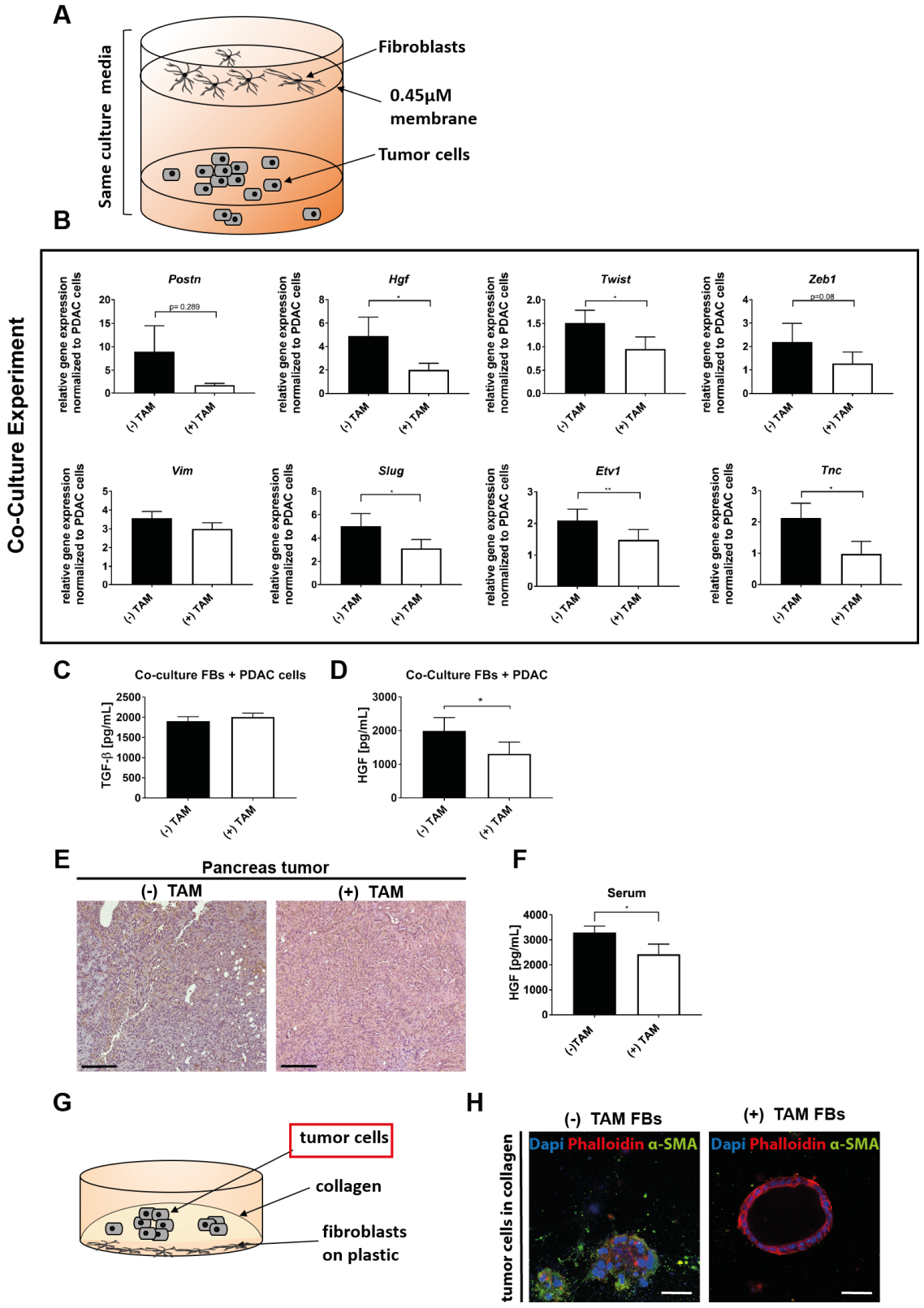

Figure 4.11 Co-culture experiment reveals paracrine HGF signaling. A) Schematic illustration of the trans well co-culture experiment. **B)** Quantitative PCR analysis of EMT markers expressed in tumor cells co-cultured with FBs; paired student t-test; n=6; * p-value: <0.05; ** p-value: 0.0018. **C)** TGF-β ELISA of the supernatant of tumor cells co-cultured with FBs in a trans well. **D)** HGF ELISA of the supernatant of tumor cells co-cultured with FBs in a trans well, t-test; p-value: 0.0475. **E)** Representative picture of the HGF staining (IHC); n=3 per group, 200µM scale bar. **F)** HGF ELISA of the serum of implanted pancreas tumors of Sm22-Cre^{ERT}; Prrx1$^{fl/fl}$ mice after 14 days; n=4 per group; unpaired student t-test; * p-value: <0.05. **G)** Schematic illustration of 3D co-culture experiment. **H)** 3D co-culture experiment, representative IF staining of tumor cells for a-SMA; Phalloidin and Dapi 50µM scale bar

HGF is also a key regulator of CAF mediated resistance toward chemotherapy (Pothula et al., 2017). It was recently published that inhibition of both HGF and c-MET combined with gemcitabine resulted in great therapy success in an orthotopic mouse model in pancreatic cancer (Pothula et al., 2017). To answer the question, whether *Prrx1* alters the sensitivity towards gemcitabine in the co-culture model, Gemcitabine treatment in a 96 trans well approach was performed.

Indeed, higher sensitivity towards Gemcitabine (GEM) was measured while co-culturing tumor cells with recombined *Prrx1*$^{fl/fl}$ FBs (Figure 4.12 A). To exclude that *Prrx1* alters the GEM metabolism in fibroblasts gene expression analysis for gemcitabine transporters as well as gemcitabine inactivating enzymes in fibroblasts and tumor cells under GEM treatment was performed. It was possible to reproduce the data from the group of Neesse (Hessmann et al., 2018), where it was already shown that tumor cells start to increase the expression of *Nt5c1A, Nt5c3,* and *ENT1* under GEM treatment (Figure 4.12 B). Interestingly, there was no significant difference in gene expression in-between the two FBs entities (*Prrx1*$^{wt/wt}$ and *Prrx1*$^{-/-}$) (Figure 4.12 B). Also co-culturing the FBs with the tumor cells under GEM treatment, shows clearly that *Prrx1* does not influence the gemcitabine metabolism in fibroblasts nor in the tumor cells significantly (Figure 4.12 C and D). This data massively supports the hypothesis that *Prrx1* ablation in FBs alters tumor differentiation and gemcitabine sensitivity by paracrine HGF signaling.

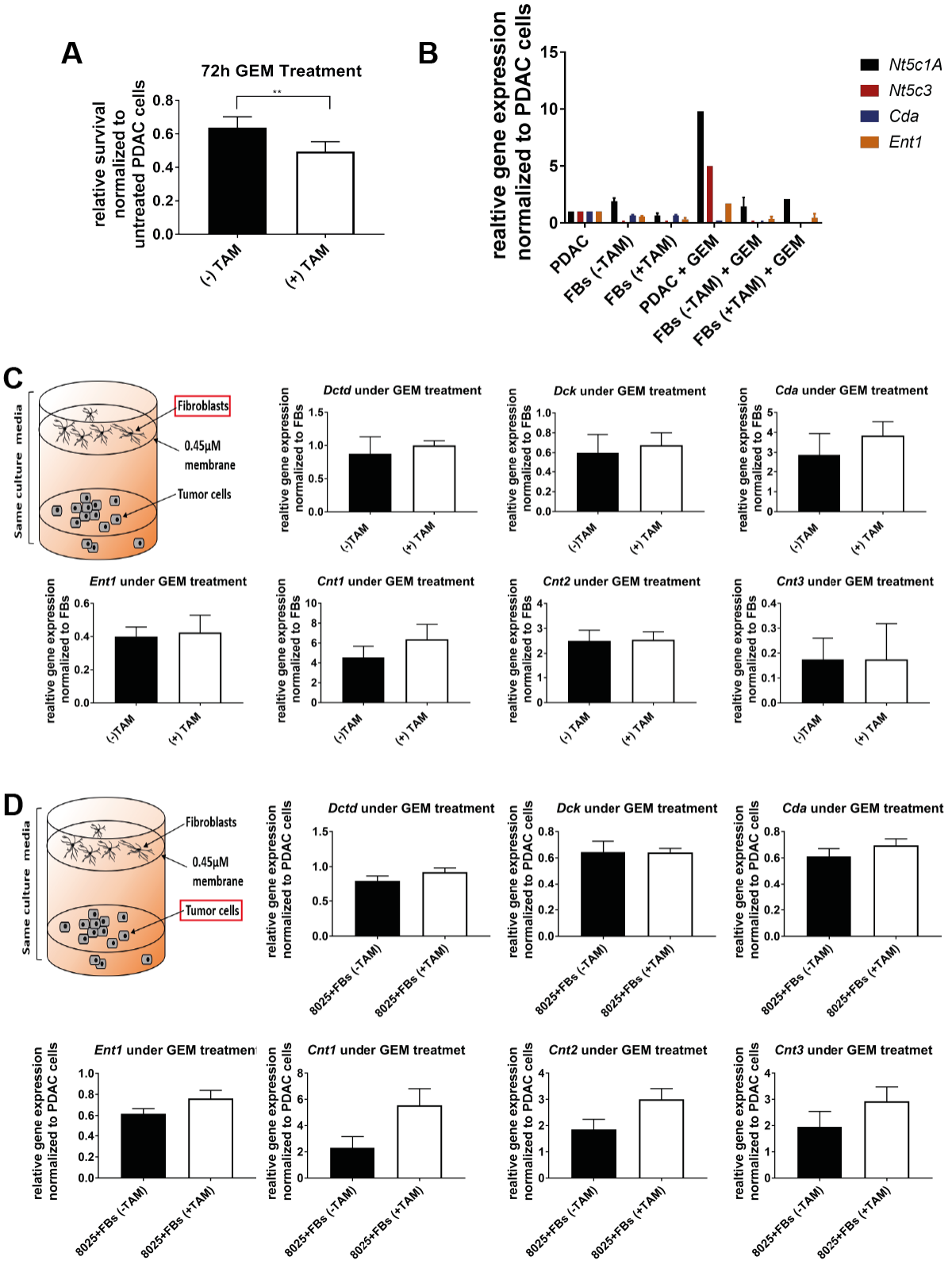

Figure 4.12 *Prrx1* does not alter the GEM metabolism in PAFs nor in PDAC cells. A) MTT assay of the tumor cells co-cultured with PAFs after 72h GEM treatment (600nM GEM), paired t-test **p-value: 0.0015. **B)** Gene expression analysis for GEM transporters and inactivating enzymes without and with GEM treatment after 24h of GEM treatment. **C)** Schematic illustration of the trans well co-culture experiment, analyzing the PAFs, quantitative PCR analysis of Gemcitabine metabolism (GEM transporters and inactivating enzymes) expressed in PAFs co-cultured with tumor cells under GEM. **D)** Schematic illustration of the trans well co-culture experiment, analyzing the PDAC cells, quantitative PCR analysis of Gemcitabine metabolism (GEM transporters and inactivating enzymes) expressed in PDAC cells co-cultured with PAFs under GEM

To confirm that paracrine HGF signaling alters the invasiveness and chemoresistance in tumor cells, recombinant HGF was added to the co-culture experiments. The data revealed that recombinant HGF overrides the effect of *Prrx1* ablation in CAFs and restore the invasiveness phenotype. This is indicated by significant upregulation of EMT transcription factors like *Slug*, *Twist, Etv1,* and *Zeb1* (Figure 4.13 A). In addition, the supplementary usage of recombination HGF during GEM treatment also restores the effect of *Prrx1* ablation in CAFs and reveals higher chemoresistance (Figure 4.13 B). This data underscores the PRRX1-HGF driven effect of EMT and gemcitabine resistance in a tumor-CAF crosstalk and highlights again the complexity of the tumor-stroma network.

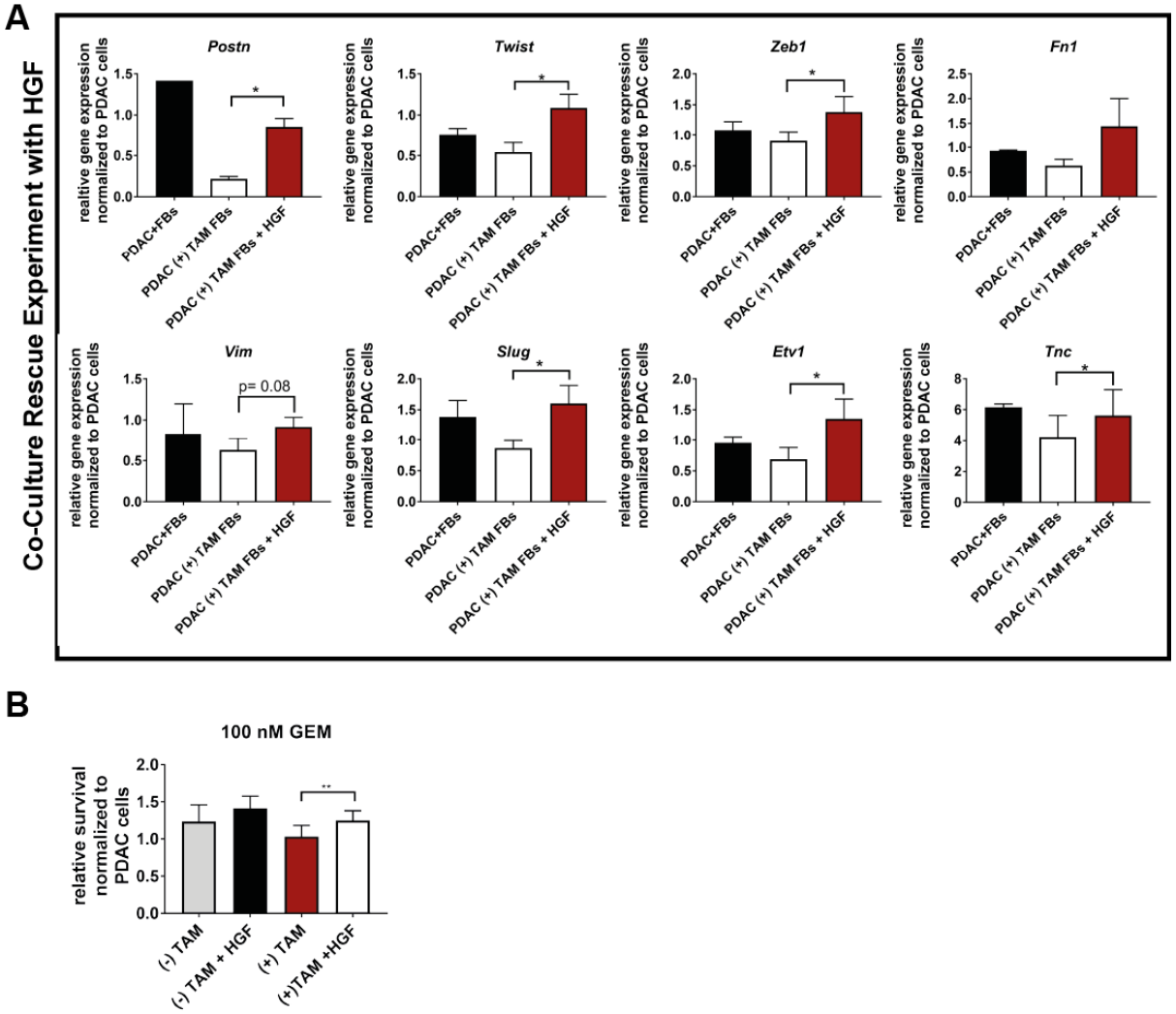

Figure 4.13 Recombinant HGF can rescue the effect of Prrx1 knockdown. A) Quantitative PCR analysis of EMT markers expressed in tumor cells co-cultured with PAFs ± HGF; paired student t-test; n=6; *p-value: <0.05. **B)** MTT Assay of the tumor cells co-cultured with PAFs ± HGF after 72h GEM treatment (600 nM GEM) t-test p-value: 0.0073

5 Discussion

In the last years, the function of CAFs has been highly discussed, especially the tumor promoting and tumor restraining role. CAFs influence the tumor biology by supporting the proliferation associated with decreased apoptosis, they increase cancer cell stemness, the migratory capability of tumor cells, the angiogenesis, the resistance towards chemotherapy, and they suppress the immune response (Vonlaufen et al., 2008; Olive et al., 2009; Xu et al., 2010; Hamada et al., 2012; Ene-Obong et al., 2013; Mace et al., 2013). For the first time Lee et al. and Rhim et al. showed a tumor restraining function of CAFs through targeting the hedgehog pathway either by genetic deletion of *shh* or by pharmacologic inhibition of the pathway (Rhim et al., 2014; Lee et al., 2015). These results were completely contradictory to the believed tumor promoting function of CAFs. The inhibition of the hedgehog pathway has led to more aggressive and poorly differentiated tumors as well as reduced stromal content and survival of the mice (Rhim et al., 2014; Lee et al., 2015). Similar findings were observed by Özdemir et al., who genetically deleted α-SMA positive cells (Özdemir et al., 2014). The contradictory results, which emerged in attempts to target the stroma, might be explained with the concept of intratumoral fibroblast heterogeneity (Bailey et al., 2008; Olive et al., 2009; Lee et al., 2014; Özdemir et al., 2014; Rhim et al., 2014). Lately, different subtypes of CAFs, the inflammatory CAFs (iCAFs) and myofibroblastic CAFs (myCAFs) were identified (Öhlund et al., 2017). The iCAFs have a more pro-tumorigenic and the myCAFs a more anti-tumorigenic function (Öhlund et al., 2017). Depending on the tumor cues the CAFs are exposed to, they interconvert into diverse phenotypic and functional subtypes. Biffi and colleagues have identified an IL1-induced signaling cascade, which promotes an inflammatory CAF state (Biffi et al., 2018). Targeting this signaling cascade resulted in a shift towards tumor suppressive myofibroblasts (myCAFs) (Biffi et al., 2018). A similar approach was published by Sherman et al. using a vitamin D receptor agonist to revert CAFs into quiescent fibroblasts (Sherman et al., 2014).

These recent findings support the hypothesis that the function of the stroma is dependent on the fibroblast subtype. Manipulating the CAF phenotype towards a tumor restraining subtype might be a more promising approach than the complete ablation of desmoplastic stroma.

In search for the explanation of the intertumoral heterogeneity, gene expression analysis of the stromal compartment revealed that the transcription factor *Prrx1* is highly upregulated in mesenchymal cells, especially in fibroblasts (Tomaru et al., 2014; Nicolle et al., 2017). This also supports the idea that EMT-TF can also regulate the plasticity program of fibroblasts in cancer.

In the previous publications of Takano and colleagues as well as Reichert and colleagues, the role of *Prrx1* as a master regulator for epithelial plasticity during embryonic development, pancreatitis, and carcinogenesis in the pancreas was shown (Reichert et al., 2013a; Takano et al., 2016). The latest publication of Yeo et al. (Yeo et al., 2018) as well as Sangrador et al. (Sangrador et al., 2018) demonstrated that manipulating the plasticity of fibroblasts via transcription factors e.g. *Twist, Prrx1* and *Zeb1* can influence carcinogenesis of the tumor.

5.1 *Prrx1* alters tumor differentiation and metastasis

In contrast to several publications describing the role of *Prrx1* as a plasticity driver in the processes of embryonic development and carcinogenesis, little is known about its part in fibroblasts (McKean et al., 2003; Yeo et al., 2018). The research field of EMT-TF in fibroblasts and how they modulate the tumor-stroma interaction is just emerging.

Gene expression analysis of different fibroblast entities revealed, that *Prrx1* is abundantly expressed in fibroblast in the pancreas. Especially the highest levels of *Prrx1* expression were measured in CAFs isolated from human PDAC tissue. Similar findings were observed for *Twist*, another EMT-TF, where Lee and colleagues showed, that CAFs express higher levels of *Twist* compared to normal fibroblasts. Indicating that EMT-TFs play an important role during the in the process of transdifferentiation from a resident fibroblast to a CAF (Lee et al., 2015).

The generation of a conditional loss-of-function allele of *Prrx1* in Dr. Reichert's group (Klinikum rechts der Isar, Technical University of Munich) allowed to study the role of *Prrx1* tissue or cell type specific for the first time, as the global knockout of *Prrx1* is lethal (Martin et al., 1995; Martin and Olson, 2000).

Therefore, the conditional loss-of function allele was crossed-in in a fibroblast specific *Cre* line (*Sm22-Cre*^{ERT}) and tumor cells were orthotopically implanted into the pancreas.

The results demonstrate that the transcription factor *Prrx1* in CAFs restrains stromal expansion but promotes invasion of tumor cells. In this process the tumor cells undergo EMT, which allows them to disseminate into the blood circulation and form metastasis. Similar findings were observed by analyzing the overall survival of patients diagnosed with PDAC. High levels of *Prrx1* expression are associated with poorer survival rate (Tang et al., 2017).

Prrx1 ablation in CAFs supports the stromal expansion through secretion of collagen, SPARC, and fibronectin in the ECM. The higher ECM content seems to restrain the tumor growth and leads to a more differentiated tumor, which is associated with less circulating tumor cells and less metastases. These findings go in hand with the publication of Özdemir et al. and Rhim et

al. who showed that the tumor microenvironment restrain rather than support the tumor growth (Özdemir et al., 2014; Rhim et al., 2014).

Although a *Prrx1* dependent regulation of the “ECM producing” phenotype in CAFs was observed, the pathway beyond this observation still needs to be revealed. Further analysis has to be performed with regard to the secretory phenotype (for example secretion of interleukins: IL-6 and IL-8, growth factors etc.) to gain more insights in the stroma-tumor crosstalk. Additionally, the regulation of ECM-degrading proteases such as MMPs might be an explanation for the higher tumor dissemination. MMPs can influence the motility and invasion capacity of tumor cells, for example MMP3 cleaves E-Cadherin and promoting thereby EMT of the tumor cells (Lochter et al., 1997).

5.2 *Prrx1* as a regulator of fibroblast plasticity

The information gained from the *in vivo* model showed that *Prrx1* impairs the synthetic phenotype of the fibroblasts and acts on several levels regarding stroma-tumor cross-talk. To support the assumption that *Prrx1* plays an important role as a plasticity driver in fibroblasts *in vitro* experiments were performed. Characterization and functional assay revealed that *Prrx1* knockout fibroblasts have a higher motility, secrete more collagen, and expresses more α-SMA, leading to the hypothesis that these cells have a more activated phenotype (Kalluri and Zeisberg, 2006; Öhlund et al., 2014).

Culturing isolated PSC in Matrigel allows these cells to revert into a quiescent state, showing that the switch from a quiescent to an activated state is reversible (Jesnowski et al., 2005; Öhlund et al., 2017).

Although some of the cultured PSCs do not lose their α-SMA expression in Matrigel, it was surprisingly to discover that *Prrx1* knockout fibroblasts express significantly higher α-SMA levels compared to the *Prrx1* wildtype fibroblasts. The loss of *Prrx1* in fibroblasts leads to reduced plasticity, because these PSCs remain in their activated state and cannot switch back to their quiescent state, reinforcing a myCAF phenotype (Öhlund et al., 2017).

It is known that TGF-β signaling is shaping the epigenetic landscape of CAFs and, therefore, their transdifferentiating status (Lamprecht et al., 2018), but no differences in TGF-β secretion was observed in between the two PSC population. Therefore, it can be assumed that the altered plasticity is due to transcriptional changes. Although little is known about the role of EMT-TF in fibroblasts, Sung et al. showed that conditioned media from Twist expressing fibroblasts significantly promote invasion of gastric cancer cells *in vitro* (Sung et al., 2011). Furthermore, they proved that Twist expression in CAFs was associated with invasion and metastasis in 195

gastric cancer samples (Sung et al., 2011). Interestingly, the proinflammatory cytokine IL-6, that is commonly expressed in tumors, was sufficient to induce Twist1 expression in normal cultured fibroblasts and to transdifferentiate them into CAFs through STAT3 phosphorylation (Sung et al., 2011). The recent publication of Yeo and colleagues (Yeo et al., 2018) support the assumption from the group of Nieto (Ocaña et al., 2012) that *Prrx1* is a downstream target of Twist.

Recently Öhlund et al. discovered that the iCAFs secrete IL-6 and other inflammatory mediators which can contribute to tumor progression, chemoresistance, and systemic effects such as cachexia and immune suppression (Feig et al., 2013; Mace et al., 2013; Flint et al., 2016; Öhlund et al., 2017).

This leads to the hypothesis that the activation of the Twist-Prrx1 axis promotes STAT3 phosphorylation, which fosters an iCAF phenotype, promoting the invasiveness of tumor cells by a secretory phenotype (Biffi et al., 2018), which has to be proven in further experiments.

This highlights the importance of Prrx1 as a plasticity driver in fibroblasts and the regulation of the ECM composition (Ocaña et al., 2012; Reichert et al., 2013a; Takano et al., 2016; Yeo et al., 2018).

5.3 *Prrx1* dependent HGF signaling can be used as a concept of patient stratification

HGF is a major component of the CAF secretome and its receptor c-MET is expressed on cancer cells (Pothula et al., 2017). Secreted HGF promotes EMT, cell scattering, proliferation, migration, and invasion of cancer cells in an HGF-dependent manner (Comoglio and Trusolino, 2002; Kalluri, 2016). Recently it was published that HGF is a transcriptional target of *Prrx1b* (Takano et al., 2016). Therefore, the capability of the *Prrx1* knockout fibroblast to secrete HGF was analyzed. Indeed, *Prrx1*$^{-/-}$ fibroblasts secrete significant less HGF into the cell culture supernatant compared to *Prrx1* wildtype fibroblasts. Accompanied with reduced HGF secretion also significant less EMT markers were expressed in cancer cells and they also kept their epithelial integrity *in vitro*. The addition of recombinant HGF into co-culture medium antagonized the effect of *Prrx1* knockout and led to a more invasive phenotype of the tumor cells, supporting the finding that HGF is a transcriptional target of *Prrx1*.

Furthermore, the analysis of the blood serum gained from the orthotopic implantation model revealed lower HGF levels, where *Prrx1* is ablated in the fibroblasts *in vivo*. The reduced HGF levels go in hand with slightly better differentiated and less invasive tumors as well as fewer metastases in the mouse model.

Transcriptional activation of *Prrx1* in fibroblasts leads to a higher secretion of HGF, which in turn binds to its receptor c-MET which is expressed on tumor cells. The dimerization of the receptor leads to an induction of the signaling pathways that support growth, survival, motility, and metastatic spread of cancer cells.

This highlights the idea, that HGF serum levels might serve as a stratification for patients in pancreatic cancer to predict disease progression and metastatic spread.

It has already been shown for other cancer types that high levels of HGF correlate with lymph node metastasis and relapse in breast cancer (Taniguchi et al., 1995; Toi et al., 1998), in multiple myeloma (Seidel et al., 1998), and in myeloid leukemia (Verstovsek et al., 2001). Also, in colon cancer patients it was shown that increased levels of HGF are associated with poor survival of patients as well as lymph node and liver metastases (Fukuura et al., 1998; Toiyama et al., 2009).

HGF might not serve only as a stratification marker for disease progression, it might also serve as a stratification marker for chemotherapy response. In *in vitro* experiments it was demonstrated that high levels of HGF secreted in the supernatant of the co-culture experiments of tumor cells and fibroblasts also correspond to chemoresistance towards gemcitabine. As shown in the gene expression analysis of the tumor cells co-cultured with fibroblasts, high levels of HGF correlate with EMT. It has been demonstrated that cells that underwent EMT are more resistant to cell death and display resistance to chemotherapy (Smith and Bhowmick, 2016). In the field of pancreatic cancer, it was already shown, that EMT suppresses cell proliferation, drug transporters, and concentrating proteins to promote resistance towards antiproliferative drugs as gemcitabine (Zheng et al., 2015). Furthermore, Li et al. demonstrated that the activation of MET also promotes a cancer stem cell phenotype resulting in resistance towards chemotherapy (Li et al., 2011).

In summary, the *Prrx1* dependent modulation of the fibroblast secretome especially for HGF influences the tumor cell plasticity via EMT and their response to chemotherapy. This underscores once again the role of *Prrx1* as a master regulator of cellular plasticity.

5.4 Modulation of fibroblast plasticity as a new treatment option

The results obtained in this dissertation highlight the role of *Prrx1* as a plasticity driver, thereby contributing significantly to ECM contribution and the stroma tumor crosstalk. Recently, the publications (Öhlund et al., 2017; Biffi et al., 2018) describe that iCAFs and myCAFs are interconvertible cell states rather than endpoints in differentiations and significantly contribute to the tumor stroma crosstalk. In the study of Biffi et al. (Biffi et al., 2018) it is highlighted that

iCAFs promote a pro tumorigenic environment and myCAFs contribute to restrain the tumor growth. The data in this dissertation reveals that *Prrx1* does not only influence the plasticity of fibroblasts but also their secretome, which massively impedes the tumor cells. Targeting the plasticity of fibroblasts via *Prrx1* could convert potential tumor-promoting CAFs into tumor-restraining CAFs. The *Prrx1* wildtype fibroblasts suggest a more iCAF like phenotype, which promotes tumor progression and chemoresistance (Straussman et al., 2012; Feig et al., 2013). Depleting *Prrx1* in CAFs leads to changes in the secretome, reducing the secretion of tumor promoting factors like HGF and shifting to a more myofibroblastic state, which increases the α-SMA positive CAF population and the secretion of ECM proteins. This population has been previously described to restrain tumor progression (Özdemir et al., 2014; Rhim et al., 2014).

These results indicate that targeting the plasticity of fibroblasts and their heterogeneity directly changes the fibroblast-tumor cell interaction. The data highlights the possibilities of new treatment designs by converting tumor promoting CAFs into a tumor-restraining CAF population.

6 Bibliography

Adamska, A., Domenichini, A., and Falasca, M. (2017). Pancreatic Ductal Adenocarcinoma. Current and Evolving Therapies. International journal of molecular sciences *18*.

Aguirre, A.J., Bardeesy, N., Sinha, M., Lopez, L., Tuveson, D.A., Horner, J., Redston, M.S., and DePinho, R.A. (2003). Activated Kras and Ink4a/Arf deficiency cooperate to produce metastatic pancreatic ductal adenocarcinoma. Genes & development *17*, 3112-3126.

Apte, M.V., Haber, P.S., Applegate, T.L., Norton, I.D., McCaughan, G.W., Korsten, M.A., Pirola, R.C., and Wilson, J.S. (1998). Periacinar stellate shaped cells in rat pancreas. Identification, isolation, and culture. Gut *43*, 128-133.

Apte, M.V., Pirola, R.C., and Wilson, J.S. (2012). Pancreatic stellate cells. A starring role in normal and diseased pancreas. Frontiers in physiology *3*, 344.

Apte, M.V., Wilson, J.S., Lugea, A., and Pandol, S.J. (2013). A starring role for stellate cells in the pancreatic cancer microenvironment. Gastroenterology *144*, 1210-1219.

Armstrong, T., Packham, G., Murphy, L.B., Bateman, A.C., Conti, J.A., Fine, D.R., Johnson, C.D., Benyon, R.C., and Iredale, J.P. (2004). Type I collagen promotes the malignant phenotype of pancreatic ductal adenocarcinoma. Clinical cancer research : an official journal of the American Association for Cancer Research *10*, 7427-7437.

Bachem, M.G., Schneider, E., Gross, H., Weidenbach, H., Schmid, R.M., Menke, A., Siech, M., Beger, H., Grünert, A., and Adler, G. (1998). Identification, culture, and characterization of pancreatic stellate cells in rats and humans. Gastroenterology *115*, 421-432.

Bachem, M.G., Schünemann, M., Ramadani, M., Siech, M., Beger, H., Buck, A., Zhou, S., Schmid-Kotsas, A., and Adler, G. (2005). Pancreatic carcinoma cells induce fibrosis by stimulating proliferation and matrix synthesis of stellate cells. Gastroenterology *128*, 907-921.

Bai, Y.-P., Shang, K., Chen, H., Ding, F., Wang, Z., Liang, C., Xu, Y., Sun, M.-H., and Li, Y.-Y. (2015). FGF-1/-3/FGFR4 signaling in cancer-associated fibroblasts promotes tumor progression in colon cancer through Erk and MMP-7. Cancer science *106*, 1278-1287.

Bailey, J.M., Swanson, B.J., Hamada, T., Eggers, J.P., Singh, P.K., Caffery, T., Ouellette, M.M., and Hollingsworth, M.A. (2008). Sonic hedgehog promotes desmoplasia in pancreatic cancer. Clinical cancer research : an official journal of the American Association for Cancer Research *14*, 5995-6004.

Bailey, P., Chang, D.K., Nones, K., Johns, A.L., Patch, A.-M., Gingras, M.-C., Miller, D.K., Christ, A.N., Bruxner, T.J.C., and Quinn, M.C., et al. (2016). Genomic analyses identify molecular subtypes of pancreatic cancer. Nature *531*, 47-52.

Baker, L.A., Tiriac, H., Clevers, H., and Tuveson, D.A. (2016). Modeling pancreatic cancer with organoids. Trends in cancer *2*, 176-190.

Bardeesy, N., Aguirre, A.J., Chu, G.C., Cheng, K.-H., Lopez, L.V., Hezel, A.F., Feng, B., Brennan, C., Weissleder, R., and Mahmood, U., et al. (2006). Both p16(Ink4a) and the p19(Arf)-p53 pathway constrain progression of pancreatic adenocarcinoma in the mouse. Proceedings of the National Academy of Sciences of the United States of America *103*, 5947-5952.

Becton, Dickinson and Company (2018). FlowJo. Online available: https://www.flowjo.com/solutions/flowjo/downloads (last visited on 12 August 2019).

Begum, A., Ewachiw, T., Jung, C., Huang, A., Norberg, K.J., Marchionni, L., McMillan, R., Penchev, V., Rajeshkumar, N.V., and Maitra, A., et al. (2017). The extracellular matrix and focal adhesion kinase signaling regulate cancer stem cell function in pancreatic ductal adenocarcinoma. PloS one *12*, e0180181.

Biffi, G., Oni, T.E., Spielman, B., Hao, Y., Elyada, E., Park, Y., Preall, J., and Tuveson, D.A. (2018). IL-1-induced JAK/STAT signaling is antagonized by TGF-beta to shape CAF heterogeneity in pancreatic ductal adenocarcinoma. Cancer discovery.

Boj, S.F., Hwang, C.-I., Baker, L.A., Chio, I.I.C., Engle, D.D., Corbo, V., Jager, M., Ponz-Sarvise, M., Tiriac, H., and Spector, M.S., et al. (2015). Organoid models of human and mouse ductal pancreatic cancer. Cell *160*, 324-338.

Bousquet, C. (2017). Pharmacological targeting of stellate cells for therapeutic gain in pancreatic adenocarcinoma (Göttingen).

Bramhall, S.R., Rosemurgy, A., Brown, P.D., Bowry, C., and Buckels, J.A. (2001). Marimastat as first-line therapy for patients with unresectable pancreatic cancer. A randomized trial. Journal of clinical oncology : official journal of the American Society of Clinical Oncology *19*, 3447-3455.

Bramhall, S.R., Schulz, J., Nemunaitis, J., Brown, P.D., Baillet, M., and Buckels, J.A.C. (2002). A double-blind placebo-controlled, randomised study comparing gemcitabine and marimastat with gemcitabine and placebo as first line therapy in patients with advanced pancreatic cancer. British journal of cancer *87*, 161-167.

Branda, C.S., and Dymecki, S.M. (2004). Talking about a revolution. The impact of site-specific recombinases on genetic analyses in mice. Developmental cell *6*, 7-28.

Bussard, K.M., Mutkus, L., Stumpf, K., Gomez-Manzano, C., and Marini, F.C. (2016). Tumor-associated stromal cells as key contributors to the tumor microenvironment. Breast cancer research : BCR *18*, 84.

Bynigeri, R.R., Jakkampudi, A., Jangala, R., Subramanyam, C., Sasikala, M., Rao, G.V., Reddy, D.N., and Talukdar, R. (2017). Pancreatic stellate cell. Pandora's box for pancreatic disease biology. World journal of gastroenterology *23*, 382-405.

Caldas, C., Hahn, S.A., da Costa, L.T., Redston, M.S., Schutte, M., Seymour, A.B., Weinstein, C.L., Hruban, R.H., Yeo, C.J., and Kern, S.E. (1994). Frequent somatic mutations and homozygous deletions of the p16 (MTS1) gene in pancreatic adenocarcinoma. Nature genetics *8*, 27-32.

Calon, A., Tauriello, D.V.F., and Batlle, E. (2014). TGF-beta in CAF-mediated tumor growth and metastasis. Seminars in cancer biology *25*, 15-22.

Ceyhan, G.O., Demir, I.E., Altintas, B., Rauch, U., Thiel, G., Müller, M.W., Giese, N.A., Friess, H., and Schäfer, K.-H. (2008). Neural invasion in pancreatic cancer. A mutual tropism between neurons and cancer cells. Biochemical and biophysical research communications *374*, 442-447.

Chu, G.C., Kimmelman, A.C., Hezel, A.F., and DePinho, R.A. (2007). Stromal biology of pancreatic cancer. Journal of cellular biochemistry *101*, 887-907.

Clevers, H., and Bender, E. (2015). Q&A. Hans Clevers. Banking on organoids. Nature *521*, S15.

Collisson, E.A., Trejo, C.L., Silva, J.M., Gu, S., Korkola, J.E., Heiser, L.M., Charles, R.-P., Rabinovich, B.A., Hann, B., and Dankort, D., et al. (2012). A central role for RAF→MEK→ERK signaling in the genesis of pancreatic ductal adenocarcinoma. Cancer discovery *2*, 685-693.

Comoglio, P.M., and Trusolino, L. (2002). Invasive growth. From development to metastasis. The Journal of clinical investigation *109*, 857-862.

Conroy, T., Desseigne, F., Ychou, M., Bouché, O., Guimbaud, R., Bécouarn, Y., Adenis, A., Raoul, J.-L., Gourgou-Bourgade, S., and La Fouchardière, C. de, et al. (2011). FOLFIRINOX versus gemcitabine for metastatic pancreatic cancer. The New England journal of medicine *364*, 1817-1825.

Cordelieres, F. (2004). Manual Tracking (ImageJ). Online available: https://imagej.nih.gov/ij/plugins/track/track.html (last visited on 12 August 2019).

Dallas, S.L., Sivakumar, P., Jones, C.J.P., Chen, Q., Peters, D.M., Mosher, D.F., Humphries, M.J., and Kielty, C.M. (2005). Fibronectin regulates latent transforming growth factor-beta (TGF beta) by controlling matrix assembly of latent TGF beta-binding protein-1. The Journal of biological chemistry *280*, 18871-18880.

Dobrynin, Y.V. (1963). Establishment and characteristics of cell strains from some epithelial tumors of human origin. Journal of the National Cancer Institute *31*, 1173-1195.

Doherty, G.J., Tempero, M., and Corrie, P.G. (2018). HALO-109-301. A Phase III trial of PEGPH20 (with gemcitabine and nab-paclitaxel) in hyaluronic acid-high stage IV pancreatic cancer. Future oncology (London, England) *14*, 13-22.

Ene-Obong, A., Clear, A.J., Watt, J., Wang, J., Fatah, R., Riches, J.C., Marshall, J.F., Chin-Aleong, J., Chelala, C., and Gribben, J.G., et al. (2013). Activated pancreatic stellate

cells sequester CD8+ T cells to reduce their infiltration of the juxtatumoral compartment of pancreatic ductal adenocarcinoma. Gastroenterology *145*, 1121-1132.

Erkan, M., Adler, G., Apte, M.V., Bachem, M.G., Buchholz, M., Detlefsen, S., Esposito, I., Friess, H., Gress, T.M., and Habisch, H.-J., et al. (2012a). StellaTUM. Current consensus and discussion on pancreatic stellate cell research. Gut *61*, 172-178.

Erkan, M., Michalski, C.W., Rieder, S., Reiser-Erkan, C., Abiatari, I., Kolb, A., Giese, N.A., Esposito, I., Friess, H., and Kleeff, J. (2008). The activated stroma index is a novel and independent prognostic marker in pancreatic ductal adenocarcinoma. Clinical gastroenterology and hepatology : the official clinical practice journal of the American Gastroenterological Association *6*, 1155-1161.

Erkan, M., Reiser-Erkan, C., Michalski, C.W., and Kleeff, J. (2010). Tumor microenvironment and progression of pancreatic cancer. Experimental oncology *32*, 128-131.

Erkan, M., Reiser-Erkan, C., Michalski, C.W., Kong, B., Esposito, I., Friess, H., and Kleeff, J. (2012b). The impact of the activated stroma on pancreatic ductal adenocarcinoma biology and therapy resistance. Current molecular medicine *12*, 288-303.

Eser, S., Schnieke, A., Schneider, G., and Saur, D. (2014). Oncogenic KRAS signalling in pancreatic cancer. British journal of cancer *111*, 817-822.

Feig, C., Gopinathan, A., Neesse, A., Chan, D.S., Cook, N., and Tuveson, D.A. (2012). The pancreas cancer microenvironment. Clinical cancer research : an official journal of the American Association for Cancer Research *18*, 4266-4276.

Feig, C., Jones, J.O., Kraman, M., Wells, R.J.B., Deonarine, A., Chan, D.S., Connell, C.M., Roberts, E.W., Zhao, Q., and Caballero, O.L., et al. (2013). Targeting CXCL12 from FAP-expressing carcinoma-associated fibroblasts synergizes with anti-PD-L1 immunotherapy in pancreatic cancer. Proceedings of the National Academy of Sciences of the United States of America *110*, 20212-20217.

Feil, R., Brocard, J., Mascrez, B., LeMeur, M., Metzger, D., and Chambon, P. (1996). Ligand-activated site-specific recombination in mice. Proceedings of the National Academy of Sciences of the United States of America *93*, 10887-10890.

Feil, S., Valtcheva, N., and Feil, R. (2009). Inducible Cre mice. Methods in molecular biology (Clifton, N.J.) *530*, 343-363.

Feldmann, G., Beaty, R., Hruban, R.H., and Maitra, A. (2007). Molecular genetics of pancreatic intraepithelial neoplasia. Journal of hepato-biliary-pancreatic surgery *14*, 224-232.

Feldmann, G., Mishra, A., Hong, S.-M., Bisht, S., Strock, C.J., Ball, D.W., Goggins, M., Maitra, A., and Nelkin, B.D. (2010). Inhibiting the cyclin-dependent kinase CDK5 blocks pancreatic cancer formation and progression through the suppression of Ras-Ral signaling. Cancer research *70*, 4460-4469.

Flint, T.R., Janowitz, T., Connell, C.M., Roberts, E.W., Denton, A.E., Coll, A.P., Jodrell, D.I., and Fearon, D.T. (2016). Tumor-Induced IL-6 Reprograms Host Metabolism to Suppress Anti-tumor Immunity. Cell metabolism *24*, 672-684.

Fukuura, T., Miki, C., Inoue, T., Matsumoto, K., and Suzuki, H. (1998). Serum hepatocyte growth factor as an index of disease status of patients with colorectal carcinoma. British journal of cancer *78*, 454-459.

Giancotti, F.G., and Ruoslahti, E. (1999). Integrin signaling. Science (New York, N.Y.) *285*, 1028-1032.

Goel, S., Duda, D.G., Xu, L., Munn, L.L., Boucher, Y., Fukumura, D., and Jain, R.K. (2011). Normalization of the vasculature for treatment of cancer and other diseases. Physiological reviews *91*, 1071-1121.

Goggins, M., Shekher, M., Turnacioglu, K., Yeo, C.J., Hruban, R.H., and Kern, S.E. (1998). Genetic alterations of the transforming growth factor beta receptor genes in pancreatic and biliary adenocarcinomas. Cancer research *58*, 5329-5332.

Gong, J., Han, J., He, J., Liu, J., Han, P., Wang, Y., Li, M., Li, D., Ding, X., and Du, Z., et al. (2017). Paired related homeobox protein 1 regulates PDGF-induced chemotaxis of hepatic stellate cells in liver fibrosis. Laboratory investigation; a journal of technical methods and pathology *97*, 1020-1032.

Gore, J., and Korc, M. (2014). Pancreatic cancer stroma. Friend or foe? Cancer cell *25*, 711-712.

Guerra, C., Schuhmacher, A.J., Cañamero, M., Grippo, P.J., Verdaguer, L., Pérez-Gallego, L., Dubus, P., Sandgren, E.P., and Barbacid, M. (2007). Chronic pancreatitis is essential for induction of pancreatic ductal adenocarcinoma by K-Ras oncogenes in adult mice. Cancer cell *11*, 291-302.

Guo, J., Fu, Z., Wei, J., Lu, W., Feng, J., and Zhang, S. (2015). PRRX1 promotes epithelial-mesenchymal transition through the Wnt/β-catenin pathway in gastric cancer. Medical oncology (Northwood, London, England) *32*, 393.

Gupta, P.B., Mani, S., Yang, J., Hartwell, K., and Weinberg, R.A. (2005). The evolving portrait of cancer metastasis. Cold Spring Harbor symposia on quantitative biology *70*, 291-297.

Hahn, S.A., Schutte, M., Hoque, A.T., Moskaluk, C.A., da Costa, L.T., Rozenblum, E., Weinstein, C.L., Fischer, A., Yeo, C.J., and Hruban, R.H., et al. (1996). DPC4, a candidate tumor suppressor gene at human chromosome 18q21.1. Science (New York, N.Y.) *271*, 350-353.

Hamada, S., Masamune, A., Takikawa, T., Suzuki, N., Kikuta, K., Hirota, M., Hamada, H., Kobune, M., Satoh, K., and Shimosegawa, T. (2012). Pancreatic stellate cells enhance

stem cell-like phenotypes in pancreatic cancer cells. Biochemical and biophysical research communications *421*, 349-354.

Hanahan, D., and Weinberg, R.A. (2011). Hallmarks of cancer. The next generation. Cell *144*, 646-674.

Heeg, S., Das, K.K., Reichert, M., Bakir, B., Takano, S., Caspers, J., Aiello, N.M., Wu, K., Neesse, A., and Maitra, A., et al. (2016). ETS-Transcription Factor ETV1 Regulates Stromal Expansion and Metastasis in Pancreatic Cancer. Gastroenterology *151*, 540-553.e14.

Heinemann, V., Reni, M., Ychou, M., Richel, D.J., Macarulla, T., and Ducreux, M. (2014). Tumour-stroma interactions in pancreatic ductal adenocarcinoma. Rationale and current evidence for new therapeutic strategies. Cancer treatment reviews *40*, 118-128.

Hessmann, E., Patzak, M.S., Klein, L., Chen, N., Kari, V., Ramu, I., Bapiro, T.E., Frese, K.K., Gopinathan, A., and Richards, F.M., et al. (2018). Fibroblast drug scavenging increases intratumoural gemcitabine accumulation in murine pancreas cancer. Gut *67*, 497-507.

Hingorani, S.R., Petricoin, E.F., Maitra, A., Rajapakse, V., King, C., Jacobetz, M.A., Ross, S., Conrads, T.P., Veenstra, T.D., and Hitt, B.A., et al. (2003). Preinvasive and invasive ductal pancreatic cancer and its early detection in the mouse. Cancer cell *4*, 437-450.

Hingorani, S.R., Wang, L., Multani, A.S., Combs, C., Deramaudt, T.B., Hruban, R.H., Rustgi, A.K., Chang, S., and Tuveson, D.A. (2005). Trp53R172H and KrasG12D cooperate to promote chromosomal instability and widely metastatic pancreatic ductal adenocarcinoma in mice. Cancer cell *7*, 469-483.

Hoff, D.D. von, Ervin, T., Arena, F.P., Chiorean, E.G., Infante, J., Moore, M., Seay, T., Tjulandin, S.A., Ma, W.W., and Saleh, M.N., et al. (2013). Increased survival in pancreatic cancer with nab-paclitaxel plus gemcitabine. The New England journal of medicine *369*, 1691-1703.

Hruban, R.H., Goggins, M., Parsons, J., and Kern, S.E. (2000). Progression model for pancreatic cancer. Clinical cancer research : an official journal of the American Association for Cancer Research *6*, 2969-2972.

Hruban, R.H., Takaori, K., Klimstra, D.S., Adsay, N.V., Albores-Saavedra, J., Biankin, A.V., Biankin, S.A., Compton, C., Fukushima, N., and Furukawa, T., et al. (2004). An illustrated consensus on the classification of pancreatic intraepithelial neoplasia and intraductal papillary mucinous neoplasms. The American journal of surgical pathology *28*, 977-987.

Jacobetz, M.A., Chan, D.S., Neesse, A., Bapiro, T.E., Cook, N., Frese, K.K., Feig, C., Nakagawa, T., Caldwell, M.E., and Zecchini, H.I., et al. (2013). Hyaluronan impairs vascular function and drug delivery in a mouse model of pancreatic cancer. Gut *62*, 112-120.

Jemal, A., Bray, F., Center, M.M., Ferlay, J., Ward, E., and Forman, D. (2011). Global cancer statistics. CA: a cancer journal for clinicians *61*, 69-90.

Jesnowski, R., Fürst, D., Ringel, J., Chen, Y., Schrödel, A., Kleeff, J., Kolb, A., Schareck, W.D., and Löhr, M. (2005). Immortalization of pancreatic stellate cells as an in vitro model of pancreatic fibrosis. Deactivation is induced by matrigel and N-acetylcysteine. Laboratory investigation; a journal of technical methods and pathology *85*, 1276-1291.

Kalluri, R. (2016). The biology and function of fibroblasts in cancer. Nature reviews. Cancer *16*, 582-598.

Kalluri, R., and Zeisberg, M. (2006). Fibroblasts in cancer. Nature reviews. Cancer *6*, 392-401.

Kim, S.K., and MacDonald, R.J. (2002). Signaling and transcriptional control of pancreatic organogenesis. Current opinion in genetics & development *12*, 540-547.

Kühbandner, S., Brummer, S., Metzger, D., Chambon, P., Hofmann, F., and Feil, R. (2000). Temporally controlled somatic mutagenesis in smooth muscle. Genesis (New York, N.Y. : 2000) *28*, 15-22.

Laklai, H., Miroshnikova, Y.A., Pickup, M.W., Collisson, E.A., Kim, G.E., Barrett, A.S., Hill, R.C., Lakins, J.N., Schlaepfer, D.D., and Mouw, J.K., et al. (2016). Genotype tunes pancreatic ductal adenocarcinoma tissue tension to induce matricellular fibrosis and tumor progression. Nature medicine *22*, 497-505.

Lamprecht, S., Sigal-Batikoff, I., Shany, S., Abu-Freha, N., Ling, E., Delinasios, G.J., Moyal-Atias, K., Delinasios, J.G., and Fich, A. (2018). Teaming Up for Trouble. Cancer Cells, Transforming Growth Factor-β1 Signaling and the Epigenetic Corruption of Stromal Naïve Fibroblasts. Cancers *10*.

LeBleu, V.S., and Kalluri, R. (2018). A peek into cancer-associated fibroblasts. Origins, functions and translational impact. Disease models & mechanisms *11*.

Lee, C.-L., Moding, E.J., Huang, X., Li, Y., Woodlief, L.Z., Rodrigues, R.C., Ma, Y., and Kirsch, D.G. (2012). Generation of primary tumors with Flp recombinase in FRT-flanked p53 mice. Disease models & mechanisms *5*, 397-402.

Lee, J.J., Perera, R.M., Wang, H., Wu, D.-C., Liu, X.S., Han, S., Fitamant, J., Jones, P.D., Ghanta, K.S., and Kawano, S., et al. (2014). Stromal response to Hedgehog signaling restrains pancreatic cancer progression. Proceedings of the National Academy of Sciences of the United States of America *111*, E3091-100.

Lee, K.-W., Yeo, S.-Y., Sung, C.O., and Kim, S.-H. (2015). Twist1 is a key regulator of cancer-associated fibroblasts. Cancer research *75*, 73-85.

Li, C., Wu, J.-J., Hynes, M., Dosch, J., Sarkar, B., Welling, T.H., Di Pasca Magliano, M., and Simeone, D.M. (2011). c-Met is a marker of pancreatic cancer stem cells and therapeutic target. Gastroenterology *141*, 2218-2227.e5.

Lim, K.-H., Baines, A.T., Fiordalisi, J.J., Shipitsin, M., Feig, L.A., Cox, A.D., Der, C.J., and Counter, C.M. (2005). Activation of RalA is critical for Ras-induced tumorigenesis of human cells. Cancer cell *7*, 533-545.

Lochter, A., Galosy, S., Muschler, J., Freedman, N., Werb, Z., and Bissell, M.J. (1997). Matrix metalloproteinase stromelysin-1 triggers a cascade of molecular alterations that leads to stable epithelial-to-mesenchymal conversion and a premalignant phenotype in mammary epithelial cells. The Journal of cell biology *139*, 1861-1872.

Lowy, A.M., Leach, S.D., and Philip, P.A. (2008). Pancreatic Cancer (Boston, MA: Springer-Verlag US).

Lv, Z.-D., Yang, Z.-C., Liu, X.-P., Jin, L.-Y., Dong, Q., Qu, H.-L., Li, F.-N., Kong, B., Sun, J., and Zhao, J.-J., et al. (2016). Silencing of Prrx1b suppresses cellular proliferation, migration, invasion and epithelial-mesenchymal transition in triple-negative breast cancer. Journal of cellular and molecular medicine *20*, 1640-1650.

Mace, T.A., Bloomston, M., and Lesinski, G.B. (2013). Pancreatic cancer-associated stellate cells. A viable target for reducing immunosuppression in the tumor microenvironment. Oncoimmunology *2*, e24891.

Maitra, A., and Hruban, R.H. (2008). Pancreatic cancer. Annual review of pathology *3*, 157-188.

Martin, J.F., Bradley, A., and Olson, E.N. (1995). The paired-like homeo box gene MHox is required for early events of skeletogenesis in multiple lineages. Genes & development *9*, 1237-1249.

Martin, J.F., and Olson, E.N. (2000). Identification of a prx1 limb enhancer. genesis *26*, 225-229.

Matano, M., Date, S., Shimokawa, M., Takano, A., Fujii, M., Ohta, Y., Watanabe, T., Kanai, T., and Sato, T. (2015). Modeling colorectal cancer using CRISPR-Cas9–mediated engineering of human intestinal organoids. Nature medicine *21*, 256.

McKean, D.M., Sisbarro, L., Ilic, D., Kaplan-Alburquerque, N., Nemenoff, R., Weiser-Evans, M., Kern, M.J., and Jones, P.L. (2003). FAK induces expression of Prx1 to promote tenascin-C-dependent fibroblast migration. The Journal of cell biology *161*, 393-402.

Metzger, D., Clifford, J., Chiba, H., and Chambon, P. (1995). Conditional site-specific recombination in mammalian cells using a ligand-dependent chimeric Cre recombinase. Proceedings of the National Academy of Sciences of the United States of America *92*, 6991-6995.

Moir, J.A.G., Mann, J., and White, S.A. (2015). The role of pancreatic stellate cells in pancreatic cancer. Surgical oncology *24*, 232-238.

Molon, B., Calì, B., and Viola, A. (2016). T Cells and Cancer. How Metabolism Shapes Immunity. Frontiers in immunology *7*, 20.

Monboisse, J.C., Oudart, J.B., Ramont, L., Brassart-Pasco, S., and Maquart, F.X. (2014). Matrikines from basement membrane collagens. A new anti-cancer strategy. Biochimica et biophysica acta *1840*, 2589-2598.

Moore, M.J., Hamm, J., Dancey, J., Eisenberg, P.D., Dagenais, M., Fields, A., Hagan, K., Greenberg, B., Colwell, B., and Zee, B., et al. (2003). Comparison of gemcitabine versus the matrix metalloproteinase inhibitor BAY 12-9566 in patients with advanced or metastatic adenocarcinoma of the pancreas. A phase III trial of the National Cancer Institute of Canada Clinical Trials Group. Journal of clinical oncology : official journal of the American Society of Clinical Oncology *21*, 3296-3302.

Moreira, L., Bakir, B., Chatterji, P., Dantes, Z., Reichert, M., and Rustgi, A.K. (2018). Pancreas 3D Organoids. Current and Future Aspects as a Research Platform for Personalized Medicine in Pancreatic Cancer. Cellular and molecular gastroenterology and hepatology *5*, 289-298.

Motulsky, H. GraphPad Prism (GraphPad Software). Online available: http://www.graphpad.com (last visited on 12 August 2019).

Mueller, S., Engleitner, T., Maresch, R., Zukowska, M., Lange, S., Kaltenbacher, T., Konukiewitz, B., Öllinger, R., Zwiebel, M., and Strong, A., et al. (2018). Evolutionary routes and KRAS dosage define pancreatic cancer phenotypes. Nature *554*, 62-68.

Muzumdar, M.D., Tasic, B., Miyamichi, K., Li, L., and Luo, L. (2007). A global double-fluorescent Cre reporter mouse. Genesis (New York, N.Y. : 2000) *45*, 593-605.

National Institutes of Health (2018). ImageJ. Online available: https://imagej.nih.gov/ij/download.html (last visited on 12 August 2019).

Neesse, A., Krug, S., Gress, T.M., Tuveson, D.A., and Michl, P. (2013). Emerging concepts in pancreatic cancer medicine. Targeting the tumor stroma. OncoTargets and therapy *7*, 33-43.

Nicolle, R., Blum, Y., Marisa, L., Loncle, C., Gayet, O., Moutardier, V., Turrini, O., Giovannini, M., Bian, B., and Bigonnet, M., et al. (2017). Pancreatic Adenocarcinoma Therapeutic Targets Revealed by Tumor-Stroma Cross-Talk Analyses in Patient-Derived Xenografts. Cell reports *21*, 2458-2470.

Nielsen, M.F.B., Mortensen, M.B., and Detlefsen, S. (2016). Key players in pancreatic cancer-stroma interaction. Cancer-associated fibroblasts, endothelial and inflammatory cells. World journal of gastroenterology *22*, 2678-2700.

Norris, R.A., and Kern, M.J. (2001). The identification of Prx1 transcription regulatory domains provides a mechanism for unequal compensation by the Prx1 and Prx2 loci. The Journal of biological chemistry *276*, 26829-26837.

Ocaña, O.H., Córcoles, R., Fabra, A., Moreno-Bueno, G., Acloque, H., Vega, S., Barrallo-Gimeno, A., Cano, A., and Nieto, M.A. (2012). Metastatic colonization requires the repression of the epithelial-mesenchymal transition inducer Prrx1. Cancer cell *22*, 709-724.

Öhlund, D., Elyada, E., and Tuveson, D. (2014). Fibroblast heterogeneity in the cancer wound. The Journal of experimental medicine *211*, 1503-1523.

Öhlund, D., Handly-Santana, A., Biffi, G., Elyada, E., Almeida, A.S., Ponz-Sarvise, M., Corbo, V., Oni, T.E., Hearn, S.A., and Lee, E.J., et al. (2017). Distinct populations of inflammatory fibroblasts and myofibroblasts in pancreatic cancer. The Journal of experimental medicine *214*, 579-596.

Olive, K.P., Jacobetz, M.A., Davidson, C.J., Gopinathan, A., McIntyre, D., Honess, D., Madhu, B., Goldgraben, M.A., Caldwell, M.E., and Allard, D., et al. (2009). Inhibition of Hedgehog signaling enhances delivery of chemotherapy in a mouse model of pancreatic cancer. Science (New York, N.Y.) *324*, 1457-1461.

Omary, M.B., Lugea, A., Lowe, A.W., and Pandol, S.J. (2007). The pancreatic stellate cell. A star on the rise in pancreatic diseases. The Journal of clinical investigation *117*, 50-59.

Özdemir, B.C., Pentcheva-Hoang, T., Carstens, J.L., Zheng, X., Wu, C.-C., Simpson, T.R., Laklai, H., Sugimoto, H., Kahlert, C., and Novitskiy, S.V., et al. (2014). Depletion of carcinoma-associated fibroblasts and fibrosis induces immunosuppression and accelerates pancreas cancer with reduced survival. Cancer cell *25*, 719-734.

Pang, T.C.Y., Xu, Z., Pothula, S., Becker, T., Goldstein, D., Pirola, R.C., Wilson, J.S., and Apte, M.V. (2017). Circulating pancreatic stellate (stromal) cells in pancreatic cancer-a fertile area for novel research. Carcinogenesis *38*, 588-591.

Paszek, M.J., Zahir, N., Johnson, K.R., Lakins, J.N., Rozenberg, G.I., Gefen, A., Reinhart-King, C.A., Margulies, S.S., Dembo, M., and Boettiger, D., et al. (2005). Tensional homeostasis and the malignant phenotype. Cancer cell *8*, 241-254.

Potenta, S., Zeisberg, E., and Kalluri, R. (2008). The role of endothelial-to-mesenchymal transition in cancer progression. British journal of cancer *99*, 1375-1379.

Pothula, S.P., Xu, Z., Goldstein, D., Merrett, N., Pirola, R.C., Wilson, J.S., and Apte, M.V. (2017). Targeting the HGF/c-MET pathway. Stromal remodelling in pancreatic cancer. Oncotarget *8*, 76722-76739.

Provenzano, P.P., Cuevas, C., Chang, A.E., Goel, V.K., Hoff, D.D. von, and Hingorani, S.R. (2012). Enzymatic targeting of the stroma ablates physical barriers to treatment of pancreatic ductal adenocarcinoma. Cancer cell *21*, 418-429.

Rahib, L., Smith, B.D., Aizenberg, R., Rosenzweig, A.B., Fleshman, J.M., and Matrisian, L.M. (2014). Projecting cancer incidence and deaths to 2030. The unexpected burden of

thyroid, liver, and pancreas cancers in the United States. Cancer research *74*, 2913-2921.

Ratajczak-Wielgomas, K., Grzegrzolka, J., Piotrowska, A., Gomulkiewicz, A., Witkiewicz, W., and Dziegiel, P. (2016). Periostin expression in cancer-associated fibroblasts of invasive ductal breast carcinoma. Oncology reports *36*, 2745-2754.

Redston, M.S., Caldas, C., Seymour, A.B., Hruban, R.H., da Costa, L., Yeo, C.J., and Kern, S.E. (1994). p53 mutations in pancreatic carcinoma and evidence of common involvement of homocopolymer tracts in DNA microdeletions. Cancer research *54*, 3025-3033.

Reichert, M., Rhim, A.D., and Rustgi, A.K. (2015). Culturing primary mouse pancreatic ductal cells. Cold Spring Harbor protocols *2015*, 558-561.

Reichert, M., and Rustgi, A.K. (2011). Pancreatic ductal cells in development, regeneration, and neoplasia. The Journal of clinical investigation *121*, 4572-4578.

Reichert, M., Takano, S., Burstin, J. von, Kim, S.-B., Lee, J.-S., Ihida-Stansbury, K., Hahn, C., Heeg, S., Schneider, G., and Rhim, A.D., et al. (2013a). The Prrx1 homeodomain transcription factor plays a central role in pancreatic regeneration and carcinogenesis. Genes & development *27*, 288-300.

Reichert, M., Takano, S., Heeg, S., Bakir, B., Botta, G.P., and Rustgi, A.K. (2013b). Isolation, culture and genetic manipulation of mouse pancreatic ductal cells. Nature protocols *8*, 1354-1365.

Rhim, A.D., Mirek, E.T., Aiello, N.M., Maitra, A., Bailey, J.M., McAllister, F., Reichert, M., Beatty, G.L., Rustgi, A.K., and Vonderheide, R.H., et al. (2012). EMT and dissemination precede pancreatic tumor formation. Cell *148*, 349-361.

Rhim, A.D., Oberstein, P.E., Thomas, D.H., Mirek, E.T., Palermo, C.F., Sastra, S.A., Dekleva, E.N., Saunders, T., Becerra, C.P., and Tattersall, I.W., et al. (2014). Stromal elements act to restrain, rather than support, pancreatic ductal adenocarcinoma. Cancer cell *25*, 735-747.

Ricard-Blum, S. (2011). The collagen family. Cold Spring Harbor perspectives in biology *3*, a004978.

Ryan, D.P., Hong, T.S., and Bardeesy, N. (2014). Pancreatic adenocarcinoma. The New England journal of medicine *371*, 1039-1049.

Sangrador, I., Molero, X., Campbell, F., Franch-Expósito, S., Rovira-Rigau, M., Samper, E., Domínguez-Fraile, M., Fillat, C., Castells, A., and Vaquero, E.C. (2018). Zeb1 in Stromal Myofibroblasts Promotes Kras-Driven Development of Pancreatic Cancer. Cancer research *78*, 2624-2637.

Schneider, G., Schmidt-Supprian, M., Rad, R., and Saur, D. (2017). Tissue-specific tumorigenesis. Context matters. Nature reviews. Cancer *17*, 239-253.

Schönhuber, N., Seidler, B., Schuck, K., Veltkamp, C., Schachtler, C., Zukowska, M., Eser, S., Feyerabend, T.B., Paul, M.C., and Eser, P., et al. (2014). A next-generation dual-recombinase system for time- and host-specific targeting of pancreatic cancer. Nature medicine *20*, 1340-1347.

Schutte, M., Hruban, R.H., Geradts, J., Maynard, R., Hilgers, W., Rabindran, S.K., Moskaluk, C.A., Hahn, S.A., Schwarte-Waldhoff, I., and Schmiegel, W., et al. (1997). Abrogation of the Rb/p16 tumor-suppressive pathway in virtually all pancreatic carcinomas. Cancer research *57*, 3126-3130.

Seidel, C., Børset, M., Turesson, I., Abildgaard, N., Sundan, A., and Waage, A. (1998). Elevated serum concentrations of hepatocyte growth factor in patients with multiple myeloma. The Nordic Myeloma Study Group. Blood *91*, 806-812.

Sherman, M.H., Yu, R.T., Engle, D.D., Ding, N., Atkins, A.R., Tiriac, H., Collisson, E.A., Connor, F., van Dyke, T., and Kozlov, S., et al. (2014). Vitamin D receptor-mediated stromal reprogramming suppresses pancreatitis and enhances pancreatic cancer therapy. Cell *159*, 80-93.

Sherr, C.J. (2000). Cell cycle control and cancer. Harvey lectures *96*, 73-92.

Shiga, K., Hara, M., Nagasaki, T., Sato, T., Takahashi, H., and Takeyama, H. (2015). Cancer-Associated Fibroblasts. Their Characteristics and Their Roles in Tumor Growth. Cancers *7*, 2443-2458.

Siegel, R., Naishadham, D., and Jemal, A. (2013). Cancer statistics, 2013. CA: a cancer journal for clinicians *63*, 11-30.

Smith, B.N., and Bhowmick, N.A. (2016). Role of EMT in Metastasis and Therapy Resistance. Journal of clinical medicine *5*.

Spizzo, G., Fong, D., Wurm, M., Ensinger, C., Obrist, P., Hofer, C., Mazzoleni, G., Gastl, G., and Went, P. (2011). EpCAM expression in primary tumour tissues and metastases. An immunohistochemical analysis. Journal of clinical pathology *64*, 415-420.

Stoker, M.G., Shearer, M., and O'Neill, C. (1966). Growth inhibition of polyoma-transformed cells by contact with static normal fibroblasts. Journal of cell science *1*, 297-310.

Straussman, R., Morikawa, T., Shee, K., Barzily-Rokni, M., Qian, Z.R., Du, J., Davis, A., Mongare, M.M., Gould, J., and Frederick, D.T., et al. (2012). Tumour micro-environment elicits innate resistance to RAF inhibitors through HGF secretion. Nature *487*, 500-504.

Strebhardt, K., and Ullrich, A. (2008). Paul Ehrlich's magic bullet concept. 100 years of progress. nrc *8*, 473-480.

Sung, C.O., Lee, K.-W., Han, S., and Kim, S.-H. (2011). Twist1 is up-regulated in gastric cancer-associated fibroblasts with poor clinical outcomes. The American journal of pathology *179*, 1827-1838.

Takano, S., Reichert, M., Bakir, B., Das, K.K., Nishida, T., Miyazaki, M., Heeg, S., Collins, M.A., Marchand, B., and Hicks, P.D., et al. (2016). Prrx1 isoform switching regulates pancreatic cancer invasion and metastatic colonization. Genes & development *30*, 233-247.

Tang, Z., Li, C., Kang, B., Gao, G., Li, C., and Zhang, Z. (2017). GEPIA. A web server for cancer and normal gene expression profiling and interactive analyses. Nucleic acids research *45*, W98-W102.

Taniguchi, T., Toi, M., Inada, K., Imazawa, T., Yamamoto, Y., and Tominaga, T. (1995). Serum concentrations of hepatocyte growth factor in breast cancer patients. Clinical cancer research : an official journal of the American Association for Cancer Research *1*, 1031-1034.

Thibodeau, S., and Voutsadakis, I.A. (2018). FOLFIRINOX Chemotherapy in Metastatic Pancreatic Cancer. A Systematic Review and Meta-Analysis of Retrospective and Phase II Studies. Journal of clinical medicine *7*.

Toi, M., Taniguchi, T., Ueno, T., Asano, M., Funata, N., Sekiguchi, K., Iwanari, H., and Tominaga, T. (1998). Significance of circulating hepatocyte growth factor level as a prognostic indicator in primary breast cancer. Clinical cancer research : an official journal of the American Association for Cancer Research *4*, 659-664.

Toiyama, Y., Miki, C., Inoue, Y., Okugawa, Y., Tanaka, K., and Kusunoki, M. (2009). Serum hepatocyte growth factor as a prognostic marker for stage II or III colorectal cancer patients. International journal of cancer *125*, 1657-1662.

Tomaru, Y., Hasegawa, R., Suzuki, T., Sato, T., Kubosaki, A., Suzuki, M., Kawaji, H., Forrest, A.R.R., Hayashizaki, Y., and Shin, J.W., et al. (2014). A transient disruption of fibroblastic transcriptional regulatory network facilitates trans-differentiation. Nucleic acids research *42*, 8905-8913.

Trapp, G., and Horn, E. (2006). Chemotaxis and Migration Tool (ibidi GmbH). Online available: https://ibidi.com/chemotaxis-analysis/171-chemotaxis-and-migration-tool.html (last visited on 12 August 2019).

Tyan, S.-W., Kuo, W.-H., Huang, C.-K., Pan, C.-C., Shew, J.-Y., Chang, K.-J., Lee, E.Y.-H.P., and Lee, W.-H. (2011). Breast cancer cells induce cancer-associated fibroblasts to secrete hepatocyte growth factor to enhance breast tumorigenesis. PloS one *6*, e15313.

van Heek, N.T., Meeker, A.K., Kern, S.E., Yeo, C.J., Lillemoe, K.D., Cameron, J.L., Offerhaus, G.J.A., Hicks, J.L., Wilentz, R.E., and Goggins, M.G., et al. (2002). Telomere Shortening Is Nearly Universal in Pancreatic Intraepithelial Neoplasia. The American journal of pathology *161*, 1541-1547.

Verstovsek, S., Kantarjian, H., Estey, E., Aguayo, A., Giles, F.J., Manshouri, T., Koller, C., Estrov, Z., Freireich, E., and Keating, M., et al. (2001). Plasma hepatocyte growth factor

is a prognostic factor in patients with acute myeloid leukemia but not in patients with myelodysplastic syndrome. Leukemia *15*, 1165-1170.

Vincent, A., Herman, J., Schulick, R., Hruban, R.H., and Goggins, M. (2011). Pancreatic cancer. The Lancet *378*, 607-620.

Vonlaufen, A., Joshi, S., Qu, C., Phillips, P.A., Xu, Z., Parker, N.R., Toi, C.S., Pirola, R.C., Wilson, J.S., and Goldstein, D., et al. (2008). Pancreatic stellate cells. Partners in crime with pancreatic cancer cells. Cancer research *68*, 2085-2093.

Vonlaufen, A., Phillips, P.A., Yang, L., Xu, Z., Fiala-Beer, E., Zhang, X., Pirola, R.C., Wilson, J.S., and Apte, M.V. (2010). Isolation of quiescent human pancreatic stellate cells. A promising in vitro tool for studies of human pancreatic stellate cell biology. Pancreatology : official journal of the International Association of Pancreatology (IAP) *10*, 434-443.

Wendt, M.K., Smith, J.A., and Schiemann, W.P. (2010). Transforming growth factor-β-induced epithelial-mesenchymal transition facilitates epidermal growth factor-dependent breast cancer progression. Oncogene *29*, 6485-6498.

Wilson, J.S., Pirola, R.C., and Apte, M.V. (2014). Stars and stripes in pancreatic cancer. Role of stellate cells and stroma in cancer progression. Frontiers in physiology *5*, 52.

Witkiewicz, A.K., McMillan, E.A., Balaji, U., Baek, G., Lin, W.-C., Mansour, J., Mollaee, M., Wagner, K.-U., Koduru, P., and Yopp, A., et al. (2015). Whole-exome sequencing of pancreatic cancer defines genetic diversity and therapeutic targets. Nature communications *6*, 6744.

Xu, Z., Pothula, S.P., Wilson, J.S., and Apte, M.V. (2014). Pancreatic cancer and its stroma. A conspiracy theory. World journal of gastroenterology *20*, 11216-11229.

Xu, Z., Vonlaufen, A., Phillips, P.A., Fiala-Beer, E., Zhang, X., Yang, L., Biankin, A.V., Goldstein, D., Pirola, R.C., and Wilson, J.S., et al. (2010). Role of pancreatic stellate cells in pancreatic cancer metastasis. The American journal of pathology *177*, 2585-2596.

Yachida, S., and Iacobuzio-Donahue, C.A. (2009). The pathology and genetics of metastatic pancreatic cancer. Archives of pathology & laboratory medicine *133*, 413-422.

Yeo, S.-Y., Lee, K.-W., Shin, D., An, S., Cho, K.-H., and Kim, S.-H. (2018). A positive feedback loop bi-stably activates fibroblasts. Nature communications *9*, 3016.

Yu, Y., Xiao, C.-H., Tan, L.-D., Wang, Q.-S., Li, X.-Q., and Feng, Y.-M. (2014). Cancer-associated fibroblasts induce epithelial-mesenchymal transition of breast cancer cells through paracrine TGF-β signalling. British journal of cancer *110*, 724-732.

Zeisberg, M., Strutz, F., and Müller, G.A. (2000). Role of fibroblast activation in inducing interstitial fibrosis. Journal of nephrology *13 Suppl 3*, S111-20.

Zheng, X., Carstens, J.L., Kim, J., Scheible, M., Kaye, J., Sugimoto, H., Wu, C.-C., LeBleu, V.S., and Kalluri, R. (2015). Epithelial-to-mesenchymal transition is dispensable for metastasis but induces chemoresistance in pancreatic cancer. Nature *527*, 525-530.

7 List of figures

8 List of tables

9 Appendix

9.1 Quantifying immunofluorescence (single color) – α-SMA

To quantify immunofluorescence (single color) staining, the protocol based on the publication from Heeg et al. was used (Heeg et al., 2016). This protocol can be found in the following.

1. Slides stained by IF for ASMA, YFP, and DAPI per standard protocol (YFP 1:250 (-20C Box4 297; Chicken), ASMA 1:7000 (-20C Oversized box Sigma 091M4832,; Mouse), Primary Ab O/N at 4C, Secondary at 1:600 CY2 Chicken, CY3 Mouse for 2 hrs at RT). 5 Slides each for 7182Y Control & 7182Y mEtv1.

2. Take images (5) of each slide at 20x. Representative images of tumor taken (each field had at least some (1-2) ASMA + cells - i.e. no areas that are completely dark, only tumor associated areas with clear YFP+ signal).

    a. Take images with same white balance and same exposure settings (AUTO – on iVision to establish baseline).

    b. Sequentially label the file names to facilitate future image processing (ie 8_1.tiff, 8_2.tiff, etc.) and place each sample's images in separate directories for each mouse.

    c. Recommend to copy the images to a hard disk where image processing below will be completed to improve performance.

3. Process images uniformly in Photoshop CS6 with AutoColor/AutoTone/AutoContrast so all are uniform.

    a. This processing can be automated in Photoshop. Create custom "Action" with Auto Color/Contrast/Tone. Then File ->Automate->Batch, select Action title, source folder, and "Save and Close" under Destination.

4. Separate out only the Red Channel (CY3) for analysis, and convert via BATCH processing in Photoshop CS6 to RGB image. Established a baseline set of threshold for sensitivity in sample population.

    a. Open sample positive and negative images in ImageJ.

    b. Select Image->Adjust->Color Threshold

    c. Make sure "Pass" is clicked for Hue, Saturation, and Brightness

d. Make sure sliders are at 0 & 255 (min and max respectively) for Hue, Saturation, Brightness.

e. Hue & Saturation were set to 0 & 255

f. Brightness was set at 40 & 255 as this best picked up stained areas with minimal background.

5. Edit Script Text below with customized max/min Hue values based on (4) above. The area to do this is indicated in the commentary text. Also edited script text with the pixel size as 10x images were used with the script previously for trichrome quantification. In this case 1 pixel = 0.2315uM.

6. Batch Process Images in ImageJ

a. In ImageJ, select Process->Batch->Macro

b. Select the Input Directory (of a single mouse)

c. Select the Output Directory (recommend for simplicity, create new directory in the mouse being analyzed). The overlays of counted area over uncounted will be generated and placed here. Please note as a default the overlay color is set to red, but if green/other is required this can be re-programmed (see commentary in code below).

d. Copy and Paste Macro Code into the area provided.

e. Click Process

f. Upon completion a results table with alternating values of total area (fixed) and measured area (variable) will be generated for all the files in the Input Directory. Click Save-As to save this file as an excel document. Confirm that overlay images have been saved to the output directory.

7. Open quantification table in Excel and calculate ratio of Total Area to IF + Area in experimental and control animals. Compare means, SD, SEM and test significance (2 tailed, paired, t-test) between the 2 averaged values for 5 different samples per group.

Script text:

```
// Change scale from inches to microns

run("Set Scale...", "distance=1 known=0.2315 pixel=1 unit=um");
```

```
//Create a duplicate image to modify with the selection

imgName=getTitle();

run("Duplicate...", "title=1.tif");


//Measure the total area of the image (denominator)

run("Set Measurements...", "area limit display redirect=None deci-
mal=3");

run("Measure");


// Threshold Color - Segment the image by color properties (Hue,
Saturation, Brightness); in this case by Hue & Brightness

min=newArray(3);

max=newArray(3);

filter=newArray(3);

a=getTitle();

run("HSB Stack");

run("Convert Stack to Images");

selectWindow("Hue");

rename("0");

selectWindow("Saturation");

rename("1");

selectWindow("Brightness");

rename("2");

// The min[0] and max[0] values are the spectrum you are choosing to
select for Hue, Saturation, and Brightness, respectively. Customize
the values based on your desired specifications.
```

```
// Run all your samples with the same min/max values to have comparable
results.

min[0]=0;

max[0]=255;

filter[0]="pass";

min[1]=0;

max[1]=255;

filter[1]="pass";

min[2]=40;

max[2]=255;

filter[2]="pass";


//Create a mask for your desired selection area

for (i=0;i<3;i++){

  selectWindow(""+i);

  setThreshold(min[i], max[i]);

  run("Convert to Mask");

  if (filter[i]=="stop") run("Invert");

}

imageCalculator("AND create", "0","1");

imageCalculator("AND create", "Result of 0","2");

for (i=0;i<3;i++){

  selectWindow(""+i);

  close();

}
```

```
selectWindow("Result of 0");

close();

selectWindow("Result of Result of 0");

rename(a);


//Apply the mask to the original image to overlay it

run("8-bit");

run("Create Selection");

selectWindow(imgName);

run("Restore Selection");


//Color in the selected area (in bright red)

run("Color Picker...");

setForegroundColor(255, 255, 255);

run("Fill", "slice");


//Measure the selected area

run("Measure");

selectWindow("Results");


//Output should be Total Area, Followed by Selection Area


//Batch run the macro for entire sequential directory of images by
going to Process ->Batch->Macro
```

9.2 Determining the Euclidian distance and the forward migration index

For the purpose of determining the Euclidian distance and the forward migration index as described in section 3.1.9, the ImageJ software was used in conjunction with the plugins (Cordelieres, 2004) and (Trapp and Horn, 2006). In order to postprocess the images, we followed the protocol received from the group of Prof. Dr. Ceyhan (Klinikum rechts der Isar, Technical University of Munich). The protocol can be found in the following pages.

Protocol – Manual cell tracking with Image J

- Install ImageJ with the manual tracking plugin and the chemotaxis plugin from ibidi on your computer
  - Image J download: http://rsbweb.nih.gov/ij/download.html
  - Manual tracking plugin: http://rsbweb.nih.gov/ij/plugins/track/track.html
  - Chemotaxis Plugin: http://www.ibidi.de/applications/ap_chemo.html

- Export your zvi-document to tif-pictures
- Open ImageJ
- Click: File -> Import -> Image Sequence and double click on the first tif-picture in your document

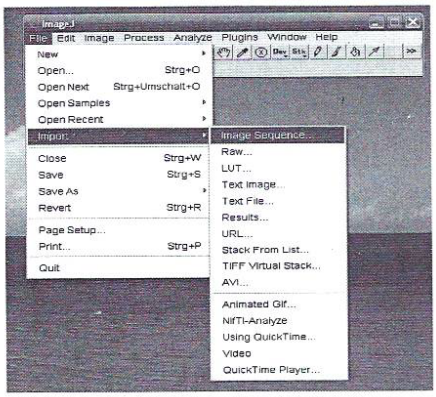

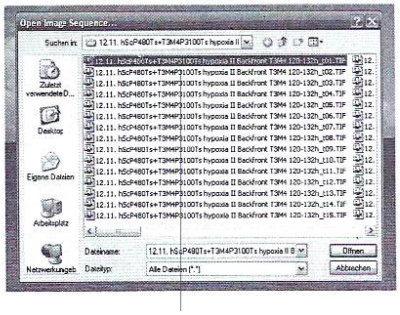

- A new box opens where we change the scale images to 70%

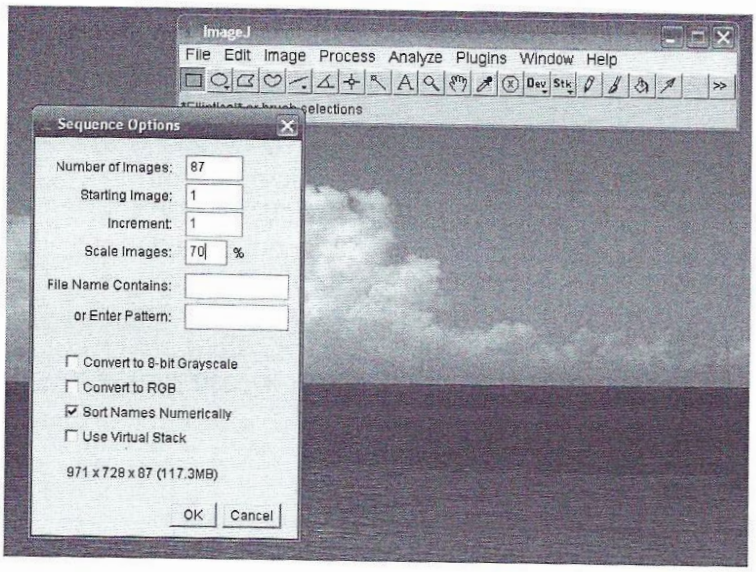

- When the video sequence is uploaded we chose: Plugins -> Manual Tracking
- A new box opens where we enter the following orders:
  - Time interval -> 5min / 30min
  - x/y calibration -> 0.645 µm
  - z calibration ->0.3
  - search square size for centring -> 1.025 pixels
  - dot size -> 6
  - line width .> 3
  - font size -> 12

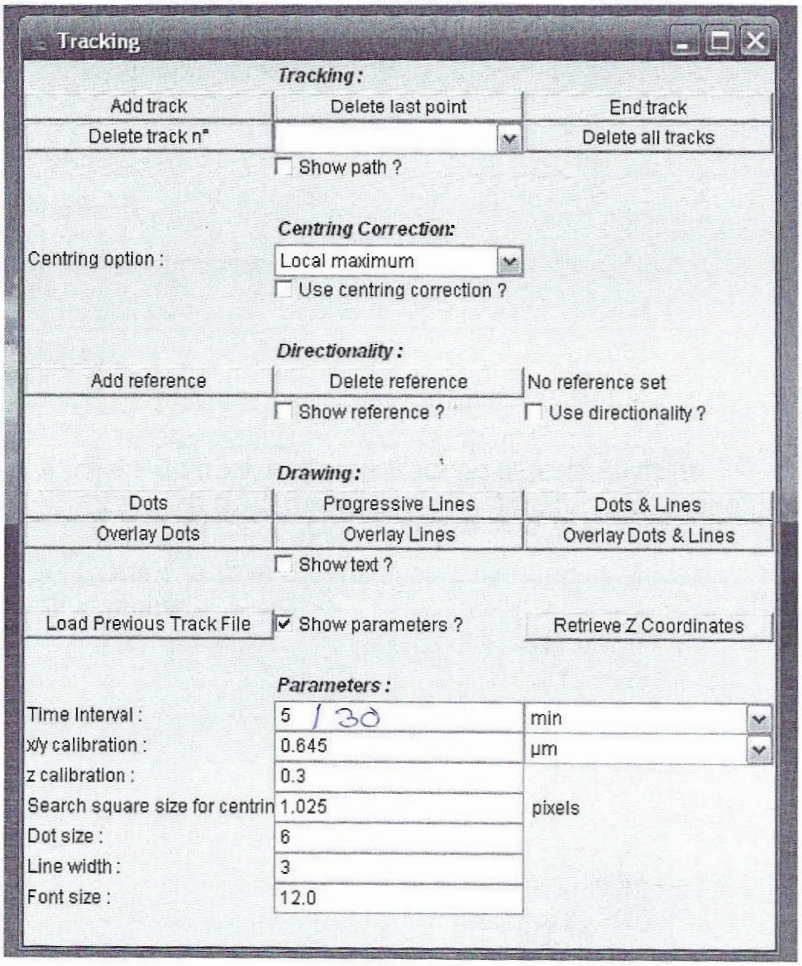

- click Add track and start tracking at least 30 cells
- After each track one has to click Add track again and then the next track can be followed
- In the end save the data you generated as a .xls data to your computer

Analysis of the tracked cells via the Chemotaxis tool from Ibidi

- Open ImageJ
- Choose: Plugins -> Chemotaxis tool

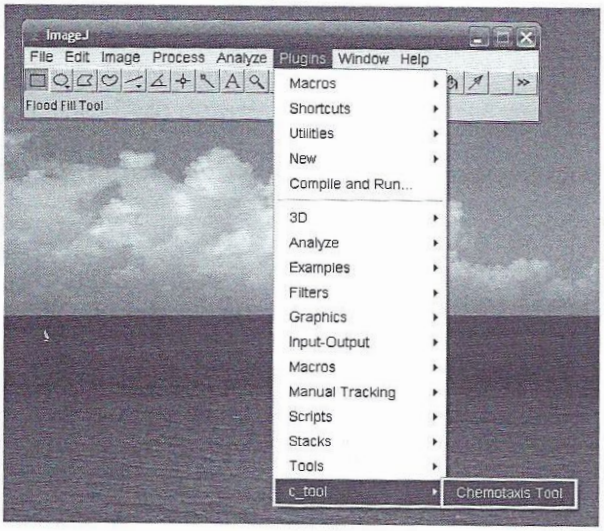

- Import your .xls data with the Import data buttom
- Fill in the number of slices you tracked
- And click Add dataset

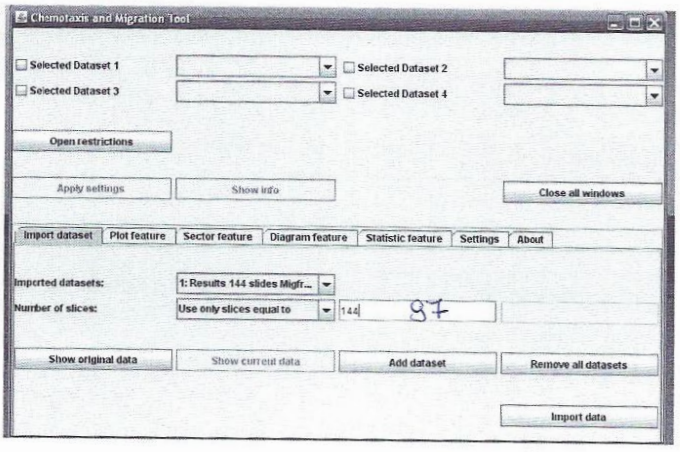

- Change the Settings:
  - Time interval -> 5min
  - x/y calibration -> 0.645 µm

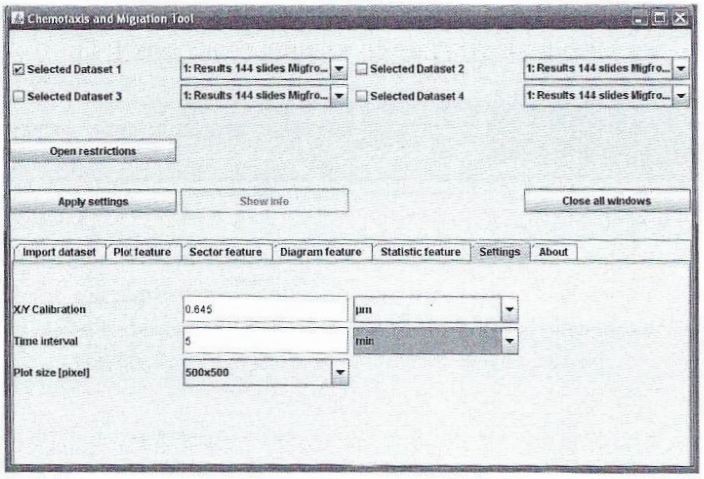

- Apply these settings with the Apply seetings buttom
- Within the statistic features one can find out the Velocity, Distance, FMI and Directionality of each tracked cell